RESPONSE OF THE MAGNETOSPHERE AND ATMOSPHERE TO THE SOLAR WIND

FINAL SCIENTIFIC REPORT FOR CONTRACT F44620-72-C-0084

Sponsored by Air Force Office of Scientific Research

BIOTECHNOLOGY AND SPACE SCIENCES SUBDIVISION
5301 BOLSA AVENUE
HUNTINGTON BEACH, CALIFORNIA 92647

MCDONNELL DOUGLAS ASTRONAUTICS COMPANY

MCDONNELL DOUGLAS CORPORATION

DISCLAIMER NOTICE

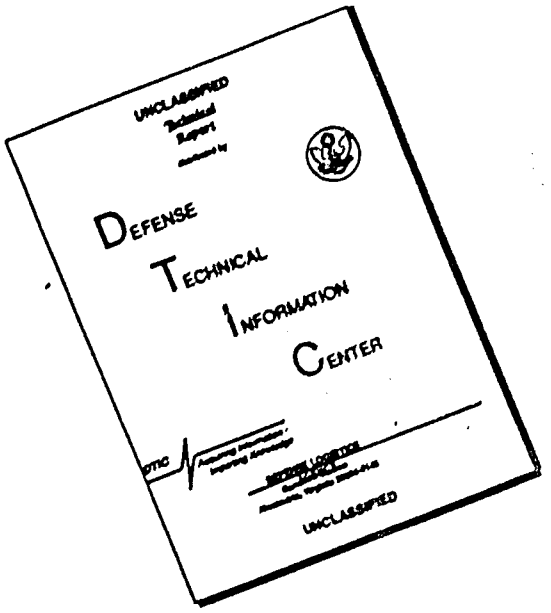

THIS DOCUMENT IS BEST QUALITY AVAILABLE. THE COPY FURNISHED TO DTIC CONTAINED A SIGNIFICANT NUMBER OF PAGES WHICH DO NOT REPRODUCE LEGIBLY.

MCDONNELL DOUGLAS

RESPONSE OF THE MAGNETOSPHERE AND ATMOSPHERE TO THE SOLAR WIND

December 1975

Final Scientific Report for Contract F44620-72-C-0084
Sponsored by the Air Force Office of Scientific Research

PRINCIPAL INVESTIGATOR: W. P. Olson

CO-INVESTIGATORS: K. A. Pfitzer and O. K. Moe

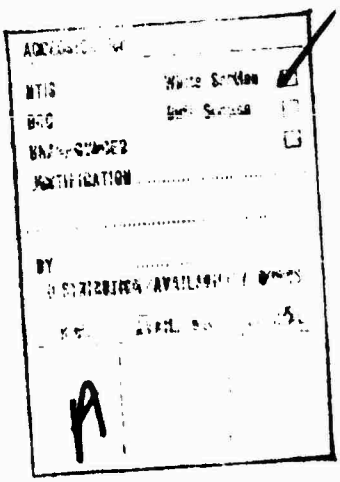

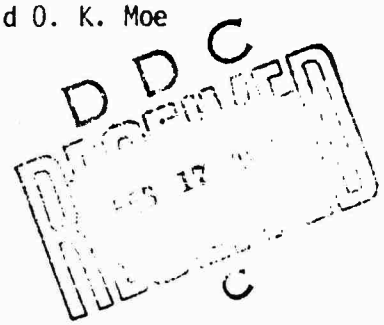

DISTRIBUTION STATEMENT A
Approved for public release;
Distribution Unlimited

MCDONNELL DOUGLAS ASTRONAUTICS COMPANY-WEST
5301 Bolsa Avenue, Huntington Beach, CA 92647

TABLE OF CONTENTS

1.0 INTRODUCTION

The solar wind (a charge neutral plasma comprised mostly of protons and electrons) is the ultimate energy source for many phenomena in the earth's upper atmosphere and ionosphere--especially at high latitudes. The solar wind also is entirely responsible for the formation and maintenance of the earth's magnetosphere. These regions of the near earth environment are strongly coupled and in turn all act to influence space and military hardware systems in many ways. Examples include: the influence of the ionosphere on radio communications and the uses of over-the-horizon radar; the influence of the neutral atmosphere on satellite trajectories and lifetimes; the effects of trapped and cosmic radiation on man and components in space; and the influence of space currents on surface systems vulnerable to magnetic field fluctuations. In order to optimize the use of these hardware systems, it is necessary to understand quantitatively these environmental influences. For the real time optimization of several systems it is necessary to predict the behavior of the environment in which these systems operate. At present, most Air Force efforts in this area are limited to the real time "specification" of environmental features. Air Force/Global Weather Central (AFGWC) routinely receives real time data from several sources which are used for specification purposes. However, to date it has not been possible to offer a bona fide predictive capability (except for the forecast of a few space averaged bulk parameters).

There are several reasons for the present lack of predictive capability. The several regions of the near earth environment and their coupling are not currently adequately understood. The energy sources that produce structures and variability in the near earth environment must be monitored. At present, this is not done routinely. Quantitative models of the environmental parameters in question and the relations to their energy sources must be developed with associated fast computer codes.

In this contract, the response of the earth's magnetosphere and upper atmosphere to the solar wind has been studied. Several goals were stated and met. The overall purpose of the work was to obtain enough understanding of

some environmental features to develop quantitative models of their behavior. This was done with the intent of examining the possibility of predicting solar wind influences on the near earth environment.

Four general problem areas were isolated with the above goal in mind.

1. Work prior to this contract was done on energy sources for the upper atmosphere (Moe, 1971; Olson, 1971). It was found in particular that at high latitudes charged particles from the solar wind precipitate directly into the ionosphere and upper atmosphere near noon (Frank, 1971, and Heikkila, 1971). This precipitation is controlled by the magnetospheric magnetic field. The "field lines" along which these particles move form the region of the magnetosphere known as the dayside cusp or cleft. The physics of the dayside cusp was studied during the first year of the contract as were the correlations discussed above. Data on precipitating particles were used to describe the extent and location of the cusps. The amount of corpuscular energy deposited through the cusps was also determined as it is an energy source for both the upper atmosphere and the ionosphere and thus an important input parameter for quantitative models of those regions. The currents in the cusp region and their associated fields were also estimated. The cusp work is discussed in Section 2.0.

2. Any attempt to <u>predict</u> atmospheric and/or ionospheric behavior must consider the coupling of both regions to the magnetosphere. This is necessary because solar wind variability must be monitored in advance of the time for which near earth environmental conditions are being predicted. The solar wind interacts with the earth's magnetic field to form the magnetosphere. The magnetospheric magnetic field in particular exerts considerable influence on the near earth environment, especially at high latitudes. Therefore, an attempt was made to more accurately model the total magnetospheric magnetic field, $\vec{B}_T$. $\vec{B}_T$ has as its main sources the earth's main (internal) field, the magnetopause field (from currents formed by the deflection of the shocked solar wind

electrons and protons in opposite directions by $\vec{B}_T$), the tail field (from particles that drift across the tail), and the ring current magnetic field (produced by particles trapped in $\vec{B}_T$ and drifting around the earth). Earlier quantitative models of $\vec{B}_T$ had neglected the ring and tail currents since it is very difficult to model a magnetic field in the region of its source currents. (Scalar potentials cannot be used in such regions.) A method was developed to overcome these problems. The result was the first accurate quantitative model of $\vec{B}_T$ that included all four of its major sources. This model is discussed in Section 3.0. This work was performed during the first and second years of the contract period.

3. The studies on the dayside cusps (or clefts) confirmed what many earlier investigations had suggested--that at high latitudes the upper atmosphere is very structured and charged particles are an important energy source in that region. These conclusions led to an attempt to construct a quantitative global model of the upper atmosphere that would for the first time include these high latitude corpuscular energy sources. This model and the model of $\vec{B}_T$ are semiempirical. That is, they use physical understanding whenever it exists, but rely on observational data in the many areas where the physics is currently not well known. Work on modeling the density of the upper atmosphere was performed during the second and third years of the contract. The atmospheric density model is discussed in Section 4.0.

4. An investigation of the several reported correlations between solar wind and near earth environmental parameters was carried out. Its purpose was twofold. First, an attempt was made to isolate highly correlated data. This would ultimately suggest a means by which some near earth environmental parameters could be predicted directly from monitored solar wind data. Such correlations also suggest that the direct monitoring of solar wind data might yield indices that are much more accurate and useful than the temporally and spatially averaged indices such as K_p, A_E, and D_{ST}. Second, such correlations must

ultimately be used to guide the development of quantitative environmental models. Such models are only useful to the extent that their input parameters are available (e.g., from a monitoring satellite) and their output parameters accurately describe environmental features (e.g., atmosphere density). These correlations are discussed in Section 5.0.

In addition to the four general problems discussed above, there were several other areas of direct or indirect results associated with performance on this contract. Both models were developed with the user's needs in mind. This is discussed in the section on modeling philosophy in Section 6.0. Other work that has grown out of this contract work is also discussed in Section 6.0. A summary of this work and conclusions regarding it are also presented in Section 6.0. Appendicies to this report appear in Section 7.0. They include listings of the quantitative magnetic field and neutral atmospheric density models. Copies of Fortran decks for these models are available upon written request from McDonnell Douglas Astronautics Company. (Contact Dr. W. P. Olson or Dr. K. A. Pfitzer for details: (714) 896-4368.) The technical references are given in Section 8.0 while the list of publications, reports, and presentations resulting from this contract is given in Section 9.0.

2.0 DESCRIPTION OF THE PROPERTIES OF THE DAYSIDE CUSPS

2.1 Observations of Cusp Parameters

Work on the physics of the dayside cusps was initiated with the following information at hand. The cusp at its intersection with the ionosphere extends a few degrees in latitude and 8-12 hours in local time with its center on the noon magnetic meridian. In the outer regions of the magnetosphere the cusp has flared so that it extends several earth radii near local noon. The position of the cusp is determined by the axis of the earth's dipole magnetic field and the direction of the solar wind. Since the magnetic and rotation axes of the earth are inclined by about 11.7°, the location of the dayside cusp in geographic coordinates is continuously changing.

Particle precipitation through the cusps yield a height integrated energy flux of $\sim$.8 ergs $(cm^2 \text{ ster sec})^{-1}$ during quiet magnetic periods, Olson (1971). (This number was obtained from the analysis of the published pitch angle and particle spectra of Frank (1971) and Heikkila (1972).) During disturbed periods the energy flux can be much larger. The protons carry most of the energy. Their peak energy transfer to the atmosphere occurs at about 170 km while the peak electron energy transfer to the atmosphere is at about 200 km (Olson, 1971). The shape of the intersection of the dayside cusp with the atmosphere is observed to be (roughly) a semi-circular region centered on the magnetic pole and extending about 180° in longitude with the central longitude at magnetic noon (see Figure 2-1). In magnetic coordinates the shape of the cusp is almost constant during quiet magnetic conditions. (It exhibits some dependence on the angle between the solar wind direction and the dipole axis.) In geographic coordinates, however, the cusp position is constantly moving. Thus, the amount of time a given point will be within the cusp region and the extent to which it will be influenced by charged particle fluxes depends on its geographic location, both its latitude and longitude. The center of the cusp is at about 75° magnetic latitude during quiet times. The seasonal variation in the cusp location is quite small (in magnetic coordinates). The region of maximum exposure of the atmosphere and ionosphere to the cusp particles is at the dipole longitude (-69° West in geographic coordinates) and about 15° below the dipole axis for the northern hemisphere.

POSITION OF CENTER OF DAYSIDE CUSP AT ATMOSPHERIC HEIGHTS AS VIEWED FROM ABOVE GEOGRAPHIC NORTH POLE

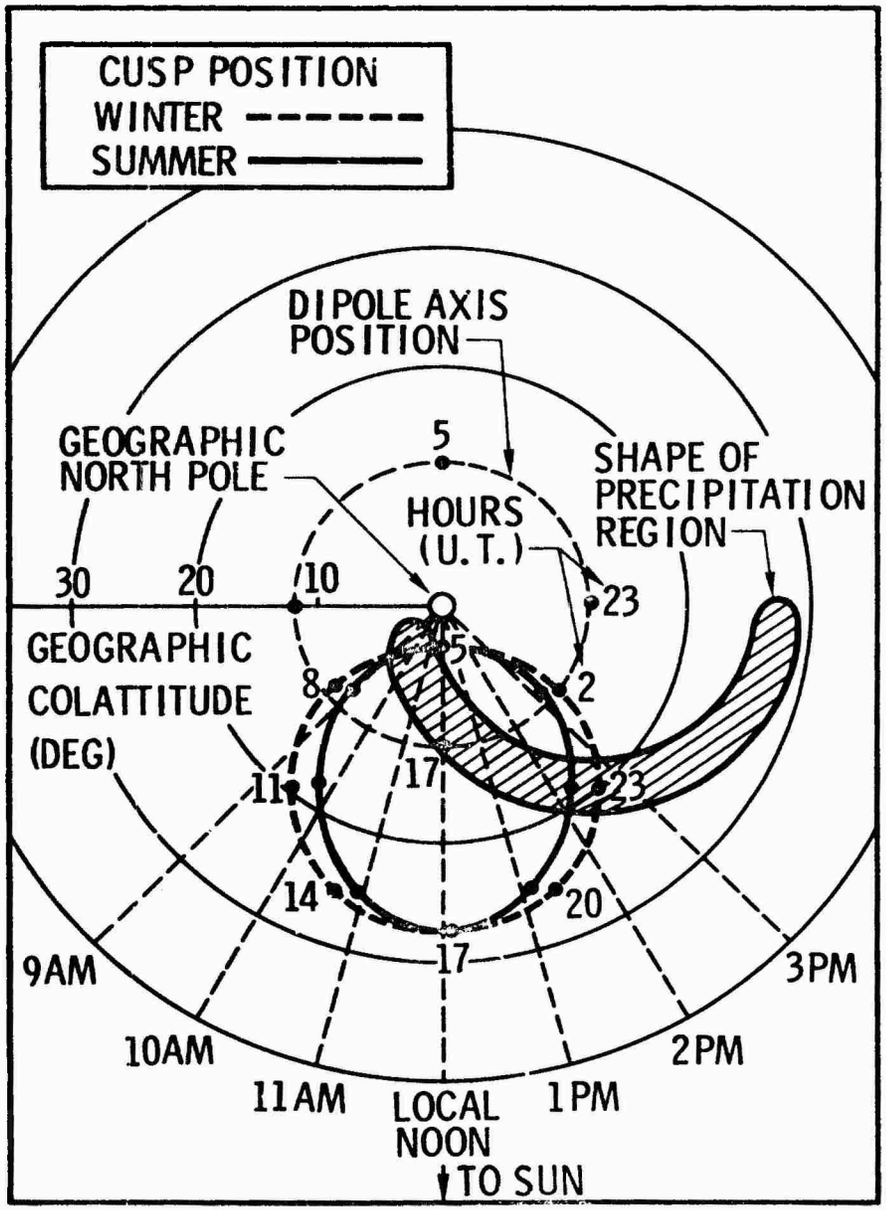

FIGURE 2-1

The geographical region that spends the most time under the cusp (and therefore receives the most energy) is near Hudson Bay. This is the location of the "fixed" atmospheric density bulge reported by Jacobs (1967). His work was based on satellite drag studies. Other better and more recent atmospheric density data also suggest heating and increased density in this region.

Since the energy input to the atmosphere via charged particles through the dayside cusps is under magnetic control it is possible to distinguish this energy source from the solar UV heating that occurs on the dayside of the earth. Near winter solstice the cusp deposits its energy on the nightside of the earth. In Figure 2-2 the zenith angle of the cusp is shown at different times of the year. A zenith angle of greater than 90° indicates that the center of the cusp (at its intersection with the atmosphere) is on the nightside of the earth. This geometric feature makes the direct testing of the extent and position of the dayside cusp energy source possible. This has been done by comparing the cusp location (given by this model) with airglow data obtained over the northern polar cap in winter (see Section 5.0).

The model discussed above permits comparison of data with cusp location and extent. In order to answer more detailed questions about the formation or maintenance of the cusp, a physical examination of the particles that move through the cusp was necessary.

2.2 The Physics of the Dayside Cusp

The presence of the cusped geometry in place of the neutral point geometry obtained from the older models had to be accounted for. For such details as the cusp geometry, the behavior of individual particles had to be considered. In particular, we found that whenever strong gradients in $\vec{B}_T$ exist just inside the magnetopause, particles can drift into the magnetosphere. $\vec{B}$ exhibits this geometry in the cusp region and in the vicinity of the equator along the tail of the magnetopause. Particle entry in the tail of the magnetopause by this mechanism is believed responsible for the cross tail currents (Olson, 1972) and much of the structure of the plasma sheet (Pfitzer and Olson, 1973). Thus, even if a model magnetosphere exhibits a closed field line geometry (all of the field lines confined within the magnetosphere), it is certain that the

DAILY AND SEASONAL VARIATION IN ZENITH ANGLE OF CENTER OF DAYSIDE CUSP AT ATMOSPHERIC HEIGHTS

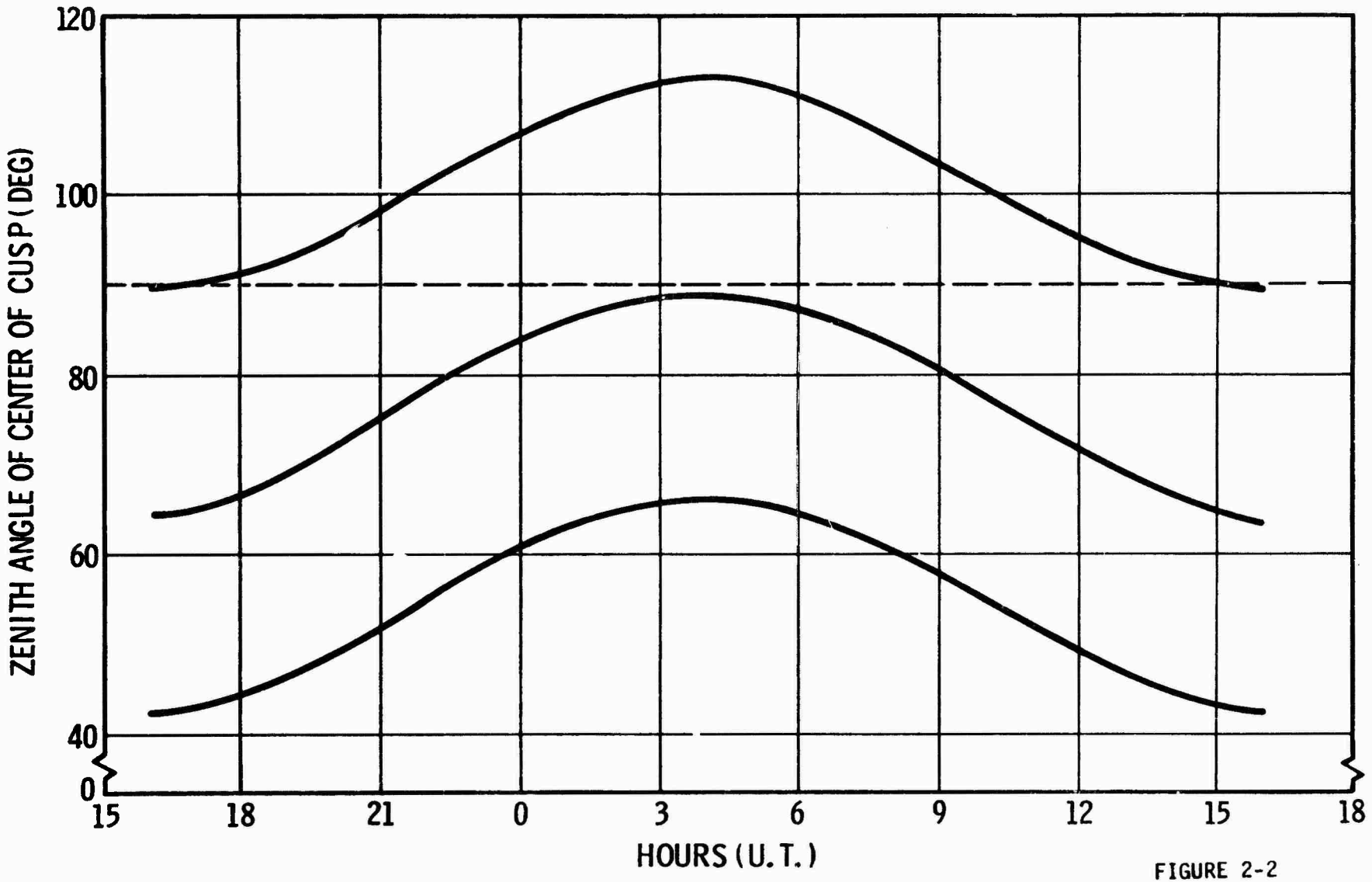

FIGURE 2-2

drift of individual particles will make the magnetosphere "open" to charged particles. That is, some of the shocked solar wind plasma (magnetosheath plasma) will penetrate the magnetosphere. This is especially true in the dayside cusp regions and the equator of the tail. We concluded that the magnetosphere cannot be adequately described in terms of pressure balance and these individual particle motions must be considered.

The magnetosheath particles initially penetrate the magnetosphere in a large region (around the neutral points in the old models). Once they enter the magnetosphere they obey the adiabatic invariants and move along field lines with most of them precipitating into the atmosphere or being mirrored back into the magnetosheath. Within the cusp the motions of the particles are diamagnetic, the particles circle the field lines such that the currents they produce tends to weaken the total field, $\vec{B}_T$. The currents of the individual particles tend to cancel each other except at the cusp boundary. The cusp currents, $\vec{J}_c$, then flow in loops only on the cusp boundary. (This cusp current system is diamagnetic, the particles that make up the current are "stationary", they move only around and up and down field lines - not around the cusp.) $\vec{J}_c$ produces a magnetic field that weakens $\vec{B}$ within the cusp. In terms of field components measured at the earth's surface (Z or V), the field from $\vec{J}_c$ is in the positive vertical direction. This suggests that the polar surface magnetic field from $\vec{J}_c$ should exhibit a daily variation in Z or V as the earth turns under the dayside cusp currents.

Near the magnetopause $\vec{J}_c$ is quite weak because many of the particles move close to the direction of the field lines. As the particles move down the field lines (toward the atmosphere) they increase their pitch angles (the angle between the particle velocity vector $\vec{V}$, and $\vec{B}$) until they "mirror" although many of them precipitate into the atmosphere. The increased average pitch angle at lower altitudes increases the magnitude of $\vec{J}$. The increased particle density also increases $\vec{J}$. However, $\vec{J}$ does not increase so rapidly as to cancel $\vec{B}$ within the cusp (like the magnetopause currents do when pressure balance formalism is used). Thus, although $\vec{B}$ is somewhat weakened (especially in the mid-altitude cusp) $\vec{B}$ is finite throughout the cusp.

The determination of $\vec{J}_c$ was guided by an empirical knowledge of n, $\vec{V}$, $\vec{V}$, A, and B which respectively are the particle number density, particle velocity components parallel and perpendicular to B, the cross sectional area of the cusp and the magnitude of the magnetic field.

In a region of the cusp when no mirroring occurs, conservation of total charge yields

$$n\ V\ A = \text{Constant} \tag{2-1}$$

while conservation of magnetic flux gives

$$AB = \text{Constant}. \tag{2-2}$$

It is assumed that A is perpendicular to B and that the edges of the cusp are parallel to B. Near the magnetopause the following values are observed for several of the variables listed above. The subscript m indicates a variable near the magnetopause end of the dayside cusp while the subscript g indicates the value of a variable at the atmospheric intersection with the cusp. From observations

$$n_m \cong 1\ cm^{-3},\ V_m = 400\ km\ sec^{-1} = V$$

(V is the total velocity - since all processes under consideration are conservative, V is constant)

$$A_m \cong 4.10^{18} cm^2,\ B_m \cong 10\gamma, \text{ while near the earth}$$

$$B_g \geq 10^4, \text{ and } A_g \geq .05R_E^2 \text{ (where } R_E \text{ is the radius of the earth).}$$

With the known values of several variables the constants in equations (1) and (2) can be evaluated near the magnetopause.

$$n_m V_m A_m \cong 1.6*10^{26}\ sec^{-1} \tag{2-3}$$

Also

$$B_m A_m \cong 4.1*10^{14}\ gauss\ cm^2 \tag{2-4}$$

Finally the first invariant constant is

$$k = V_\perp^2/B = 10^8 \text{ cm sec}^{-1} \text{ gauss}^{-1}. \tag{2-5}$$

With (1) and (2) and the known values of several variables it is possible to determine the strength of $\vec{J}_c$ as a function of altitude in the cusp. The number of particles that pass through a unit length, ℓ, along the cusp surface is given by:

$$n_\ell = \ell \, R \cdot 2\pi r \cdot n$$

where R is the particle gyroradius and r is the radius of the cusp. The average velocity of the particles is $V \frac{2}{\pi}$. Thus, the total flux of charges per second past ℓ is

$$J = N_\ell \cdot q \, \frac{V_\perp 2}{\pi} \, \frac{1}{2\pi r} \cdot \quad \text{Since } R = \frac{m V_\perp}{qB}$$

where m is the particle mass - and the (constant) first adiabatic invariant is defined by $\mu \equiv m V_\perp^2/2B$, the current per unit length $j_c = j/\ell$ becomes

$$j_c = \frac{4n\mu}{\pi} . \tag{2-6}$$

Since μ is constant j depends only on n. The change in n with altitude in the cusp can then be determined (1) provided the dependence of $V_\parallel$ on altitude is known. Since $V_\perp^2/B$ is constant (a form of the first adiabatic invariant) and V is constant, we find $V_\parallel^2 = V^2 - V_\perp^2 = V^2 - kB$ where $k \equiv V_\perp^2/B$, thus $V_\parallel = (V^2\text{-}kB)^{1/2}$ and from (1) $n(V^2\text{-}kB)^{1/2} A = 1.6 \times 10^{26}$. A varies as the inverse of B according to equation (2). However, it is realized that equation (2) provides only a guideline in a region where currents are flowing and that the product AB is not precisely constant. Combining these results yields

$$n \, \frac{V^2 - kB}{B}^{1/2} = 3.8 \times 10^{11}$$

or, when the constants are used

$$n = 3.10^{18.5} B/(1.6\text{-}3B)^{1/2} \tag{2-7}$$

when $B = .3$ $n \simeq 1.8 \times 10^{17.5}$
when $B = .0001$ $n \simeq 2 \times 10^{14.5}$

Thus n varies by almost 3 orders of magnitude in this simple analysis. Actually, the currents on the cusp boundary and the distribution of pitch angles at any given altitude within the cusp tend to diminish this range of densities. Although the solar wind has a directed velocity component, the particles do not all enter the cusp moving along field lines as has been assumed here. Further, if the particle distribution was isotropic, there would be no increase in n toward the base of the cusp. An intermediate case where the density increases by a factor of 10 or 15 from the top to the base of the cusp is not unreasonable. Similarly the strength of $\vec{J}_c$ should then increase by the same amount. The value of $\vec{B}$ near the currents (at a point close enough to $\vec{J}$ that the currents appear to be planar) is linearly proportional to $\vec{J}$. Thus, if B is 7γ near the magnetopause it will be about 100γ in the ionosphere. At points more distant than this $\vec{B}$ will be somewhat smaller. At the base of the cusp then B will have a component of about 100γ opposite to the dipole contribution. Thus, a ground based magnetometer should measure a daily variation on the order of 100γ at points that pass under the dayside cusp. Such behavior in the polar surface magnetic field has long been observed. The largest daily variations occur at the cusp latitude - about 75° magnetic latitude. Also, the daily variation has the proper phase. The vertical component (positive out from the earth) is largest near noon.

3.0 QUANTITATIVE MODEL OF THE TOTAL MAGNETOSPHERIC MAGNETIC FIELD

In order to use solar wind data to predict atmospheric and ionospheric behavior it is necessary to have a quantitative model of the total magnetospheric magnetic field, $\vec{B}_T$. Charged particles precipitating through the dayside cusps and solar cosmic rays are controlled by $\vec{B}_T$. The model of $\vec{B}_T$, therefore, should be capable of accepting as input descriptors, several solar wind parameters capable of being monitored by satellite borne sensors. Output from the model can then be used to predict the location and extent of the dayside cusp regions and the variation in those other field locations that control particle precipitation from the tail and middle magnetosphere.

Existing magnetic field models have proven inaccurate for many applications. A study of the observations of the magnetospheric magnetic field was therefore made in order to determine those regions of the magnetosphere where existing models were grossly in error. Two important conclusions were reached. First, on average, in the tail of the magnetosphere, field lines from the two lobe regions are connected to the equatorial region of the tail. In earlier models an infinitesimally thin current sheet flowed across the equatorial region of the tail and prohibited the return of field lines through the equator. Second, observations of the magnetic field in the inner magnetosphere (in the range of geocentric distances from 2 to 6 earth radii) indicate that even during quite magnetic times the magnetic field is depressed. This indicates that a distributed ring-like current flows through the inner magnetosphere at all times. The observed field then is better represented by a simple dipole main field with no contributions from the magnetosphere than by some of the older models which incorrectly represented this region as being one of augmented magnetic field. These two features are of major importance for many magnetospheric phenomena. The weak field region in the inner magnetosphere will cause field lines at a given equatorial location to intersect the earth at lower latitudes than given by previous models. Because of this, the poleward extent of the trapping region for adiabatic particles and the cutoff for solar cosmic ray particles should be at lower latitudes than those given by previous models. The return of field lines through equatorial regions of the tail dictates that charged particles

cannot gain access to the inner magnetosphere via that region of the tail as has been assumed many times in work on solar cosmic rays.

In order to use this information on the observed magnetospheric magnetic field to develop a magnetic field model it was first necessary to try to understand the currents responsible for the magnetic fields. Work on this aspect of the problem resulted in a model of the distributed magnetospheric current systems (Olson, 1974). The procedure developed for obtaining currents is quite different from previous ones. Instead of calculating self-consistent particle and field distributions it was demanded that the currents produce magnetic fields similar to those observed. This procedure was used because it most readily permits the development of quantitative models of the currents and the fields. The currents that produce the magnetic field features described above are themselves produced by the drift of electrons and ions in opposite directions in the non-uniform total magnetospheric field and by diamagnetic currents caused by gradients in the plasma density. In the inner magnetosphere the analysis of OGO-3 and 5 magnetometer data by Sugiura and his coworkers (Sugiura et al., 1971; Sugiura, 1972; Sugiura and Poros, 1973) provided important information on the currents produced by trapped particles. In particular, they developed contours of ΔB, the scalar difference between the magnitudes of the total field and the earth's main field. Their plots provide an indication of the scalar magnitude of the field produced by currents flowing in the magnetosphere. A noon midnight plot of ΔB for low K_p values is shown in Figure 3-1. The considerable structuring in the equatorial region suggests that currents must flow there.

The procedure for determining the currents was then as follows. The general form of the currents as suggested by the observations were used to select the positions of "wires" and the strength of the current flowing through each of them. Integration over these currents then yielded values of the field from the distributed currents that were added to the magnetopause magnetic field (which had been previously determined) and the earth's main field and compared with observations. Differences in the observed and computed values of the field were noted and changes made in the positions and strengths of the

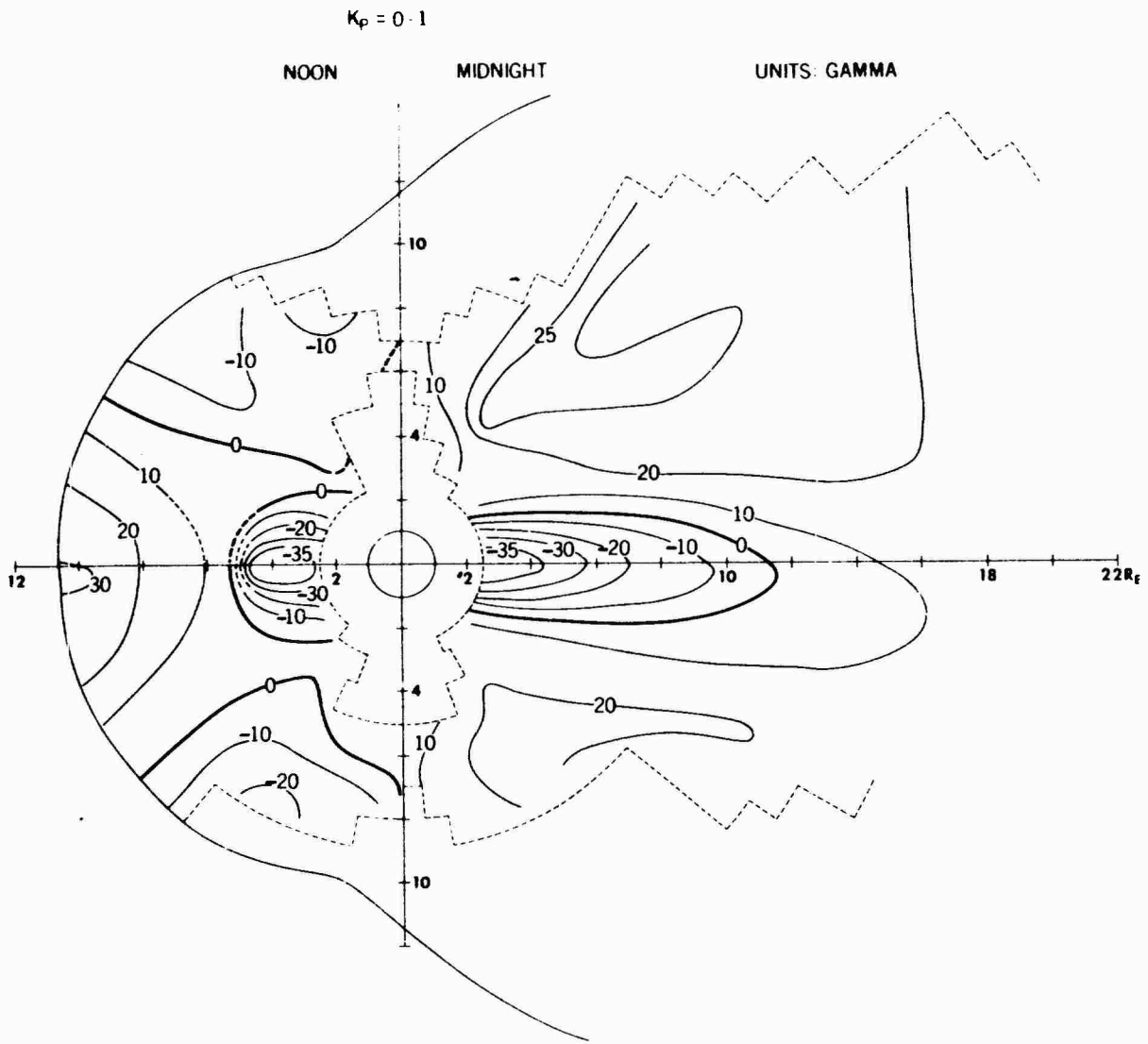
K_p = 0-1
NOON
MIDNIGHT
UNITS: GAMMA
10
4
4
10
-10
-10
0
10
0
-20
-35
-30
-10
20
30
12
2
2
-35
-30
-20
-10
0
10
18
22R_E
25
20
10
20
0
-10
-20
10

FIGURE 3-1

currents in order to decrease the differences. The currents in the inner magnetosphere and in the tail were considered separately. The ΔB contours obtained from the final model are shown in the noon-midnight meridian plane in Figure 3-2. It is seen that the model correctly reproduces the main observed field (older models produced grossly incorrect ΔB values).

In the tail regions it was demanded that the model fit both the observed decay of the lobe field with distance down the tail and the decay of the northward component through the equatorial region with distance down the tail. Several attempts were made at fitting these features with the standard "θ" current loop (e.g., Axford et al., 1965; Siscoe, 1966). With the cross tail currents constrained to a thin equatorial sheet it was not possible to model both the lobe and equatorial field simultaneously. A good fit was obtained only when the cross tail currents were allowed to flow through the plasma sheet and the return currents were not constrained to flow in planes of constant X_{SM}. In order to fit these features it was also necessary to have the loop current contribute locally to the northward component of the field at the equator. The observed flare of the radius of the tail was also input to the study. Although tests with varying flare rates indicated that the tail shape had only a small effect on the field, an analytic expression for the tail flare was developed from reported values (Siscoe, 1971) for use in the study.

Although the main purpose of this work on distributed currents was to provide an input for the development of a quantitative magnetic field model, it also shed light on several other magnetospheric features. (1) It became evident in the study that dynamic processes must be involved in the maintenance of the quiet magnetosphere. The magnetosheath plasma continuously supplies the distributed currents that flow across the tail but the quiet time ring current is formed by trapped particles whose drift shells do not intersect the magnetopause. Thus, the magnetosheath cannot directly be the source of the inner loop currents. They must instead be fed by the tail at irregular (substorm or storm) intervals and so can be formed and maintained only by temporal changes in the tail magnetic field or the presence of a cross tail

electric field, either of which can act to accelerate particles into orbits that close around the dayside magnetosphere. (2) A study of the distant tail field suggests that the currents flowing across the tail may be larger near the boundary of the plasma sheet but are not particularly strong in the neutral sheet region and that the neutral sheet should be thought of merely as that region where the total magnetic field is quite small. (3) These distributed currents also contribute to the magnetic field at the earth's surface, and therefore must be included in the study of the quiet daily variation in the surface field (S_q) and in the study of D_{st} which is a measure of the strength of the ring current. These magnetospheric currents make a significant contribution to S_q (the observed noon-midnight difference in the S_q field at mid-latitudes is about 20 to 40 gammas during quite times). At the equator, the noon-midnight difference in the north component of the field from these currents is just under 9 gammas and about 14 gammas when the effects of induced currents are included. However, it is still believed that they are not the predominant source of S_q as was suggested by Sarabhai and Nair (1969) and that ionospheric currents produce most of the observed S_q pattern although the magnetospheric currents must contribute significantly to the daily variability in S_q. (4) Magnetosheath plasma flows across the tail of the magnetosphere and contributes simultaneously to the plasma sheet and the distributed currents in the tail. This penetration of magnetosheath plasma suggests that the magnetosphere is "open" to low energy particles over several regions of the magnetopause. This work suggested that both high and low particles can enter the magnetosphere even if it is magnetically closed. Thus, although details of merging geomagnetic and interplanetary fields have not been studied quantitatively, it is quite certain that the magnetosphere is always open to the entry of charged particles and that in any self-consistent quantitative model of magnetospheric particles and fields, the fields will not be completely confined.

The total magnetospheric magnetic field can be found by integrating over these distributed currents and adding the field value to the field produced by the magnetopause currents and the earth's main field. However, this is a very time consuming process. For the model to be useful it must be capable of returning the total magnetospheric magnetic field at any position in the

34843

ΔB CONTOURS OBTAINED FROM DISTRIBUTED CURRENT MODEL, ΔB=B (MEASURED) -B (DIPOLE)

UNITS: GAMMA

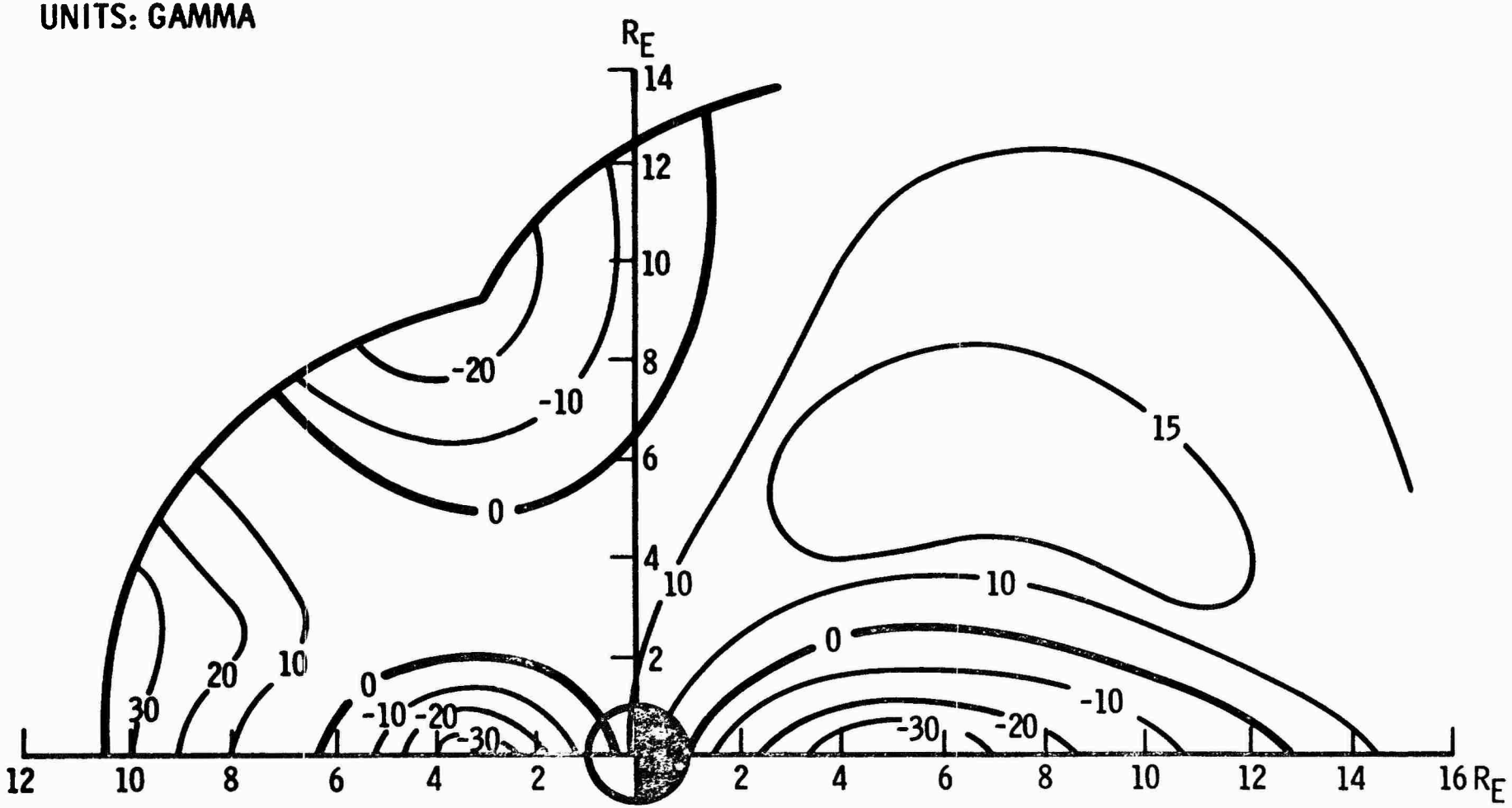

FIGURE 3-2

magnetosphere with a minimal expenditure of computer time. Therefore, the values of the magnetic field were found at many points by direct integration over the distributed and magnetopause currents. These values of the field were then input to a least squares best fit computer program to determine coefficients of the polynominal series to be used in the analytic field representation. Previous representations of the magnetopause magnetic field have been given in the terms of the scalar potential. Since the field from the distributed currents must be fit in the region of the source currents, a scalar potential can no longer be used since $\nabla \times \vec{B}$ must be permitted to be non-zero. Another constraint on the form of the series representation is dictated by the rather sharp structuring that the field from the distributed currents exhibits in the inner magnetosphere. Thus, the series must simultaneously fit a very structured region near the earth and the weak field region in the distant tail. A standard one-dimensional orthonormal least squares fitting program was generalized for use to find coefficients in n variables (K. A. Pfitzer, unpublished reference, 1973). In order to fit both the structure of the inner magnetosphere and the tail field topology, it was necessary to include terms of up to sixth order in a power series plus similar terms multiplied by an exponential. A final requirement for the model is that the field must vary smoothly between the points where it was computed for input to the fitting program. Calculations of both the distributed magnetic field and the magnetopause magnetic field show that the model fields do vary smoothly over the region where they are defined. This finding is particularly important for the distributed magnetic field since "wires" were used initially to represent source currents (Olson, 1974). The form of the series representation for the distributed magnetic field and the coefficients have been published in Olson and Pfitzer (1974). A listing of the computer deck is included in Appendix A.

Field lines at various latitudes are shown for different local times in Figure 3-3 using the analytic version of the model. Note that the field lines from 76° magnetic latitude cross the equator at midnight farther from the earth than the 82° lines shown by Mead (1964). It is this feature, the extension of the near earth field lines produced by the inclusion of the distributed magnetic field, that makes this model capable of reproducing

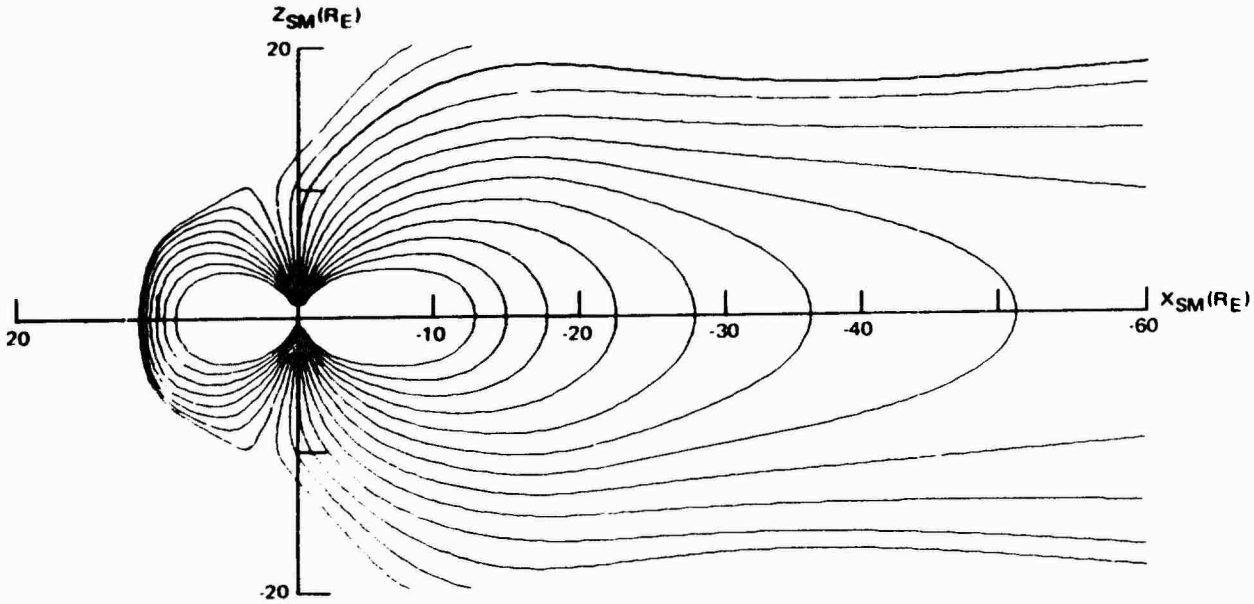

FIGURE 3-3

many particle and field observations that previously were not properly modeled. Generally, the field line geometry in the tail remains quite dipolar. There are no lines that run parallel to the equator for large distances. It is emphasized that this model magnetic fie'd is intended to represent only the quiet (and most dipolar) state of the magnetosphere. The accuracy of the model has been tested by comparing model calculations with particle and field observations. Optical tracking data (Adamson et al., 1973) from the NASA-MPE Barium Cloud Experiment has shown that the field lines in the inner magnetosphere are more elongated than the lines calculated from models consisting of main field and earlier external field representations (Barrish and Roederer, 1973). A computer program that combines any series expansion of the main field with various representations of the magnetospheric field (K. A. Pfitzer, unpublished manuscript, 1973) used the GSFC 9/65 main field expansion and the present model to generate field lines and compare them with the optical track of the barium clouds (see Figure 3-4). The model field fits the observations quite accurately because it includes the depressed inner magnetosphere field feature produced by the quiet time ring current. The earth intercept of field lines from geosnychronous orbit have been determined for various local times (see Figure 3-5). The foot of the field line lies between 65 and 66° magnetic latitude depending on the time of day. This is almost 3° lower than the values given by previous boundary models (Mead, 1964; Olson, 1970). The model was used to compute high and low energy charged particle behavior in the magnetosphere. The high latitude earth intercept of the trapping boundary calculated from the model agrees well with the observed boundary which is four to five degrees lower than that calculated from previous models (Pfitzer, 1972). The trapping boundary computed with the present model is in good agreement with observations at all latitudes (see Figure 3-6). The high latitude cutoff for cosmic ray particles calculated from previous models have been in error with observation by 5 to 7°. With the present models the calculated cutoffs are essentially in agreement with the observed values (Masley et al., 1973). It is the depressed field region from 3 to 6 radii geocentric distance produced by the distributed currents that causes the field lines at a given latitude at the earth's surface to cross the equator at larger geocentric distances than those calculated from previous models. In turn, it is this field geometry that allows charged particles to penetrate to

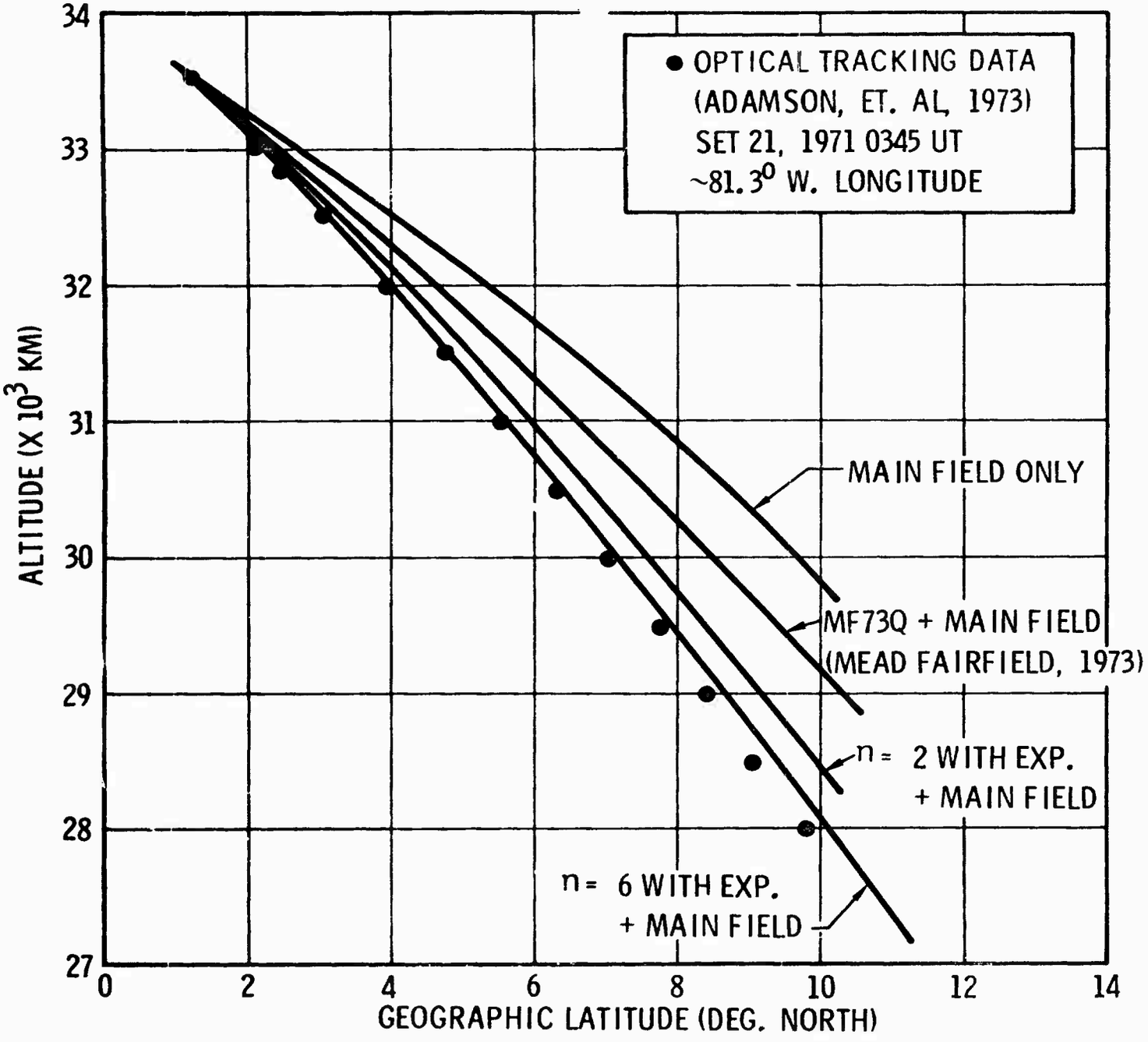
● OPTICAL TRACKING DATA
(ADAMSON, ET. AL, 1973)
SET 21, 1971 0345 UT
~81.3° W. LONGITUDE
MAIN FIELD ONLY
MF73Q + MAIN FIELD
(MEAD FAIRFIELD, 1973)
n = 2 WITH EXP.
+ MAIN FIELD
n = 6 WITH EXP.
+ MAIN FIELD
ALTITUDE (X 10³ KM)
GEOGRAPHIC LATITUDE (DEG. NORTH)
34
33
32
31
30
29
28
27
0
2
4
6
8
10
12
14

FIGURE 3-4

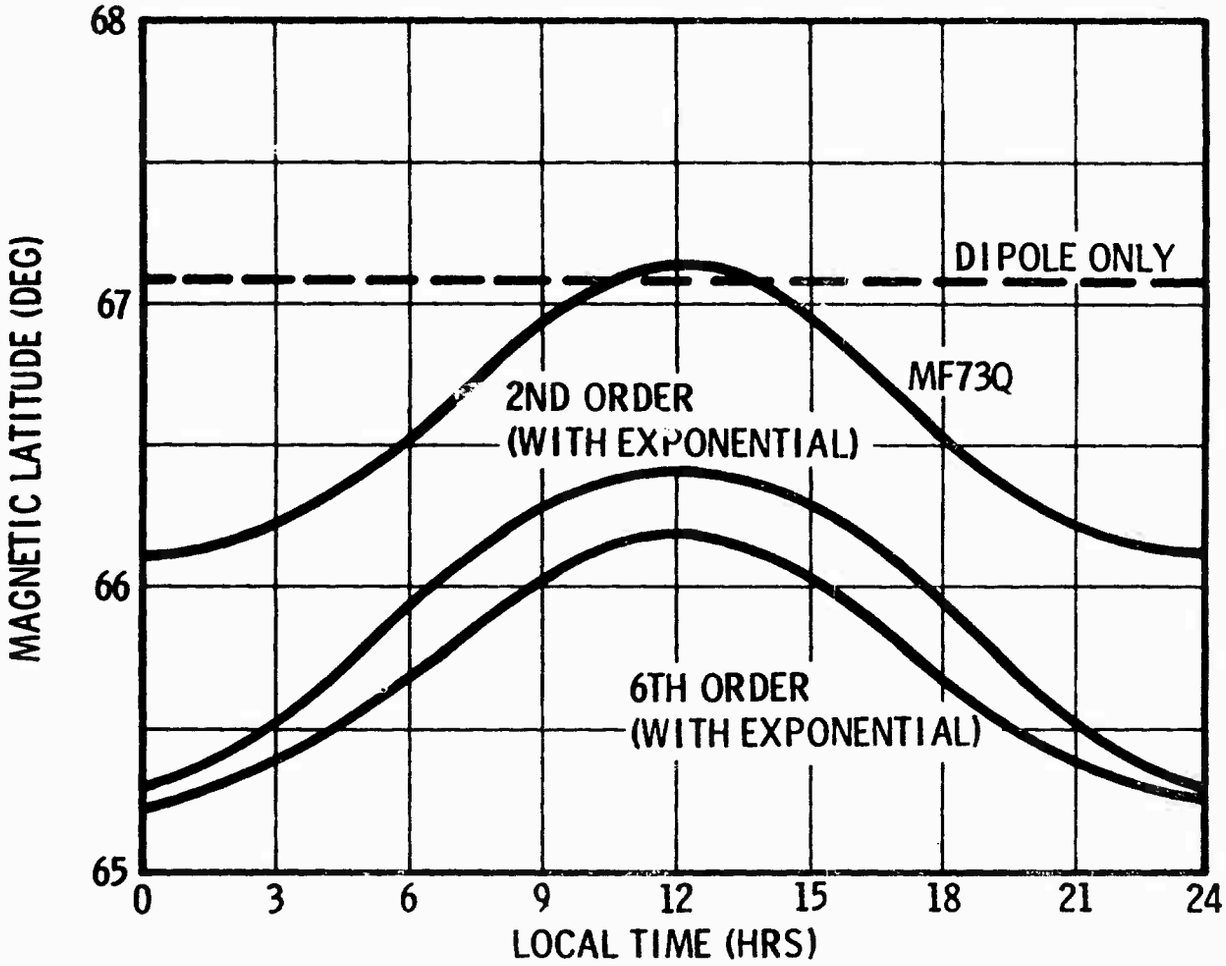
68
67
66
65
MAGNETIC LATITUDE (DEG)
DIPOLE ONLY
MF73Q
2ND ORDER
(WITH EXPONENTIAL)
6TH ORDER
(WITH EXPONENTIAL)
0
3
6
9
12
15
18
21
24
LOCAL TIME (HRS)

FIGURE 3-5

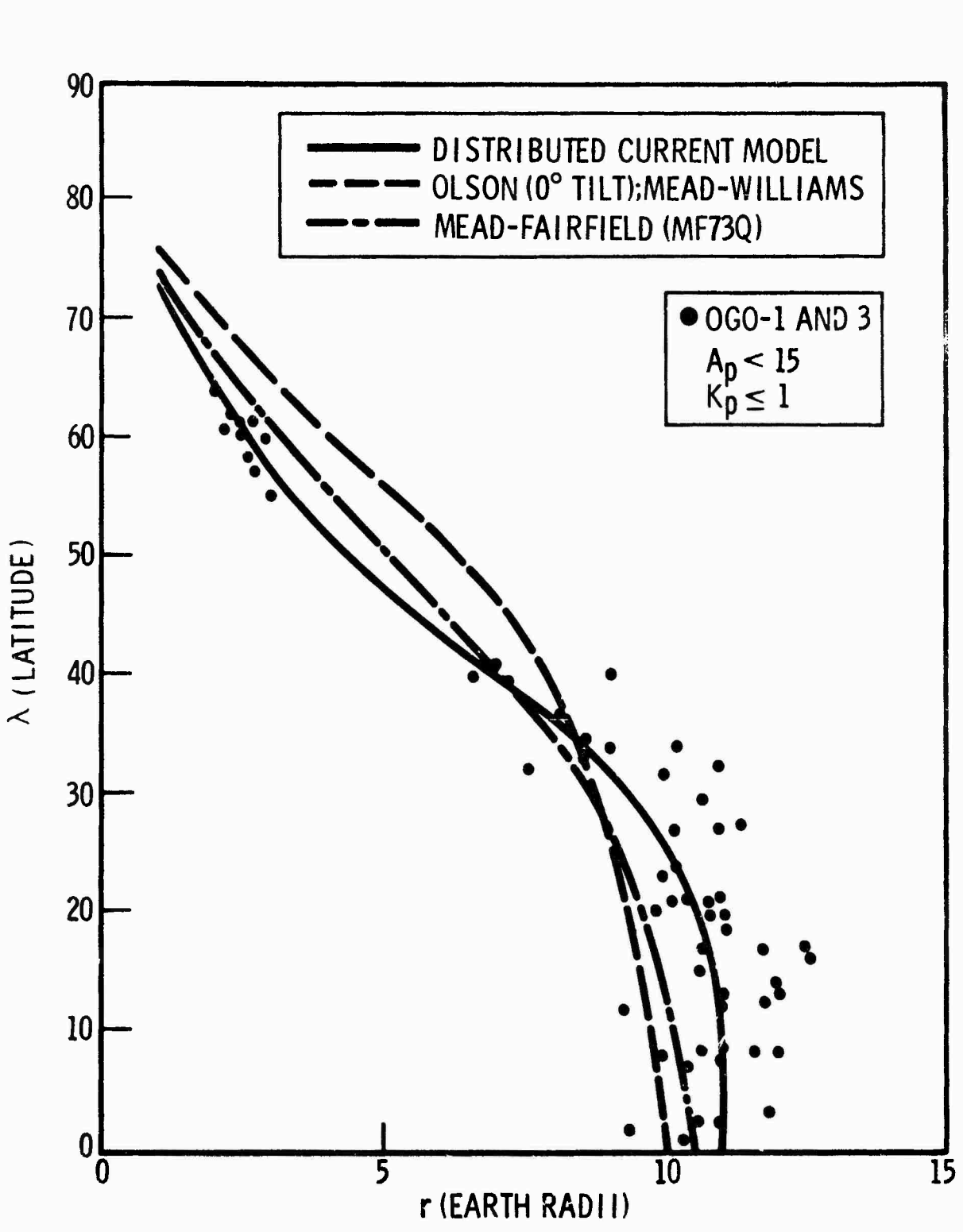
DISTRIBUTED CURRENT MODEL
OLSON (0° TILT);MEAD-WILLIAMS
MEAD-FAIRFIELD (MF73Q)
OGO-1 AND 3
$A_p < 15$
$K_p \leq 1$
λ (LATITUDE)
r (EARTH RADII)
90
80
70
60
50
40
30
20
10
0
0
5
10
15

FIGURE 3-6

lower latitudes than is possible with models that do not include the effects of the distributed currents that flow through the inner magnetosphere.

This total magnetic field model has been restricted in two ways. First, it represents only the symmetric magnetosphere. This geometry occurs only when the solar wind is incident perpendicular to the earth's magnetic dipole axis. The second "limitation" of the model is that it represents quiet magnetic conditions. Extensions and improvements to this model are discussed in Section 6.0. (Work on the development of this field model was supported jointly by this contract, the Office of Naval Research (ONR), and the MDAC Independent Research and Development Program.)

4.0 A MODEL OF THE NEUTRAL ATMOSPHERE

Recent satellite experiments and previous analyses of satellite drag data have shown that the high latitude neutral atmosphere is quite structured. Both the incoming cusp particle fluxes and their influence on the neutral atmosphere have been measured. To understand and ultimately predict the effects of these environmental features on space hardware systems, it is necessary to develop a quantitative model of the density of the upper atmosphere that includes the energy input from the dayside cusp particles. Such a model was developed under this contract and is described in this section. It includes both the solar ultraviolet and charged particle energy sources. The model is semi-empirical--it is based on available satellite data and our present understanding of both the UV and corpuscular energy sources. It offers a global description of the atmosphere above 120 km. The model takes into account the dependence of atmospheric density on the value of the solar flux constant. The UV and corpuscular effects are computed in separate coordinate systems and their contributions added. It is believed that the work on the atmospheric density described here represents significant progress in environmental modeling. It is the first time that corpuscular energy inputs have been considered quantitatively in a neutral density model. It is also believed that this is the first quantitative, analytic, global model of the upper atmospheric density. This model should be useful in several theoretical studies and in systems applications.

Ever since an accelerometer was first flown on a polar satellite (Bruce, 1968), it has been apparent that there are at least two density bulges in the lower thermosphere during geomagnetically quiet times. The low-latitude bulge is usually attributed to heating by solar UV radiation (although other energy sources may contribute importantly), but the high-latitude bulge is almost certainly caused by energy carried by the plasma which makes up the solar wind.

There are several charged particle sources that heat the upper atmosphere, but only those particles that precipitate through the dayside cusps constitute a

steady source with corresponding "permanent" atmospheric density features. (Charged particles that precipitate into the upper atmosphere during substorms and magnetic storms produce large and sudden changes in density but their presence is irregular.) The dayside cusp particles consist of magnetosheath protons and electrons. The protons can penetrate to about 110 km and the electrons to just below 100 km (Olson, 1971; Olson, 1972). The protons carry the bulk of the energy that is transferred to the neutral atmosphere. Their peak energy loss per unit change in altitude is at 169 km. The particle energy transferred to the atmosphere eventually produces heating which causes neutral particles at a given altitude to rise and increase the density at heights above the heating source region. Thus, it is expected that although atmospheric density should be influenced by the particles to altitudes as low as 100 km the largest effects should occur near and above 169 km.

Two coordinate systems are used in the model. The solar UV source is best described in geographic coordinates. Thus, inputs to the computer subroutine must include the universal time and the time of year. Local time is also entered as a function of the coordinates of the point where the atmospheric density is to be determined. The dayside cusp particles are constrained to precipitate into the atmosphere along magnetic field lines. The cusp intersection with the atmosphere is nominally 15 degrees below the magnetic dipole axis with its longitude center on the magnetic noon meridian plane as defined by the dipole axis and the sun-earth line). The extent of this intersection in longitude is about 12 hours. The extent of the cusp in latitude is several degrees (3-5). The region of the atmosphere actually heated by these particles is of course much larger because the impact energy is spread out by winds, thermal conduction, and possibly by gravity waves. In the development of the present model, the input energy sources have been considered quantitatively. The determination of the extents of their heating influence, however, has not considered dissipation mechanisms such as winds and wave phenomena. Rather, the extents of the heating regions have been determined from satellite measurements (both direct and indirect) of the atmospheric density. The corpuscular contribution is then found in magnetic coordinates and combined with the UV contribution. The form of the equations used in the model is now discussed.

4.1 Model Description

In the Interim Reports to AFOSR, mathematical descriptions of a neutral density model were developed. Those reports concerned themselves with the description of the functions necessary to describe the neutral density model and the development of an understanding of the high latitude corpuscular energy source. Here, a fast FORTRAN computer deck which can be used to describe the atmosphere from 0-450 km is described. In several cases, shorter expansions or simpler functions than discussed in the Interim Reports were used whenever such usage did not compromise the accuracy of the model within current experimental error. We believe that during quiet times in the range 120-450 km (the principle altitude range covered by this study) the model has an accuracy of about 10 percent. From 0-120 km a simple power series expansion extends the 120-450 km model to the ground by fitting it to the CIRA 72 mean reference atmosphere (COSPAR, 1972). The average deviation from CIRA 72 between 0-120 km is less than one percent with a 7th order fit.

The FORTRAN deck has as inputs position and time as well as parameters describing solar activity. The input parameter for the UV heating is the 10.7 cm solar flux and the input parameter for the particle heating is proportional to the particle flux and the location and size of the cusps.

The following paragraphs define the equations utilized in the development of the FORTRAN code. The entire functional representation is contained in this report, so that the reader can develop his own FORTRAN code if so desired. Appendix B contains the MDAC FORTRAN code for the density model. It has been carefully optimized to minimize the calls to elementary functions (sines, cosines, square roots, etc.) and to minimize the number of multiplies. A test program and a sample computer output are also listed to assist the reader in usage of the program.

4.1.1 Functional Form for the Total Density

The total density is expressed as the sum of two terms: the first term, ρ_μ, describes the combined effects of ultraviolet heating and effects other than

those due to the corpuscular energy sources. The second term, $\Delta\rho_c$, gives the contribution due to the density associated with corpuscular heating caused by particles entering the atmosphere through the magnetospheric cusps. Thus we may write the density as

$$\rho = \rho(z, \lambda, \phi, T, D, F, P) = \rho_\mu + \Delta\rho_c \qquad (4\text{-}1)$$

where

ρ is the total neutral density in gm/cm^3
ρ_μ is the density due to non-corpuscular energy sources
$\Delta\rho_c$ is the density due to corpuscular energy sources
z is the altitude in km
λ is the geographic latitude in degrees (+ is North, - is South)
ϕ is the geographic longitude in degrees east (0-360°)
T is the universal time in hours
D is the day of year
F is the decimetric solar flux
P represents the particle heating parameters

The function ρ_μ is expressed as a product of four terms (See Eq. (2) Interim Report Sept 75)

$$\rho_\mu = \rho_0(z, F)\, B(z, \lambda, t)\, J(z, \lambda, D)\, Q(z, D) \qquad (4\text{-}2)$$

where t is the local time in hours and is given by $t = T + \phi/15$,
ρ_0 is the mean equatorial density as a function of height,
B gives the diurnal variation in the density,
J gives the seasonal and latitudinal dependence,
Q is the semi-annual variation.

Each of the above terms is now explained in some detail.

4.1.2 Altitude Dependence

For average conditions the mean equatorial neutral density, $\rho_0(z, F)$, can be expressed as

$$\rho_o = \rho(120)\ \exp\left[\frac{-(z - 120)}{1.737\sqrt{z - 103}}\right] \qquad (4\text{-}3)$$

for 120 km < z < 450 km,

where $\rho(120)$, the mean equatorial density at 120 km, is 2.7×10^{-11} gm/cm^3. The square root relationship in the denominator of the exponent is used because of experimental evidence that scale heights in the thermosphere vary approximately as the square root of the altitude (Moe, et al., 1968).

At the lowest altitudes, ρ_o is based on Moe (1973). At the higher altitudes, parameters are chosen to make this model in approximate agreement with the forthcoming U.S. Standard Atmosphere.

Equation 4-3 can be modified to take into account the dependence of the equatorial density on solar activity by replacing the constant 1.737 with the function A, where

$$A = 0.99 + .518\left(\frac{F + \bar{F}}{110}\right)^{1/2} \qquad (4\text{-}4)$$

F is the 10 cm solar flux constant measured at Ottowa, Canada and $\bar{F}$ is its average over the preceding three months. They are given in units of 10^{-22} watts/m^2/Hz. The function A has been developed to represent the solar cycle variations deduced from satellite measurements by King-Hele and Quinn (1966), and Moe (1969).

4.1.3 Diurnal Variation

The function B (z, λ, t) which represent the diurnal variation is given by the expression B (z, λ, t) = $[1 + (f(t) - 1) \cos \lambda]^{\mu(z)}$, where f(t) is the diurnal variation in density at the equator. The function f(t) is represented as a Fourier series such that given $\mu(z) = 1$ at 450 km, the density at the equator accurately models the density variation observed by Hedin et al. (1974). Development of the series is described in Appendix D. However, use of the full six term Fourier series expansion is not justified at this time because of the large scatter in the data of Hedin et al. In

the FORTRAN deck we limit the expansion to the first three terms. This modifies the fit by only two percent and is well within the ten percent accuracy of Hedin et al.'s curve. Thus

$$f(t) = .994 + .545 \cos[\tfrac{\pi}{12}(- 14.745)] + .102 \cos [\tfrac{\pi}{6}(t - 1.838)] \quad (4\text{-}5)$$

The function $\mu(z)$ which gives the height dependence of the diurnal variation must satisfy the following conditions:

1. $\mu(450) \approx 1.$ i.e., f(t) must reproduce Hedin et al.'s values at 450 km

2. $\mu(186) \approx .4$ in order to match the LOGACS data near noon

3. $\mu(230) \approx .57$ in order to fit the data of Ching and Carter (1974) near local midnight

4. $\mu(120) = 0.$ i.e., the diurnal variation must approach zero at 120 km, the lower limit of the model where it is to interface with CIRA 72.

The expression $\mu(z) = 1.1 \times (1 - \exp(-(z-120)/150))$ satisfies the above four conditions.

4.1.4 Latitudinal and Seasonal Dependence

The 1974 and 1975 Interim Reports differ substantially in their treatment of the term $J(z, \lambda, D)$ which describes the latitudinal and seasonal dependence. The 1975 Interim Report introduces a relatively complex function which depends on 18 empirically determined coefficients in order to improve the fit of the density model with the mid-latitude LOGACS data. Although this function significantly improved the fit to the LOGACS data, it introduced a rather large seasonal latitude dependence. For example, at solstice a ratio in the North to South polar densities of 10 to 1 is introduced at 186 km. At 450 km the ratio exceeds 100 to 1. Hedin et al. (1974) observe only a 2 to 1 latitudinal variation at 450 km. Therefore, even though the more complex

function does improve the fit to LOGACS during northern summer day, it cannot be used at this time in a FORTRAN deck representing a global density model. Therefore, the much simpler expression defined in the 1974 Interim Report is used in the model construction. We thus write

$$J(z, \lambda, D) = [1 - \alpha(1 - \cos(\lambda - \lambda_s))]^{m\mu(z)} \qquad (4\text{-}6)$$

λ_s is the latitude of the sun's subsolar point and is given by $\lambda_s = 23.5 \sin \frac{2\pi(D - 81)}{365}$. A value of $\alpha = .25$ is consistent with observations indicating only a small latitude dependence due to UV heating. A value of 2.5 for m is also consistent with the requirement that $m\mu(186) = 1$ at 186 km to best fit the LOGACS data and $m\mu(450) = 2.5$ in order to best fit the latitude dependence observed by Hedin et al. (1974) at 450 km. Since mu(z) approaches zero as z approaches 120 km, the function J approaches unity as z approaches 120 km, and thus the latitude and seasonal variation goes to zero as z approaches 120 km.

4.1.5 The Semi-annual Variation

Derivation of the semi-annual variation represented as the term Q in Eq (4-2) is explained in considerable detail in Appendix E. The function Q is expressed as

$$Q(z, D) = 1 + [R(z) - 1]\, G(D) \qquad (4\text{-}7)$$

where

$$R(z) = .98 + .27 \times 10^{-2} z - .85 \times 10^{-6} z^2 - .59 \times 10^{-9} z^3 \qquad (4\text{-}8)$$

and

$$G(D) = .143 \cos(\tfrac{2\pi}{365}(D - 4)) + .239 \cos(\tfrac{4\pi}{365}(D - 109)) + .044 \cos(\tfrac{6\pi}{365}(D - 66)) \qquad (4\text{-}9)$$

The semi-annual variation does not approach zero as z approaches 120 km. Observations indicate that a significant diurnal variation is observed only to as low as 90 km. Therefore, Q is allowed to vary below 120 km such that no diurnal variation exists below 75 km and the total density agrees with CIRA 72. This damping is explained in Section 4.1.7 which described the model from 0-120 km.

4.1.6 Corpuscular Heating

$\Delta\rho_c$, the density increase due to the corpuscular heating, is given in the 1974 Interim Report as

$$\Delta\rho_c = \rho_\mu \cdot C(z, \lambda_m, t_m, P) \tag{4-10}$$

and in the 1975 Interim Report as

$$\Delta\rho_c = \rho_o\, C(z, \lambda_m, t_m, P) \tag{4-11}$$

where C is the cusp heating function. We have chosen to use equation 4-10 instead of 4-11 because studies by Hedin et al., indicate a definite high latitude peak in the summer hemisphere, but none or a smaller one in the winter hemisphere. Equation 4-10 introduces a summer-winter dependence into the cusp heating term whereas equation 4-11 has north south particle heating symmetry for all seasons. The term C is given a scale height factor of about 50 km since we wish to have zero heating at 120 km and approach maximum heating near 170 km (Olson; 1971, 1972). Thus

$$C(z, \lambda_m, t_m, P) = \exp(-(z - 120)/50)C(\lambda_m, t_m, P) \tag{4-12}$$

The function $C(\lambda_m, t_m, P)$ is dependent on the magnetic latitude, λ_m, the magnetic local time, t_m, and the cusp heating parameters represented in the above equation by P. The parameters represented by P are the particle precipatation intensity, I, the half width of heating region in magnetic latitude, ε_o, the half-width of the heating region in magnetic local time, Σ, and the

magnetic latitude of the center of the northern cusp heating region, λ_{mc}. The geomagnetic coordinate system is defined such that the North geomagnetic pole is located at 69° W and 78.5° N geographic. The zero in magnetic longitude is along 69° W geographic longitude.

Magnetic local time, t_m, is defined such that zero is in the anti-solar direction. The magnetic local time, t_m, is measured in degrees. The magnetic local time of the observation, t_{mo}, is given by

$$t_{mo} = 15 \cdot UT + \phi_m - 69 \tag{4-13}$$

where ϕ_m is the magnetic longitude. The local time of the center of the cusp, t_{mc}, is always located at the subsolar longitude (magnetic local noon) and thus, $t_{mc} = 180°$. The difference in magnetic local time between the observation point and the cusp center, Δt_m, is given by

$$\begin{aligned} \Delta t_m &= 15\ UT + \phi_m - 69 - 180 \\ &= 15\ UT + \phi_m - 249 \end{aligned} \tag{4-14}$$

Δt_m is restricted to the range -180° to +180°. Therefore

if $\Delta t_m > 180$ $\quad\quad$ $\Delta t_m \rightarrow \Delta t_m - 360$

if $\Delta t_m < 180$ $\quad\quad$ $\Delta t_m \rightarrow \Delta t_m + 360$

The magnetic latitude, λ_m, is restricted to ± 90° (+ is North - is South). The difference in magnetic latitude, $\Delta\lambda_m$, between the observation point, λ_{mo}, and the center of the cusp, λ_{mc}, is given by the equation

$$\Delta\lambda_m = |\lambda_{mo}| - |\lambda_{mc}| \tag{4-15}$$

Given the above definitions we can now express the function C by the following expressions:

$$C(\lambda_m, t_m, P) = 0 \qquad \text{if } |\Delta\lambda_m| \geq \varepsilon_o$$

$$C(\lambda_m, t_m, P) = I \times L \times \left(1 + \cos\frac{\pi\Delta\varepsilon}{\varepsilon_o}\right) \qquad \text{if } |\Delta\lambda_m| < \varepsilon_o \tag{4-16}$$

where

$$\left.\begin{aligned} L &= 2 - \frac{|\Delta t_m|}{\Sigma} \\ \Delta\varepsilon &= \Delta\lambda \end{aligned}\right\} \text{if } \Delta t_m \leq \Sigma$$

$$\left.\begin{aligned} L &= 1 \\ \Delta\varepsilon &= \cos^{-1}[\sin\lambda_{mo}\sin\lambda_{mc} + \cos\lambda_{mo}\cos\lambda_{mc}\cos(|\Delta\lambda_m| - \Sigma)] \end{aligned}\right\} \text{if } \Delta t_m > \Sigma \tag{4-17}$$

The above defined expression for C defines a density bulge that wraps itself around the geomagnetic pole and is most intense at local magnetic noon.

4.1.7 Density Below 120 km

In order to make the FORTRAN deck a more useful tool, a fit to the CIRA 72 mean reference atmosphere was added to the model. The junction between the 0-120 km model and the 120-450 km model is everywhere continuous and the slopes are closely matched, but not mathematically continuous. Below 120 km the density is given by

$$\rho = \left(1.2252 \times 10^{-3} \exp\left(\sum_{i=1}^{7} a_i z^i\right)\right) Q' \tag{4-18}$$

where

$$\begin{aligned} Q' &= Q \qquad \text{when } z \geq 90 \text{ km} \\ Q' &= 1 + (Q - 1)\exp(-(z-90)^2/200) \qquad \text{when } z < 90 \text{ km} \end{aligned} \tag{4-19}$$

Q is the diurnal variation defined by equation 4-7. The coefficients for the expansion in equation 4-18 are

$$a_1 = -.8015593 \times 10^{-1}$$
$$a_2 = -.3366924 \times 10^{-2}$$
$$a_3 = +.1821500 \times 10^{-4}$$
$$a_4 = +.1739634 \times 10^{-5}$$
$$a_5 = -.3658010 \times 10^{-7}$$
$$a_6 = +.2688846 \times 10^{-9}$$
$$a_7 = -.6820457 \times 10^{-12}$$

The seventh order expansion produces a fit to CIRA 72 below 75 km which has an RMS error of less than one percent and a maximum error of 2.5 percent. Additional terms can easily be added to improve the fit.

4.2 Model Results and Comparisons with Observations

This model of the density of the neutral upper atmosphere is functionally very simple and computationally very fast. Yet, it considers most of the known variations in the atmosphere. It treats latitude, longitude, diurnal, seasonal, semi-annual, altitude, solar cycle and particle precipitation variations and can thus be used to predict the density of the atmosphere as a function of time, position, solar and magnetospheric parameters. Since it includes the heating effect of particles precipitating into the high latitude regions, it is especially valuable in the study and prediction of the density of the polar atmosphere. Furthermore, since this high latitude effect is parameterized, it can be used to predict increases in the high latitude density when the solar wind particle flux increases and the cusp location is observed to change. The model is analytic and thus differentiable. Only three regions exist where the derivative of the density is discontinuous. These are at: 120 km where the 120-450 km model is matched to CIRA 72; over the geographic poles; and over the geomagnetic poles. In all three cases, however, the density is continuous and the slopes, although not mathematically continuous, are closely matched.

The three dimensional mercator projections in Figures 4-1, 4-2 and 4-3 give an overview of the model's features. Figure 4-1 shows the density at 400 km during summer solstice at a universal time of 1600 hours. The UV density peak

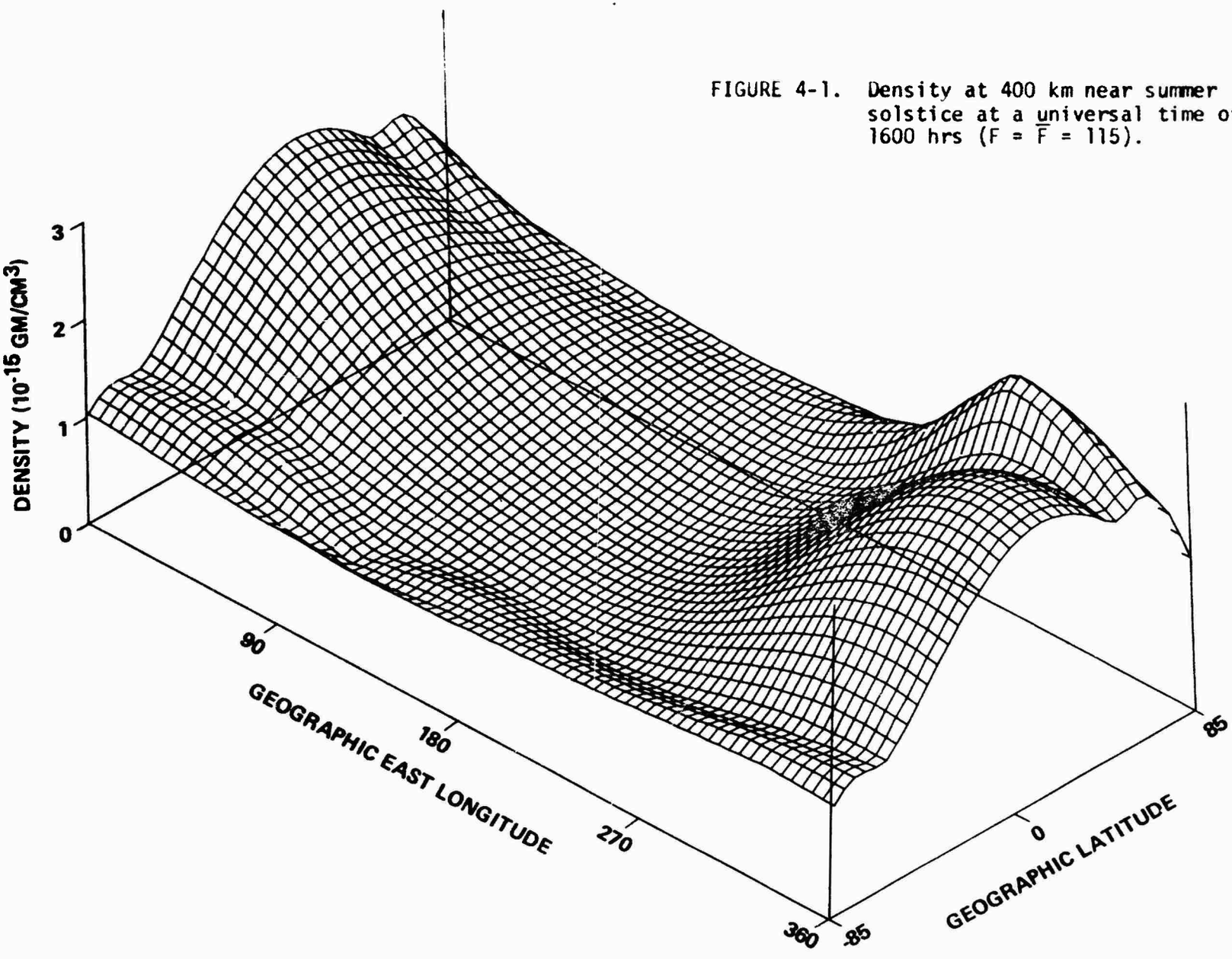

FIGURE 4-1. Density at 400 km near summer solstice at a universal time of 1600 hrs ($F = \overline{F} = 115$).

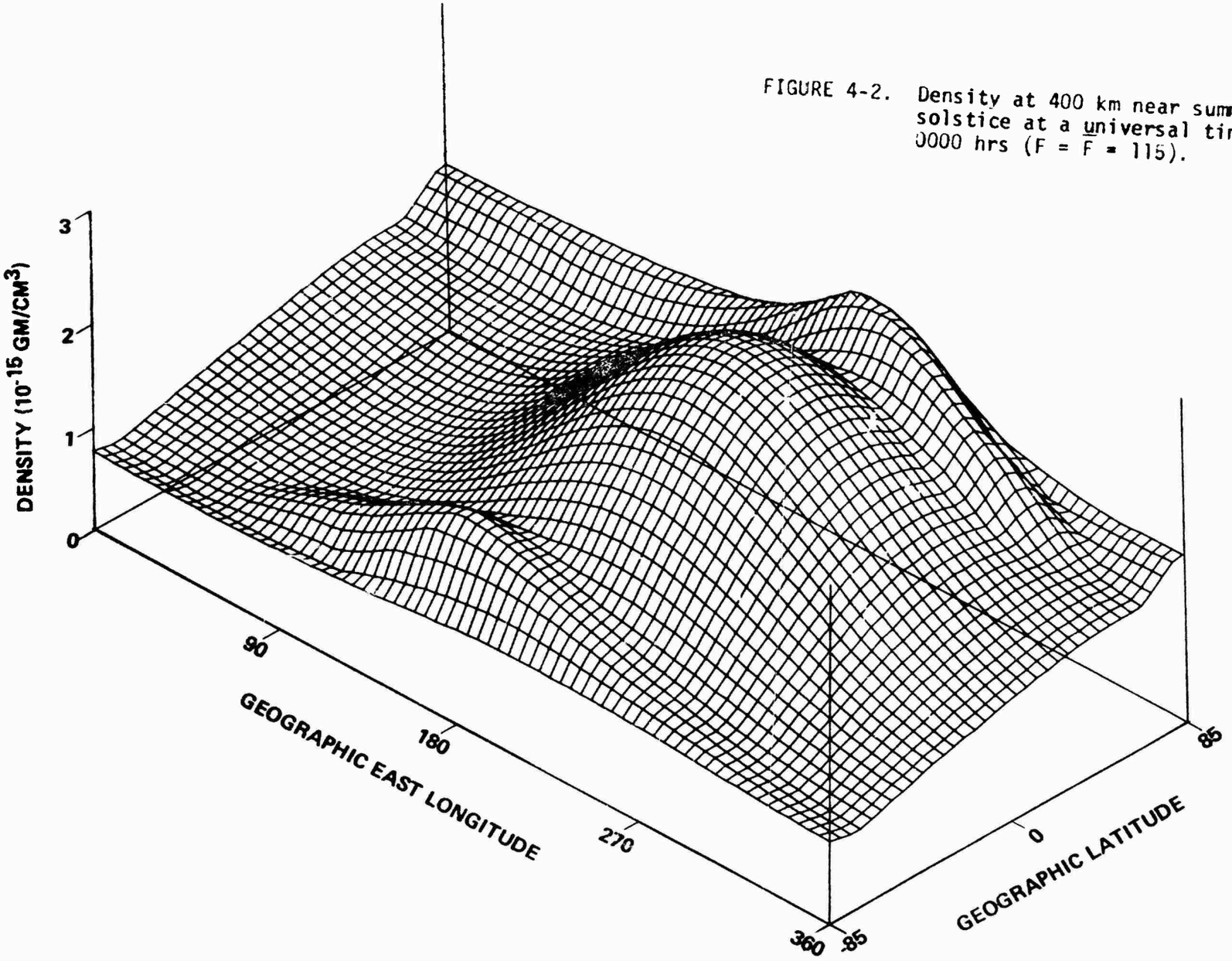

FIGURE 4-2. Density at 400 km near summer solstice at a universal time of 0000 hrs ($\bar{F} = F = 115$).

FIGURE 4-3. Density at 150 km near summer solstice at a universal time of 0000 hrs (F = F = 115).

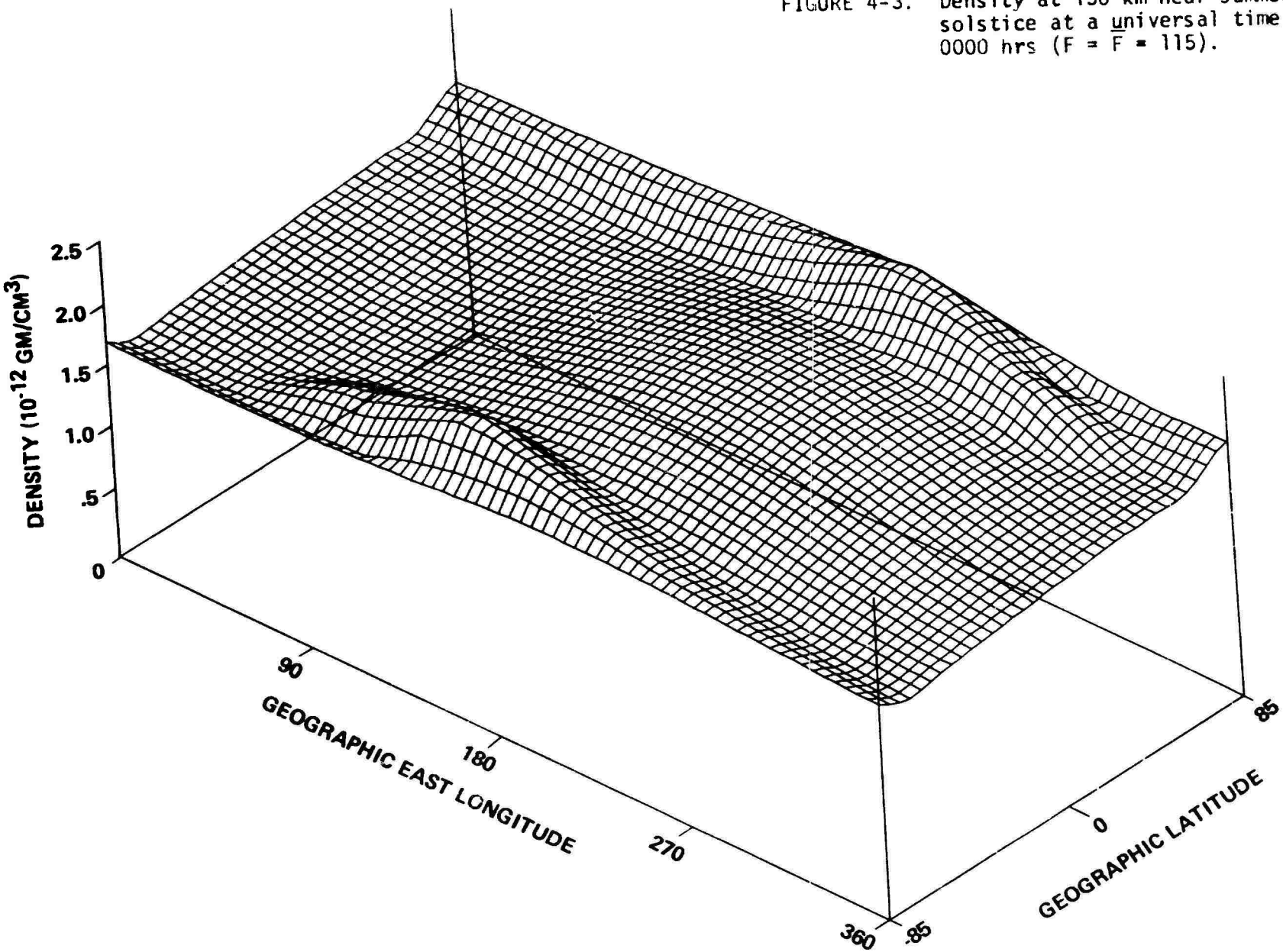

is located to the north of the equator and at about 1400 hours local time. The particle heating peak is most intense on the subsolar magnetic longitude containing the magnetic dipole. Since the total density is dependent on the particle heating effect as well as the UV heating, the northern particle heating peak which is in sunlight is much more pronounced than the southern particle heating peak which is far into darkness during the summer solstice night. Notice, furthermore, that the North pole-South pole density difference during solstice is about a factor of 2 and is in agreement with Hedin et al. (1974). Figure 4-2 is the same as 4-1 except that the universal time is equal to zero. The southern particle heating peak seen in Figure 4-2 is now somewhat larger since the southern dipole is now on the day side of the earth. The UV heating peak still lags the sun by about two hours. Figure 4-3 is a similar mercator projection at 150 km. At 150 km, the amplitudes of the UV and the particle heating peaks are considerably reduced. All of the variations except the semi-annual variation approach zero as the altitude approaches 120 km. The semi-annual variation approaches 0 as the altitude approaches 75 km.

A three dimensional polar plot is used in Figure 4-4 to represent the density bulge introduced at high latitudes due to particle precipitation. The particle heating region surrounds the geomagnetic pole and is maximum in the solar direction and drops to zero in the anti-solar direction. Its amplitude, location in geomagnetic latitude, and its size are adjustable parameters related to solar wind and magnetospheric properties. The adjustable parameters have been set to give a best fit to the LOGACS data during quiet times. Figure 4-5 shows a comparison between the current model and the LOGACS data. The current model is able to represent both the low latitude UV bulge as well as the high latitude particle heating bulge. Several passes of LOGACS data were available and these were used to determine the particle heating intensity parameter, I. I = .15 gives a best fit to the LOGACS data. It is the parameter I that must be varied to compensate for changes in the precipitating particle fluxes. The static diffusion models (e.g., Jacchia, 1971) do not model this high latitude phenomenon.

FIGURE 4-4. Polar view of the densi y around the geographic North pole at an altitude of 250 km at UT = 0000 hrs ($F = \bar{F} = 115$).

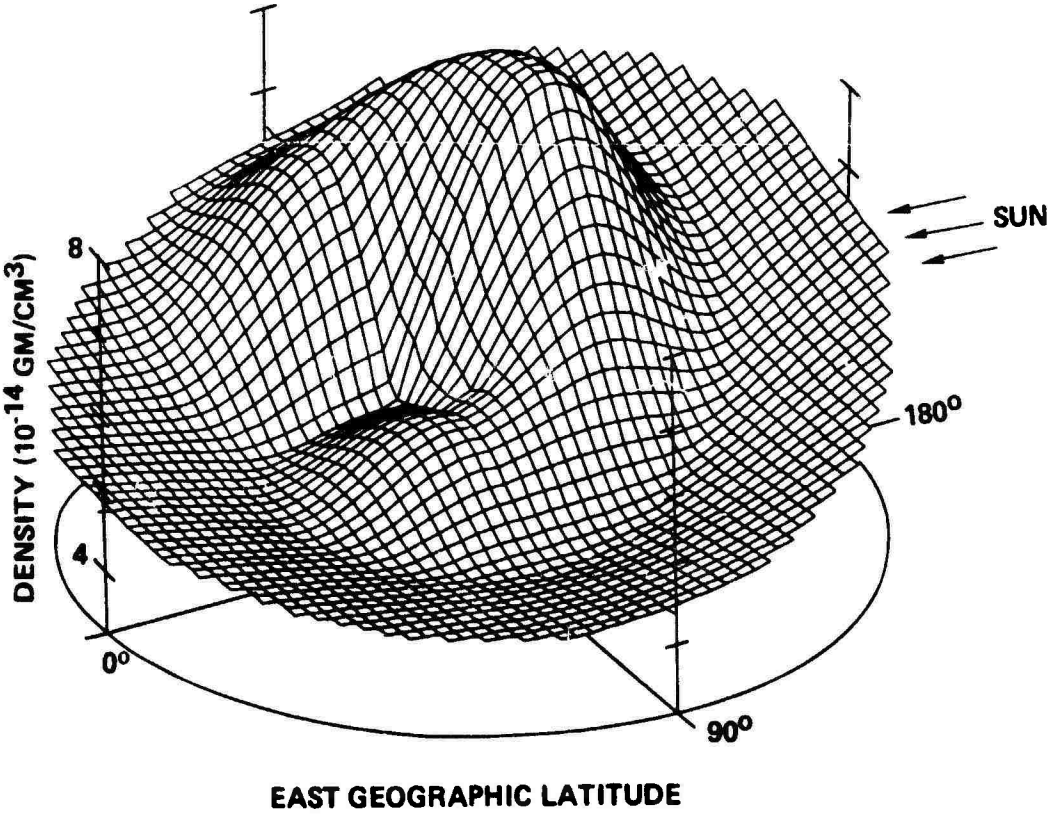

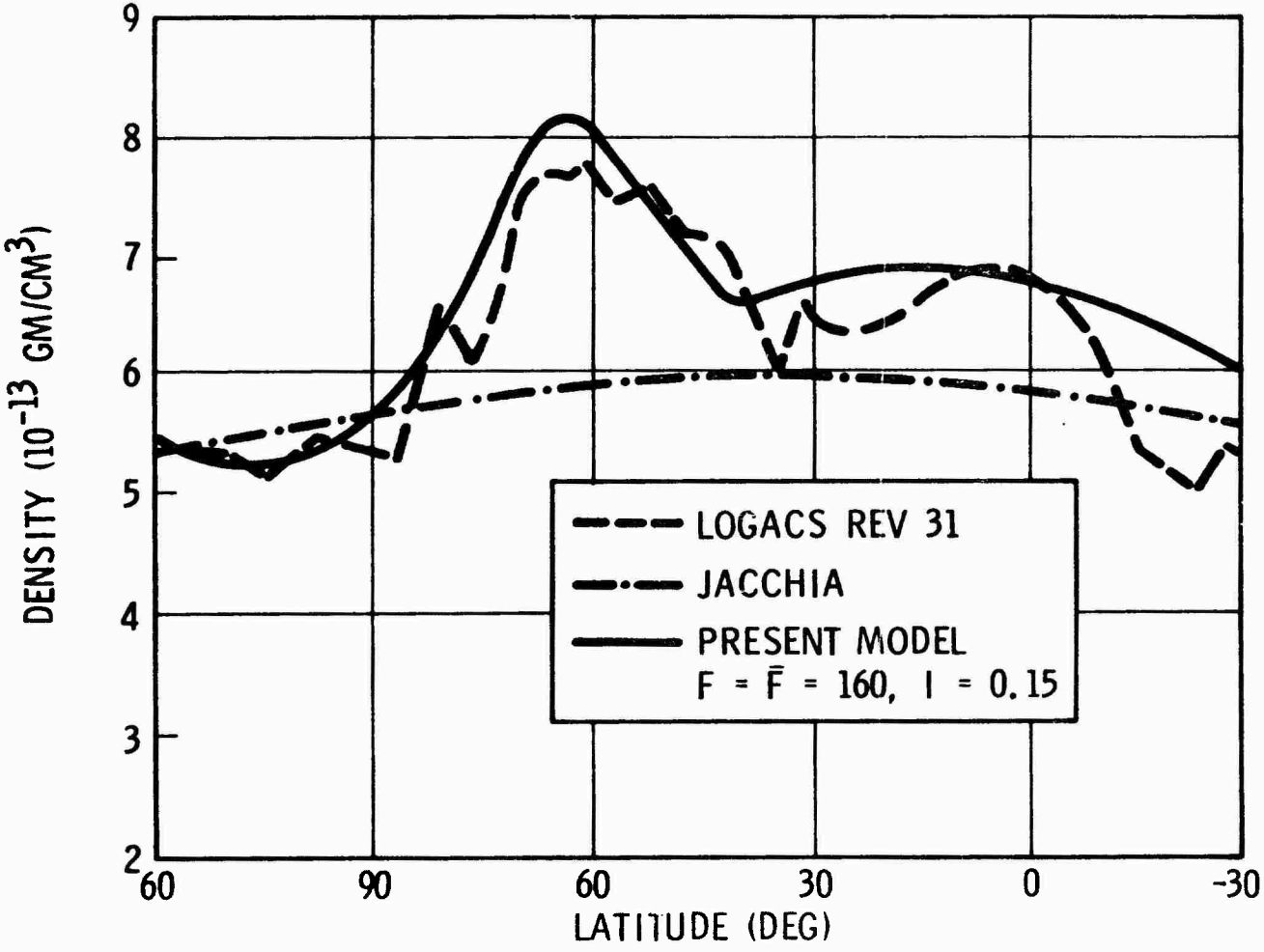

FIGURE 4-5. Comparison of the model with the data of the LOGACS satellite. The LOGACS data has been reduced to 186 km. $F = \bar{F} = 160$ and $I = .15$.

The semi-annual variation was adjusted to match the results of Hedin et al. (1974) at 450 km. Figure 4-6 shows the comparison between the current model and Hedin et al.'s OGO-6 data. The fit at 450 km for both 0 and 45 degrees is within experimental error. The amplitude of the diurnal variation decreases with decreasing altitude. The rate of decrease was adjusted to fit the LOGACS data (Figure 4-5) at 186 km near local noon and the data of Ching and Carter (1974) at 230 km near local midnight (Figure 4-7). The data of Ching and Carter were taken during April 1972 when the 10 cm solar flux was 115 x 10^{-22} watts/m^2/Hz. The agreement in absolute density is excellent except for high northern latitudes. For night time and latitudes above 60 degrees, this model as well as others consistently underestimate the density by about 20 percent. This region on April 24th is very near the light-dark terminator and perhaps the model's dependence on the rate of change of density with respect to the solar angle is too rapid. The effect is probably not due to neglected particle precipitation effects since similar discrepancies do not occur near the south pole. The southern measurements were made well within the darkness region and were far removed from the light-dark terminator over the pole. This region where the difference between observation and model averages about 20 percent is small in size. In almost all other regions where the model has been tested, agreement between model and data is better than 10 percent.

Several additional comparisons between the model and <u>average</u> atmospheric densities can be performed by averaging outputs from the model. Figure 4-8 shows the altitude dependence of the density for solar minimum ($F = \bar{F} = 70$) and solar maximum ($F = \bar{F} = 220$) at 0400 and 1400 hours local time (i.e., near the minimum and the maximum in the diurnal cycle). Also shown are points from the CIRA 72 mean reference atmosphere which represent a diurnally and seasonally averaged atmosphere at a latitude of 30 degrees when the 10 cm solar flux has a value of 145 x 10^{-22} watts/m^2/Hz. The dashed curve represents the model with $F = \bar{F} = 145$ and averaged over universal time and the days of the year at a latitude of 30 degrees North and a longitude of 0 degrees East. We note the excellent agreement with CIRA 72.

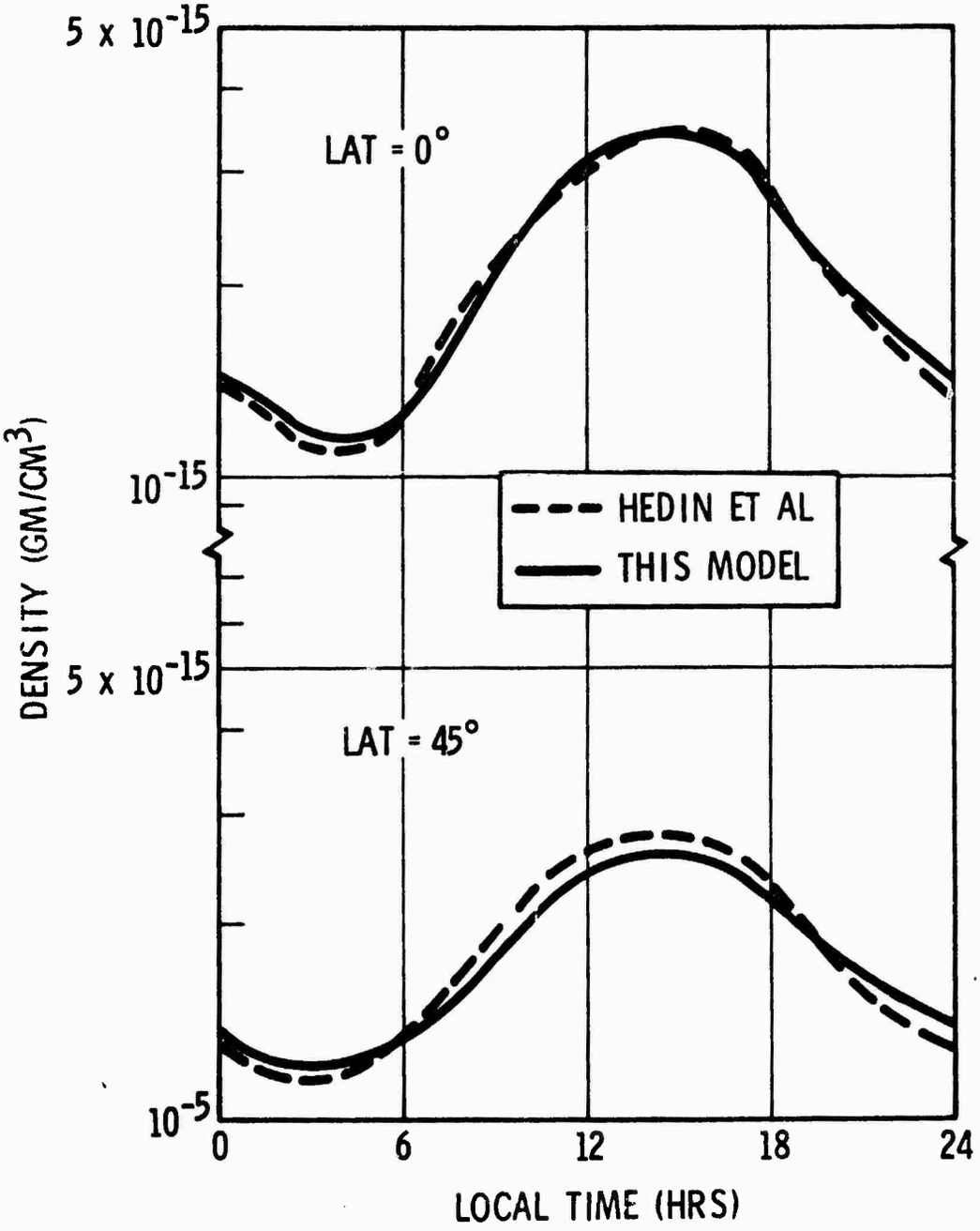

FIGURE 4-6. Diurnal variations at 450 km at a latitude of 0° and 45°. The OGO-6 data of Hedin et al. (1974) is compared with the model at λ=0° and 45° at an altitude of 450 km near equinox when $F = \bar{F} = 150$.

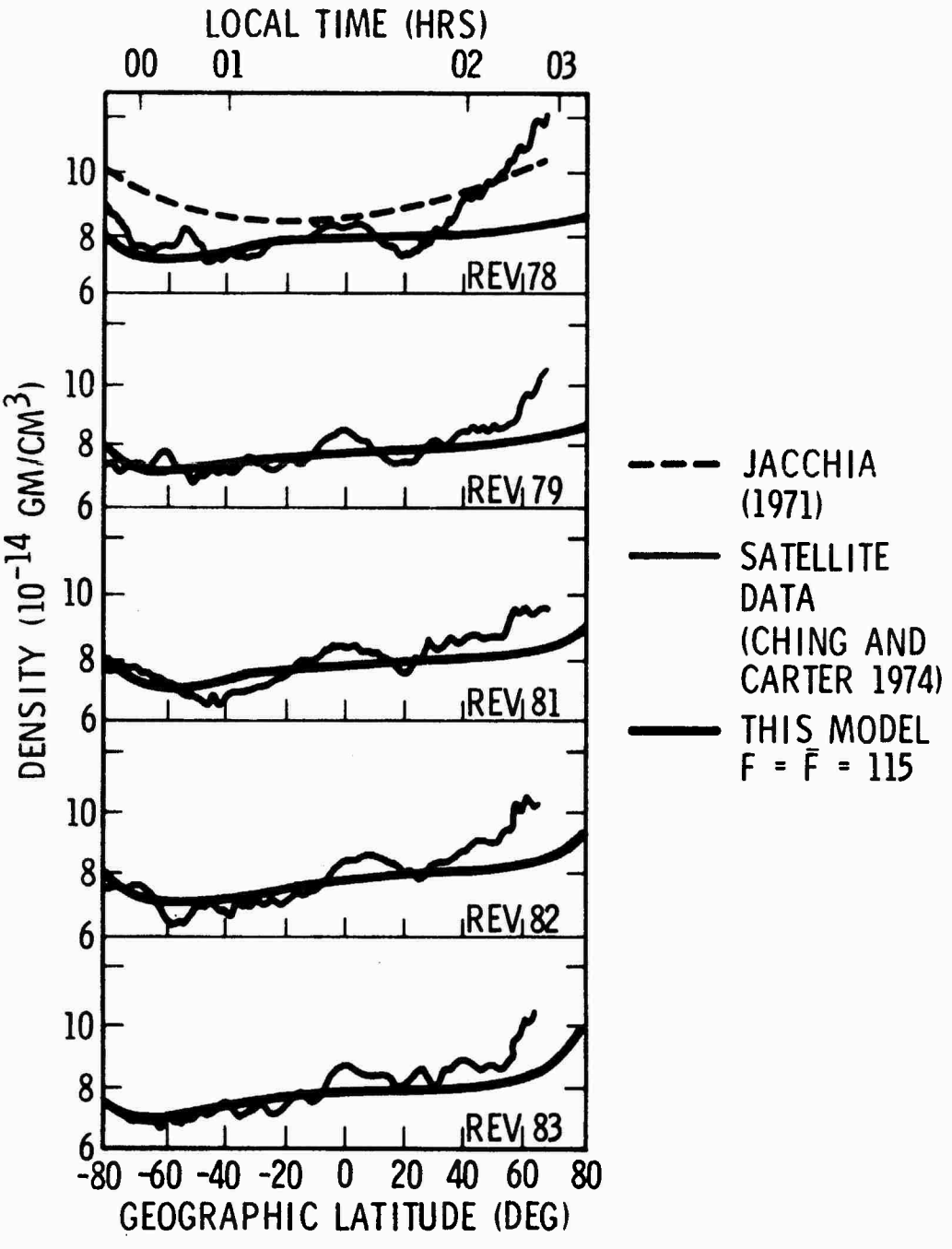

FIGURE 4-7. The nighttime data of Ching and Carter (1974) is compared with the model. The average 10 cm solar flux during April 1972 was ∿ 115. This value was input to the model for the comparison.

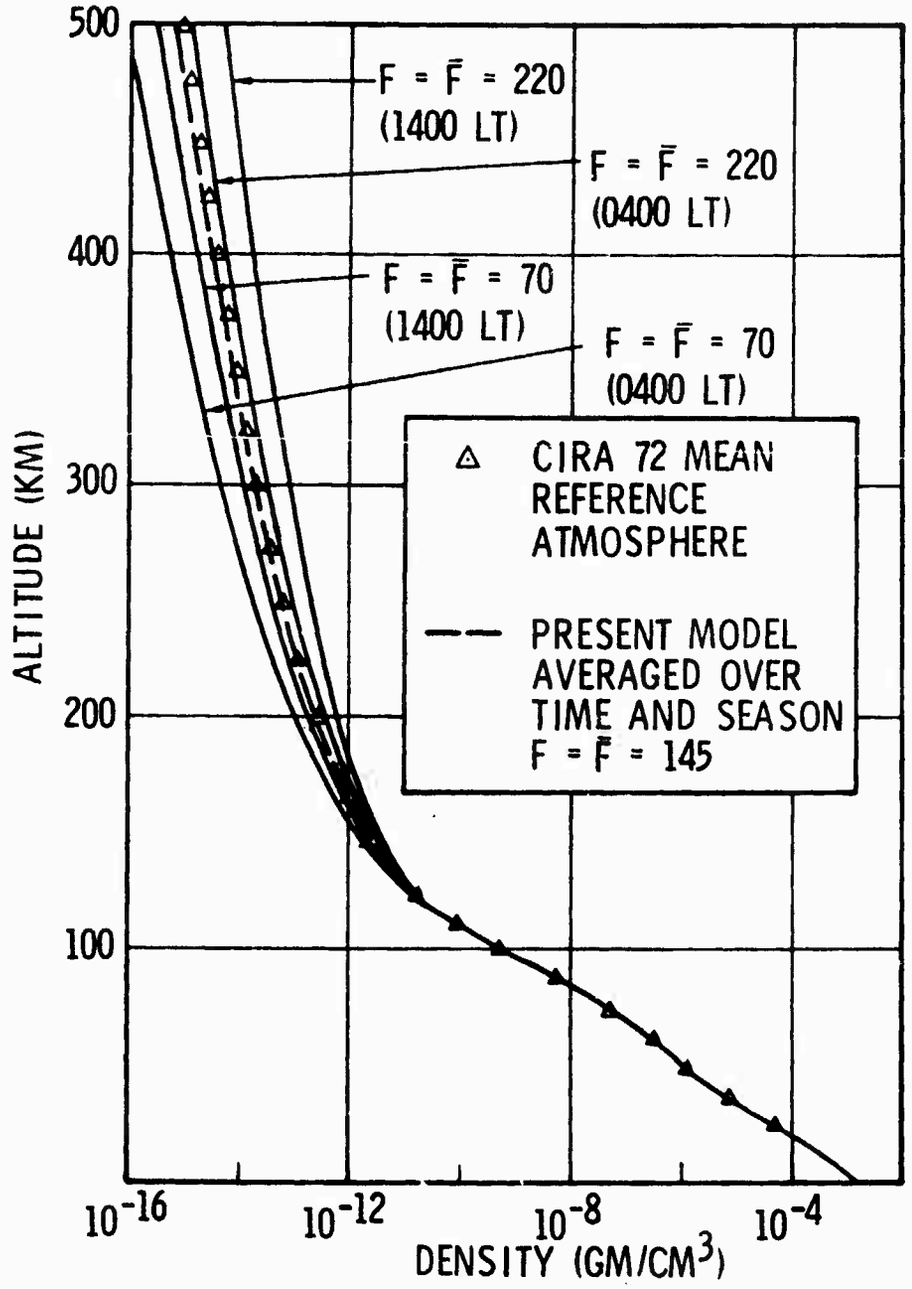

FIGURE 4-8. Density versus altitude for solar minimum ($F = \bar{F} = 70$) and solar maximum ($F = \bar{F} = 220$) near the daily maximum (LT = 1400 hrs) and the daily minimum (LT = 0400 hrs). Also shown is a comparison between a universal time and the seasonally averaged model output at a latitude of 30° ($F = \bar{F} = 145$) with the CIRA 72 mean reference atmosphere.

Hedin et al. (1974) also presents a diurnally averaged curve for solstice showing the data as a function of latitude. When the present model is averaged over universal times and geographic longitudes at solstice a curve very similar in appearance to Hedin et al.'s OGO-6 curve is obtained (See Figure 4-9). In the summer hemisphere a second high latitude maximum (separate from the UV maximum) is produced due to the particle precipitation. This agrees well with the double maximum observed by OGO-6. The major differences between the OGO-6 data and the model, defined by this report, are that the OGO-6 data are about 25 percent higher and that the model determined summer high latitude peak is slightly low (when the LOGACS determined value for I, I = .15, is used). Hedin et at. state that their seasonal dependence, in particular the annual and semi-annual variation is poorly defined and thus the absolute amplitude has a large uncertainty. The shape in latitude dependence is, however, quite accurate. The summer hemisphere high latitude difference is easily corrected by increasing the particle heating parameter by ~ 30 percent to I = .2. Since no data are available during this time period for determining the average particle flux entering the cusp, a value of .2 is not inconsistent. The average variation predicted by the model is in substantial agreement with the OGO-6 data.

4.3 Use of Model to Describe the Disturbed Atmosphere

The model described above was developed with a very general set of input parameters that describe variability in charged particle and ultraviolet heat sources. To date those parameters have been adjusted such that the model describes the "undisturbed" atmosphere. Work on the description and parameterization of the disturbed atmosphere was initiated in the past year and described in the 1975 Interim Report. By appropriately determining the dependence of the input parameters on magnetic and solar activity and taking into account storm time dependent behavior, the model can be extended for use over a range of disturbance conditions. For example, charged particle heating during magnetospheric substorms (via the plasma sheet lobes) and during magnetic storms (from the decay of the ring current) can readily be incorporated into the model by appropriate expansion of the dayside cusp region. (Particle precipitation through the lobes of the plasma sheet will extend the corpuscular heating region

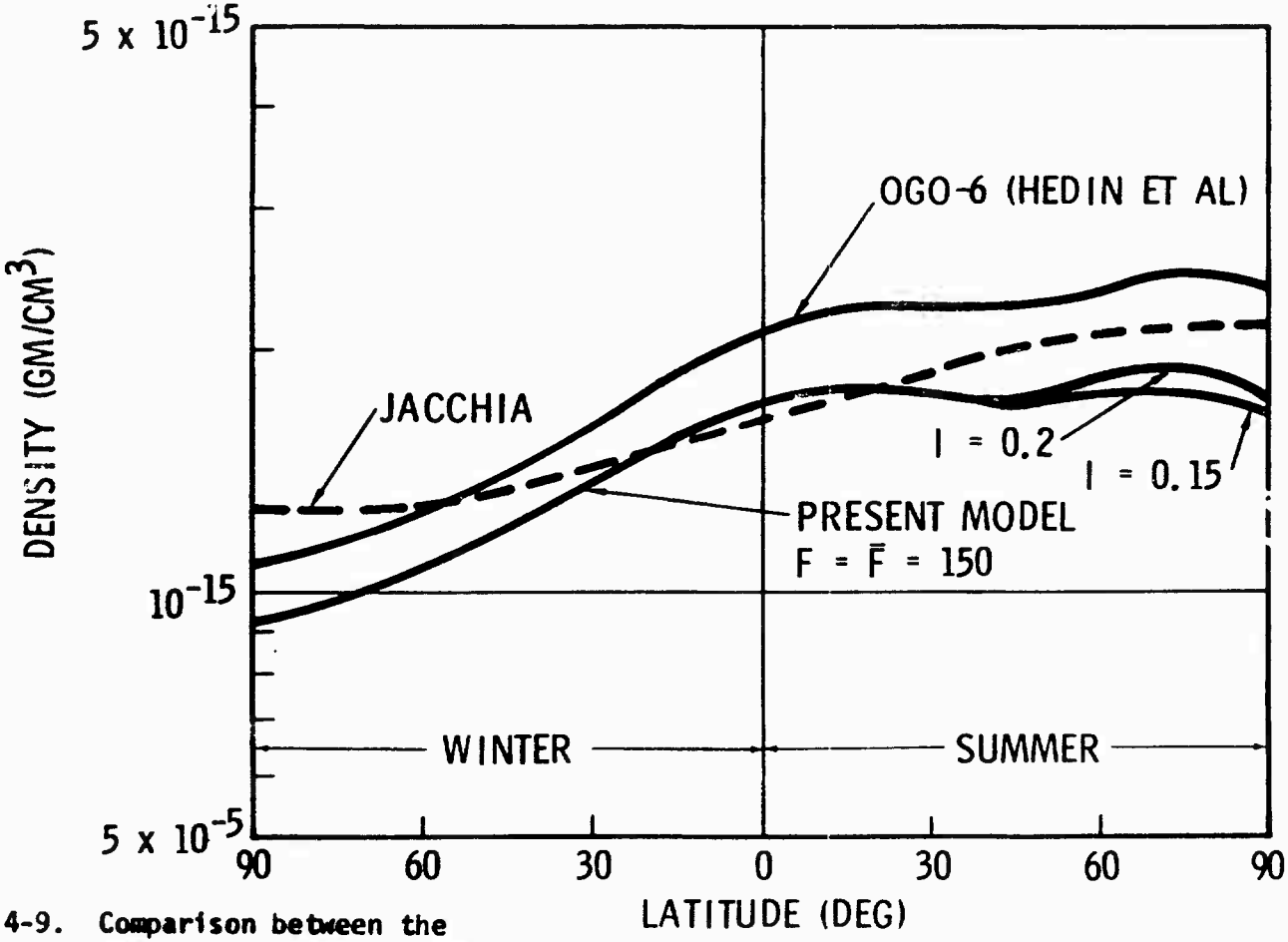

FIGURE 4-9. Comparison between the longitudinal and diurnally averaged model at solstice with the solstice averaged data of Hedin et al. Two values for the cusp heating (I = .15 and I = .2) are shown. Also shown for reference is the model curve of Jacchia (1971).

to all longitudes and to lower altitudes on the nightside due to the relatively larger primary particle energies - from 10 to 50 keV. Particle heating from ring current decay will extend the corpuscular energy source to much lower latitudes and introduce a dependence on storm onset time.) As has been our general modeling philosophy (see Section 6.0) the variability in the input parameters could be determined by comparing preliminary model output data with observations. As with our magnetic field modeling work, an attempt is made to represent all conditions with one basic model. For purposes of prediction and satellite monitoring we also believe that the input parameters should be capable of direct and continuous observation and not be temporally and spatially averaged indicies.

5.0 SOLAR WIND AND NEAR EARTH ENVIRONMENTAL PARAMETERS

The models discussed in the previous two sections (and all other near earth environmental models) require input parameters that can be monitored in real time if the models are to be used for prediction purposes. Thus, a study was made of several observational data sets to find observables that directly described near earth environmental features (e.g., the extent of dayside aurora provides a gross picture of the location of the dayside cusps). Possible correlations between solar wind parameters and near earth environmental features were also sought. (They would provide a source of "predictive" input parameters for the models.)

Density measurements deduced from orbital perturbations of the balloon satellites Explorer 19 and Explorer 24 (Jacchia and Slowey, 1972) were graphed for comparison with Vela 3 and 5 solar wind measurements over a period of several years in order to determine how the relationships vary with the sunspot cycle. Comparative data covering four months are shown in Figures 5-1 and 5-2 to illustrate the relationships for a wide range of solar and geomagnetic activity. The correlation between air drag and solar wind speed in Figures 5-3 and 5-4 suggests that nearly every change in the solar wind produced a corresponding change in the energy input to the upper atmosphere.

Evidence for a high-latitude density bulge at quiet times was furnished by the low-g accelerometer aboard the Air Force satellite 1967-50B ("LOGACS") (Bruce, 1968, 1972; De Vries, 1972). In Figure 5-5 selected LOGACS data are replotted to show two energy sources not explicitly included in static diffusion models. The solid line in the Figure represents the observed density when the geomagnetic planetary amplitude, A_p was 4, indicating quiet conditions. (The nocturnal values of density are extrapolated.) The data were adjusted to a constant altitude of 100 nautical miles (186 km). The observed latitudinal variation of density differs considerably from that given by the Jacchia Model (1970). The measured density appears to represent thermal expansion in response to two discrete energy sources: (1) The ultraviolet source at low latitudes and (2) the corpuscular source at high.

FIGURE 5-1

CORRELATIONS, JAN. TO FEB. 1967

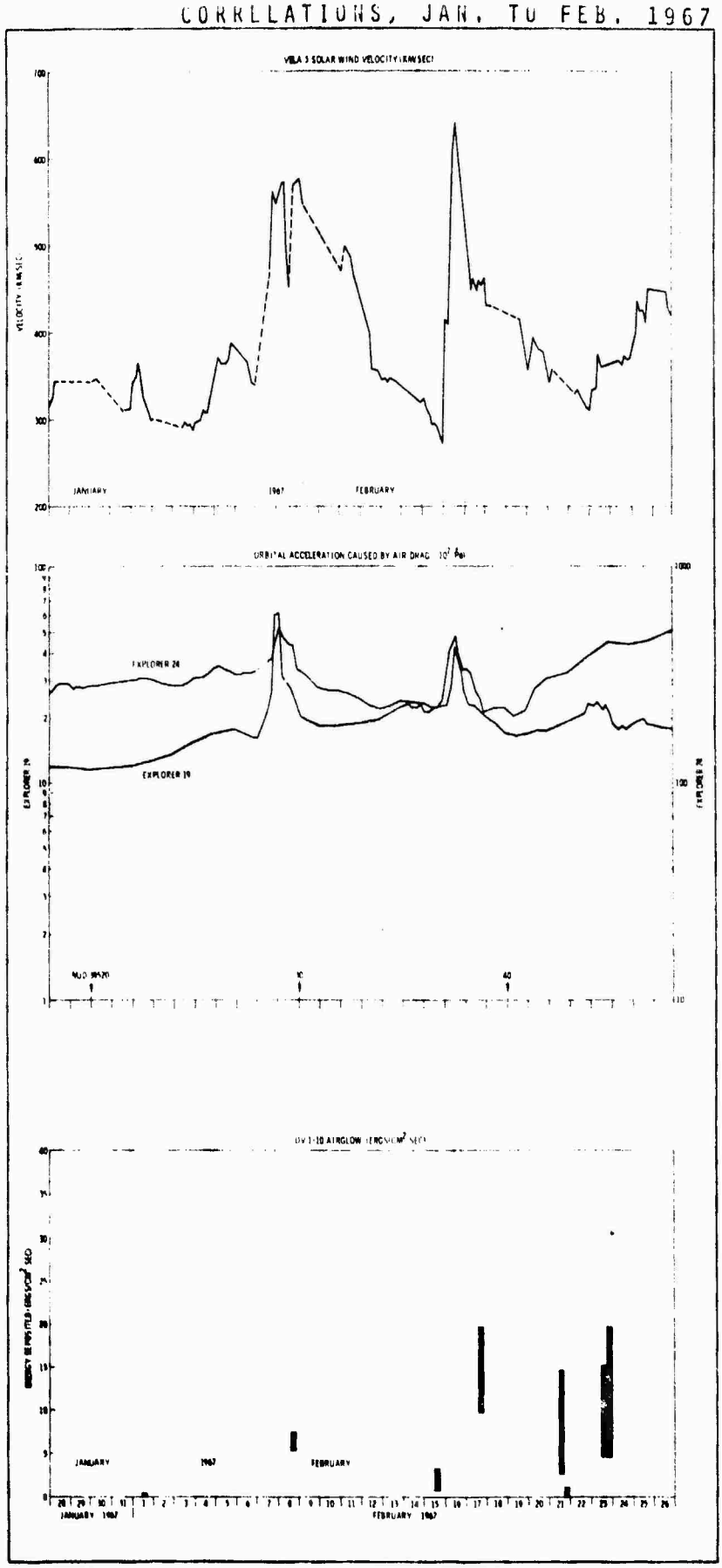

FIGURE 5-2

CORRELATIONS, MAY, 1967

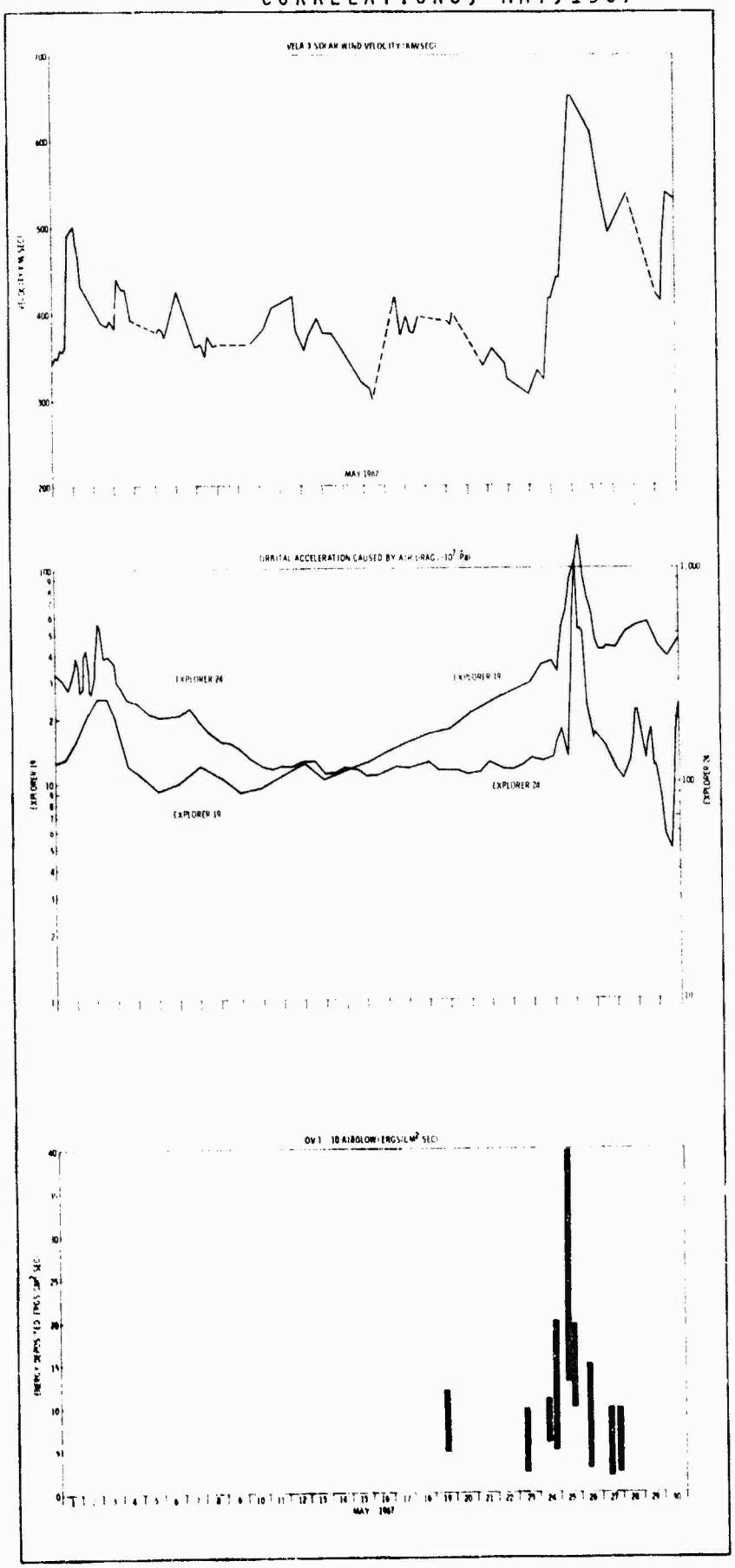

FIGURE 5-3

CORRELATIONS, DEC. 1965 TO JAN. 1966

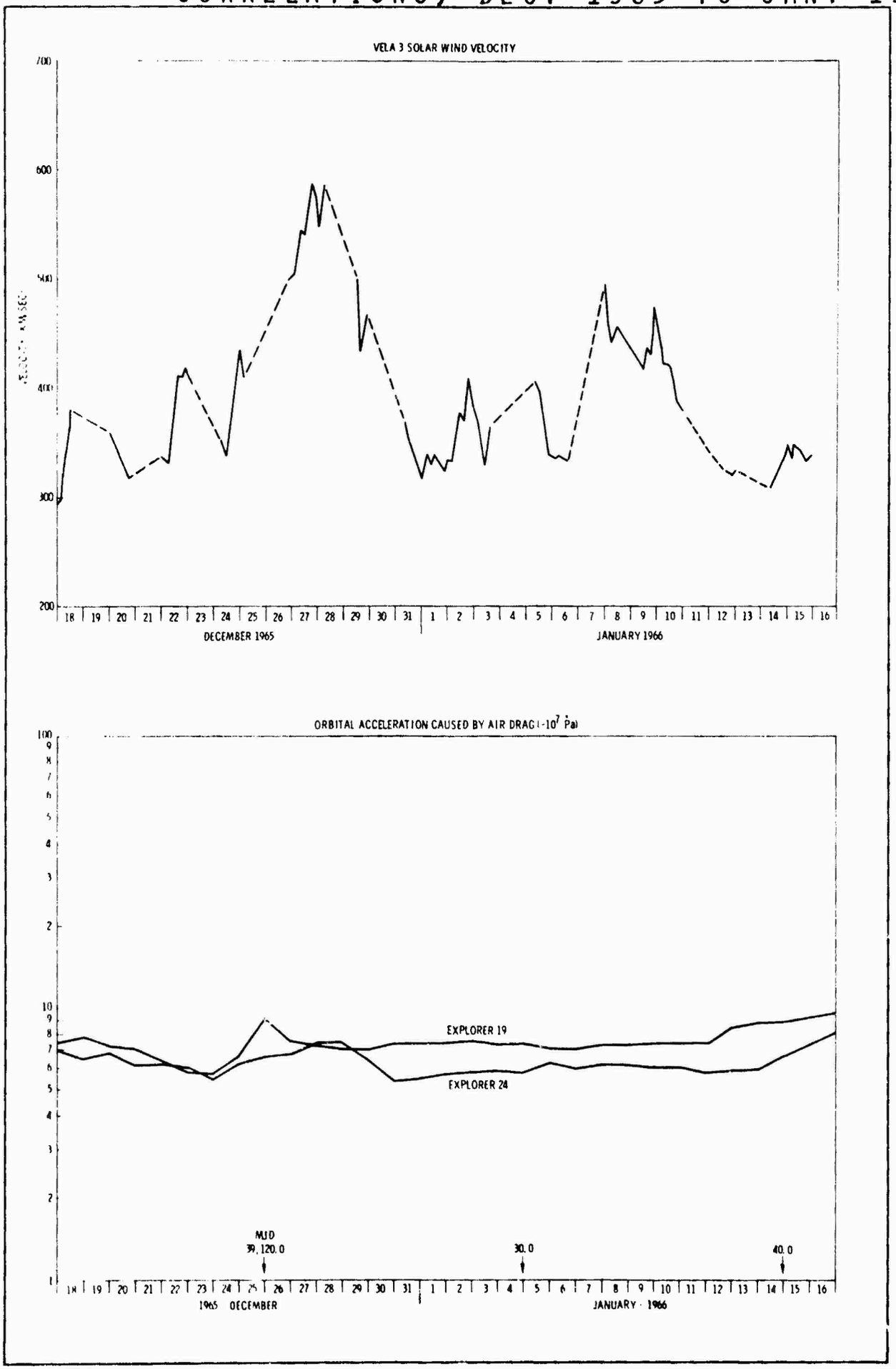

FIGURE 5-4

CORRELATIONS, JAN. TO FEB. 1966

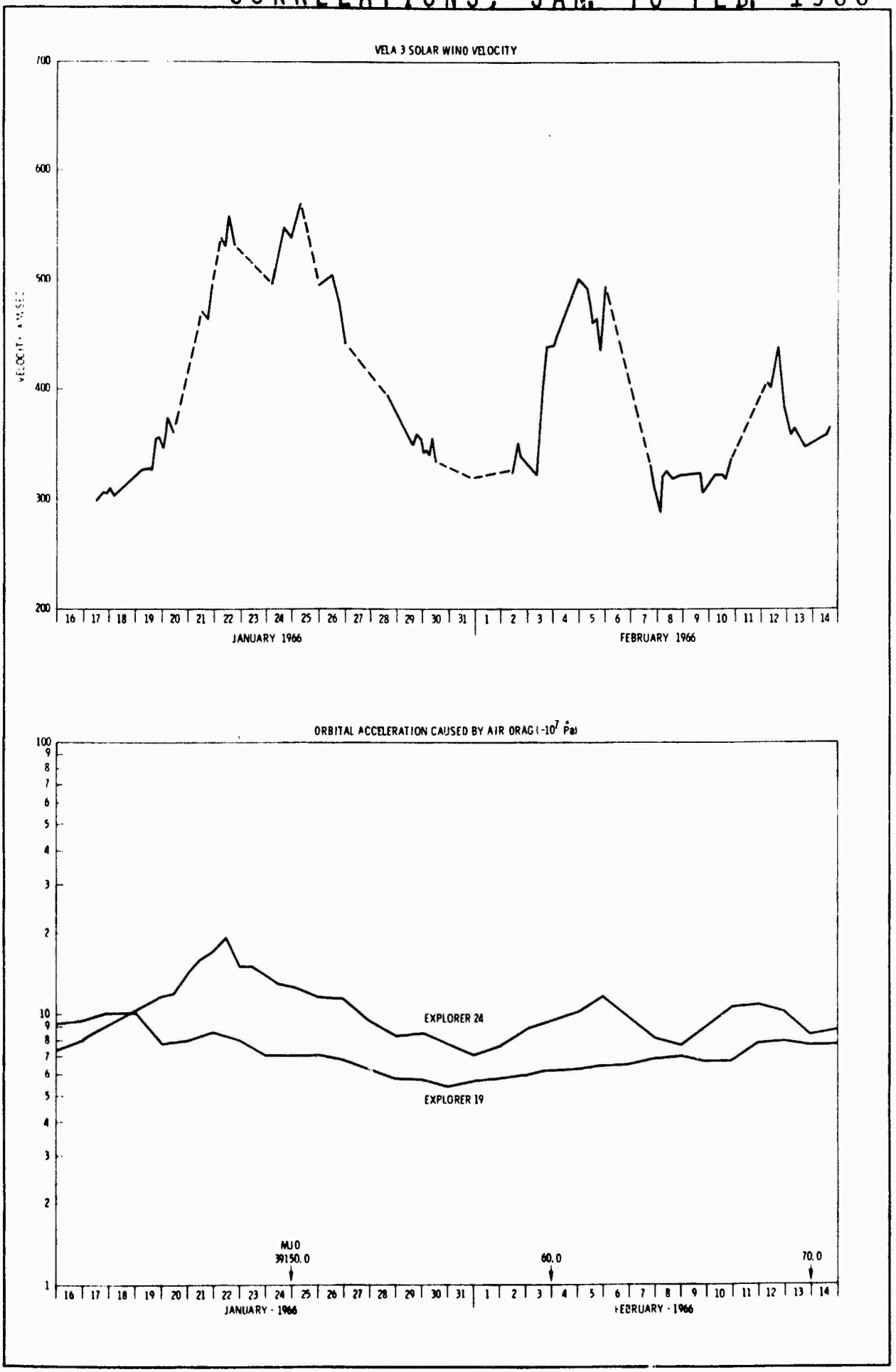

AIR DENSITY AT 100 N.MI. (186 KM.) IN MAY, 1967

P360
27223

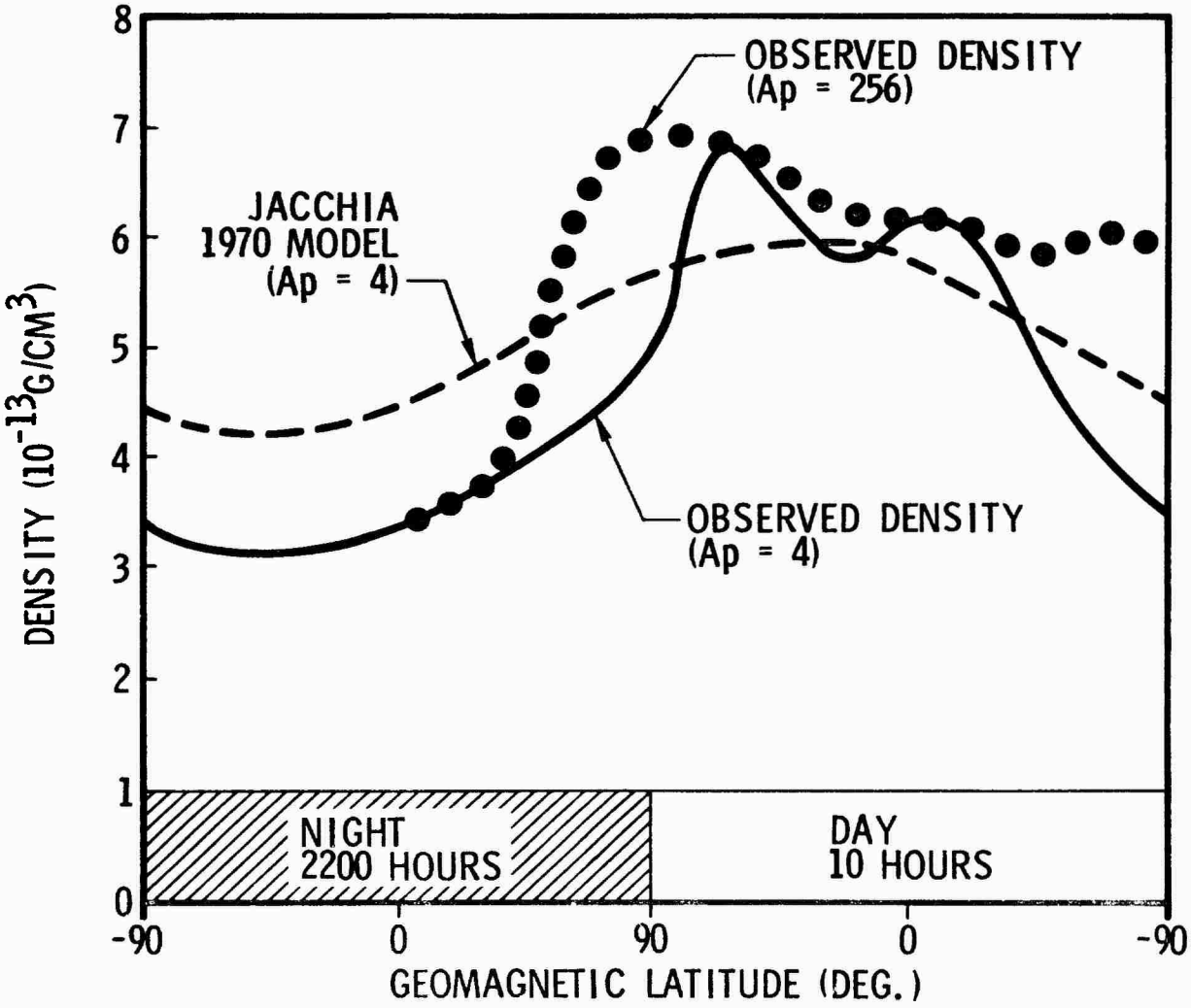

FIGURE 5-5

5.1 Composition Measurements

Longitudinal variations of thermospheric composition have been observed by the mass spectrometer on OGO 6 (Hedin and Reber, 1972), who attribute them to geomagnetic control of polar heat input. The contours of N_2 concentration in the Antarctic atmosphere at two local times are illustrated in Figures 5-6 and 5-7. Their geographic extent correlates well with the average cusp location. The absolute maximum N_2 concentration occurs at about 0800 UT (3 hours after local noon) at an invariant latitude of 70°S. Similar persistent longitudinal variations of positive ions occur (Taylor, 1971). (It requires some time for the density and composition to respond to energy sources, while a nearly instantaneous response is provided by the airglow.)

5.2 Airglow and Auroral Measurements

The ISIS-II Satellite generated global maps of the 6300 Ångstrom line of atomic oxygen (Shepherd and Thirkettle, 1973). The most prominent feature observed is a band of permanent red aurora on the dayside of the earth, centered on magnetic noon at about 78° invariant latitude. The intensity contours of this aurora measured near 0535 UT on 14 December 1971 are shown in Figure 5-8. The overall shape resembles the contour of the dayside cusp at 0535 UT. The computed instantaneous cusp region is projected on the airglow contours in Figure 5-9.

The airglow measurements furnish detailed information about the instantaneous energy distribution within the cusp. Figure 5-8 also shows the aurora on the nightside, which is produced by precipitation from the tail. By combining the ISIS-II airglow observations with magnetospheric modeling calculations, information about the atmospheric energy sources provided by the magnetosphere during the day and night at quiet and disturbed times can be obtained.

Measurements of Lyman-alpha aurora and airglow have been reported by Clark and Metzger (1969) and by Metzger and Clark (1971), who flew a narrow-band scanning photometer on the Air Force research satellite, OV1-10. This experiment clearly showed the enhancements which occur during geomagnetic storms, as well as the variation with latitude during quiet times. In the various measurements reported, the inferred particulate flux in the auroral zone varied from less than 1 erg/cm^2 sec during several quiet periods to 36 at one point

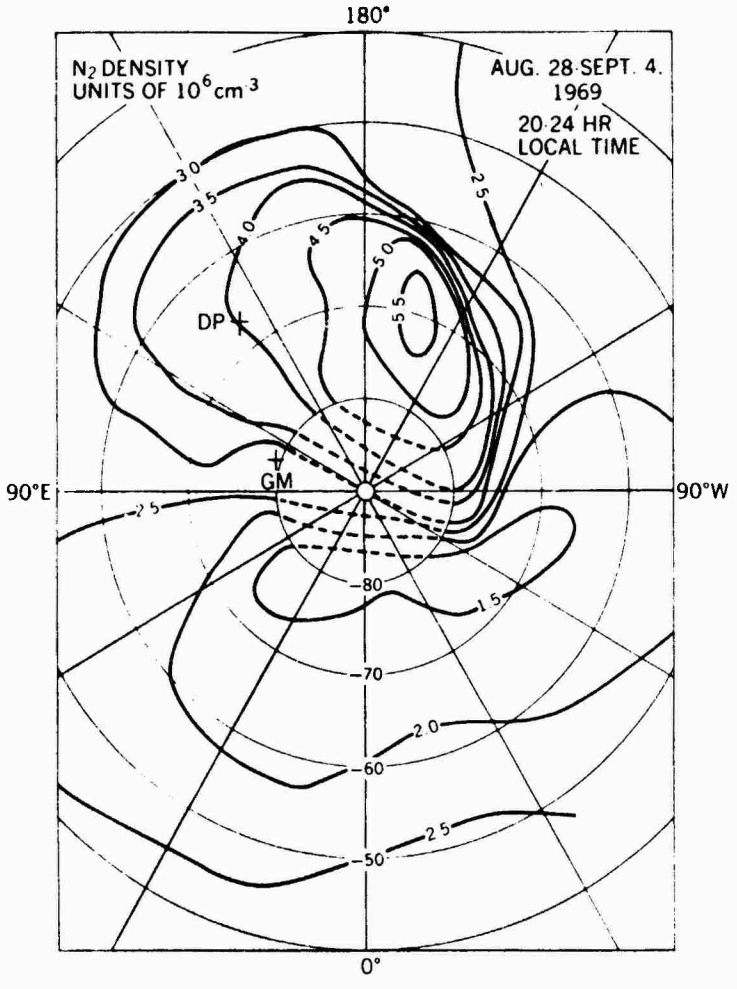

FIGURE 5-6 CONTOUR PLOT IN GEOGRAPHICAL COORDINATES OF N_2 DENSITY EXTRAPOLATED TO 450 KM FOR 2000-2400 LT AND AVERAGED OVER DATA FROM AUGUST 28 TO SEPTEMBER 4, 1969, WHEN $A_p \leq 12$. DASHED LINES INDICATE LACK OF DATA. DP INDICATES DIP POLE, AND GM INDICATES GEOMAGNETIC POLE.

(AFTER HEDIN AND REBER)

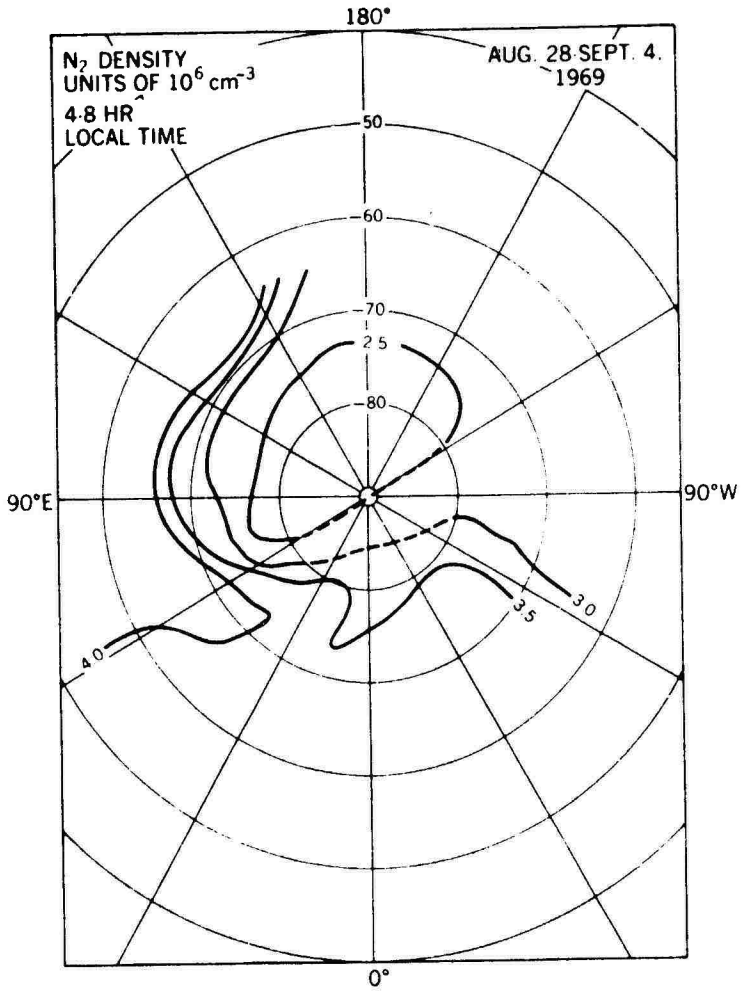

FIGURE 5-7 CONTOUR PLOT OF N_2 DENSITY UNDER THE SAME CONDITIONS AS FIGURE 3-7 EXCEPT FOR 0400-0800 LT.

(AFTER HEDIN AND REBER)

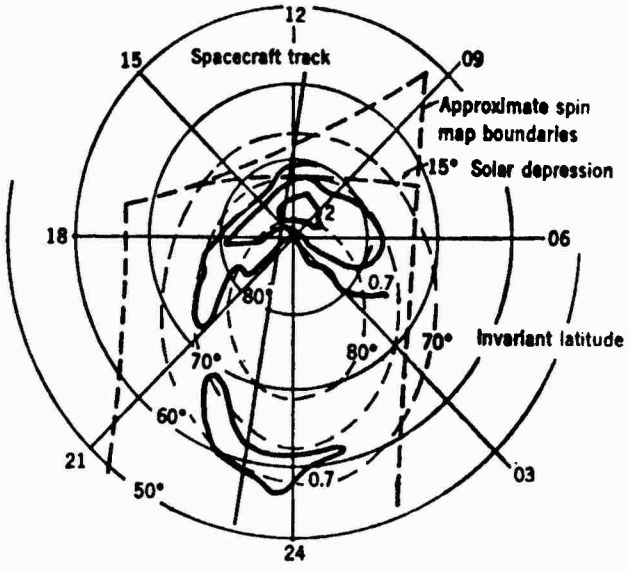

FIGURE 5-8 INTENSITY CONTOURS FOR 6300-Å EMISSION PLOTTED ON COORDINATES OF GEOGRAPHIC LATITUDE AND LOCAL TIME. THE INTENSITIES SHOWN ARE IN KILORAYLEIGHS. ALSO SHOWN (DASHED) ARE SOME INVARIANT LATITUDE CONTOURS, THE SPIN MAP BOUNDARIES, THE 15° SOLAR DEPRESSION ANGLE LINE, AND THE SPACECRAFT TRACK.

(AFTER SHEPHERD AND THIRKETTLE)

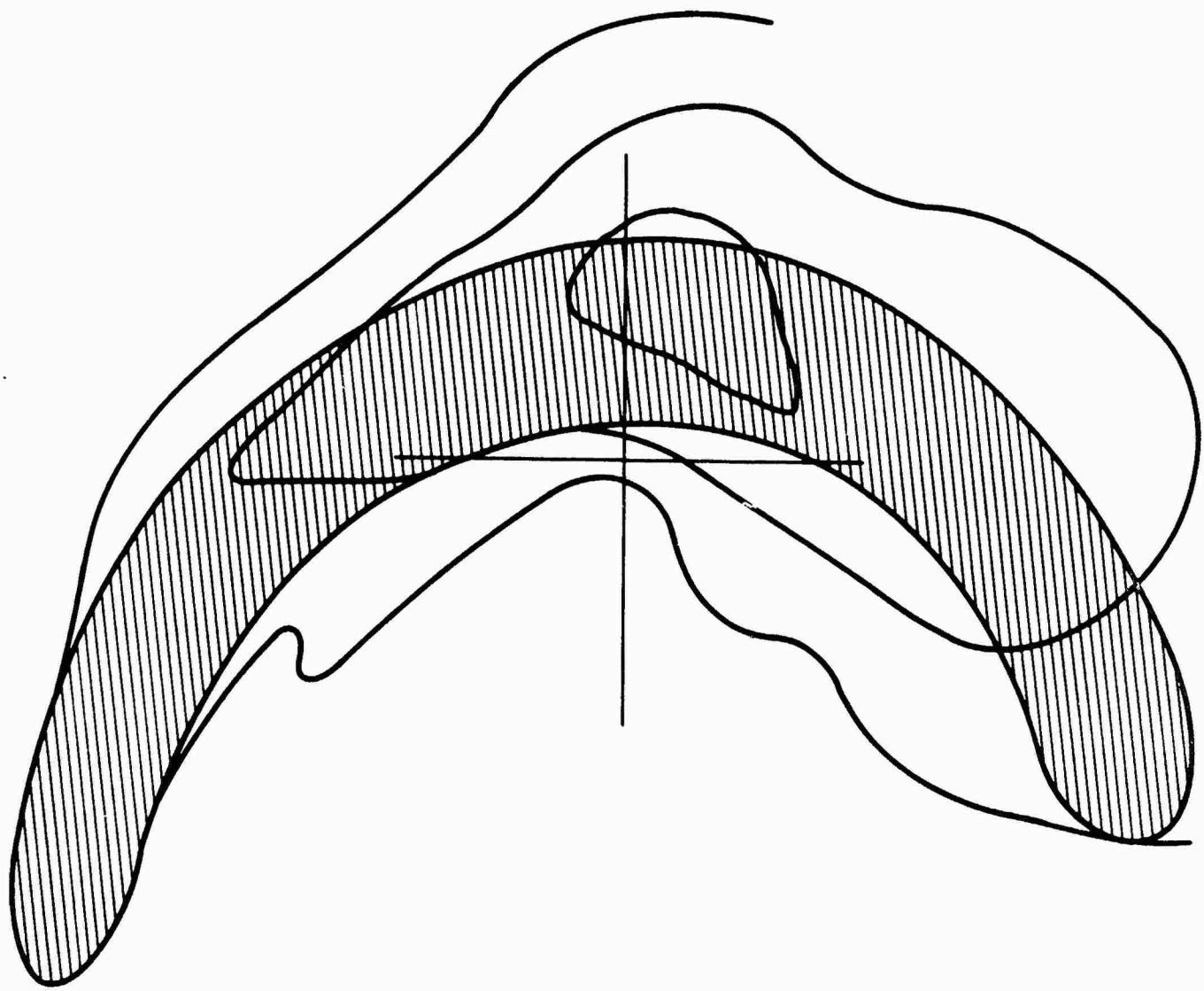

FIGURE 5-9 COMPUTED REGION OF PRECIPITATION FROM THE DAYSIDE CUSP (SHADED) COMPARED WITH MEASURED AIRGLOW CONTOURS FROM FIG. 3-9.

during the great geomagnetic storm of May 1967. The OV1-10 auroral zone measurements are compared with solar-wind velocities from Vela 3 and 5 in Figures 5-1 and 5-2. (If an auroral measurement begins at zero, it means that an upper bound was determined.) There was a rather good correlation among the reported data, but the data are far from complete. Complete density data for comparison with solar-wind data were provided by the balloon satellites, Explorers 19 and 24, which are also shown in Figures 5-1 and 5-2. These data were discussed in Section 5.0.

The rates of energy deposition in the auroral zone which Clark and Metzger deduced from airglow measurements are plotted for 17 orbital revolutions of the OV1-10 satellite during the months February and May 1967. The ranges of reported measurements have been extended by $\pm$20 percent, to allow for possible random errors of measurement. When the solar wind is very quiet and about 300 km/sec, the rate of energy deposition is usually below 5 ergs/cm^{2}sec, and sometimes below 1 erg/cm^{2}sec. But during disturbed times, the rate is higher, sometimes much higher (especially during the great storm of May 25 and 26, 1967). The fact that the airglow as measured in this experiment is much more variable than the solar wind illustrates the importance of detailed modeling of the magnetospheric and atmospheric processes.

6.0 SUMMARY AND CONCLUSIONS

The development of these magnetic field and neutral density models has lead us to recognize that at present, because of our lack of physical understanding of many environmental features, any environmental model of practical utility must be semiempirical. The magnetic field model has become a useful tool to many investigators because it accurately represents many observed features of the magnetospheric magnetic field. We have learned then that the first requirement of any environmental model is not that it be based on a complete understanding of all the physical phenomena involved, but rather that it be useful. In order to be useful to groups whose hardware systems are influenced by environmental features (and for most basic research applications), a model of one of those features must possess several qualities. First, it must quantitatively and accurately represent the environmental feature it is intended to describe. Second, it must be analytic. For many applications it is necessary that the parameter to be described is defined continuously over a region and that its representation be differentiable. Third, it must be possible to represent the model with a computer code that is fast. The model is not useful if its output parameters can be obtained only after large amounts of computer time have been expended. This has important implications for future decisions on model development and data collection. The ultimate goal of predicting near earth environmental effects will not be reached by continuing to increase the amount of monitored data to the point that effectively the whole environment is monitored continuously. Large data sets and slow computer codes will not prove useful in the attempt to develop a capability for real time monitoring of environmental features (although such codes and data sets may be of some merit for increasing our understanding of some of the physical processes operating in the environment). Rather, the ultimate predictive system will operate with a small set of well chosen input parameters and a set of very fast computer codes. Fourth, the model must be usable over a large region of space. For example, models of the upper atmosphere and ionosphere should be global while models of the magnetosphere should be valid from the subsolar region to the distant tail (at least to lunar orbit). Fifth, the model must also be compatible with other models. This dictates that care be used in deciding on the proper input and output parameters. It must also be

constructed so that environmental data observed by satellite and ground based detectors can be used as input parameters.

The magnetic field modeling work has led directly to two other modeling efforts. In one the work on magnetospheric magnetic fields ($\vec{B}_T$) is being extended to include variations produced in $\vec{B}_T$ by changes in the angle between the geomagnetic dipole axis and the solar wind direction. (This angle influences the gross shape of the magnetosphere and related magnetic field topology.) This work is being done for AFWL with monitoring function provided by OSR. (AFWL became interested in the work on magnetic fields because of their need to keep track of charged particles released by nuclear bursts. It was believed that some of their problems were related to the use of inaccurate field models.) This work includes the modification of the "B, L" coordinates so that with the improved model, charged particle data can conveniently be organized out and beyond synchronous orbit (Pfitzer and Olson, 1975). This work will provide an accurate description of the magnetospheric magnetic field during "quiet" magnetic conditions and provide a means for organizing charged particle data during such periods. The other effort, funded by ONR, is to construct a quantitative model of total ionospheric electron density. In both of these efforts the model philosophy, described above, is being used.

We believe that we are now close to having a first order set of models that describe the near earth environment. The magnetic field and atmospheric density models now exist. The procedures for developing the associated electric field model have been developed with support from the ONR. These models together with the ionospheric electron density model now under construction can be used to test the possibility of predicting near earth environmental behavior. Such a test would be valuable in at least two ways. First, it would serve to verify the accuracy of the models. Second, it would demonstrate that at least some bulk parameters describing the environment can be predicted. The second item is particularly important since such a test would call modeling efforts to the attention of many people caring for and optimizing the performance of hardware systems. One such test of predictive capability might be performed

as follows. Data from the SOLRAD-HI and HELIOS satellites on solar wind parameters could be used as input to the magnetic field model. Variation in magnetic field topology calculated with the model could be used as input to the neutral atmospheric density and ionospheric electron density models to indicate the location and extent of charged particle energy sources. The satellite data would be used directly to provide inputs on the intensity of the charged particle fluxes. The ionosphere and atmosphere models could then be used to "predict" several parameters that could be checked against truth data provided by polar orbiting satellites such as those used on the DMSP satellites. Such an effort would at the same time permit questions on systems problems to be answered. Examples are: What is the optimal data sampling rate? Is the satellite coverage adequate? What are the optimum orbits for this monitoring function? Are the data the best for this monitoring/predicting purpose or should new sensors be developed?

Compatibility of models must also be tested. Each model must individually be examined to guarantee that meaningful input parameters have been used. The set of models should also be checked to make certain they provide the proper output parameters. (The output parameters should provide meaningful input to other codes that will be used to compute such things as radio wave paths through the ionosphere, the trajectories of satellites and missiles moving in the earth's atmosphere and radiation dose rates for components and man in space.)

In addition to their practical applications, this zero order set of models should also make possible several pure research endeavors that previously could not be considered. An example is the study of upper atmospheric winds on a global scale. The density of the earth's upper atmosphere and the electron density in the ionosphere are necessary inputs to such a study. It would be hoped that such scientific studies at the basic research level would provide the new insights necessary to improve these models and make them even more useful for the prediction of near earth environmental effects on hardware systems. We are also quite interested in the interaction of electric and magnetic fields with charged particles and would hope that these models could be used to quantitatively study many charged particle phenomena in the

earth's magnetosphere. We believe that the use of quantitative field models will make possible the quantitative explanation of several storm time and magnetospheric substorm associated phenomena observed over short periods of time.

The realization that quantitative models are necessary for both basic and applied research led us to propose that a conference be held on "Quantitative Magnetospheric Models". The conference was held May 6-8 in La Jolla Shores, California, with the American Geophysical Union as the prime scientific sponsor. AFOSR, ONR, AIAA, and MDAC also supported this conference. A summary of the conference is given in Appendix C. A summary of the meeting was presented to the 10th ESCAB symposium (Vienna), the annual (Washington) meeting of the AGU, and to the IMS Workshop at the IUGG (Grenoble) meeting. At the IUGG meeting, IAGA formed a new working group on Quantitative Models with W.P. Olson as its Chairman. The models developed under the present contract will be considered by that working group for use during the IMS.

Since completion of work on the magnetic field model, over 50 requests for information concerning the model have been made and over 35 copies of the computer subroutine that computes the magnetic field have been distributed to users. In addition to the successful tests of the model listed above, the model has been used by various groups for such purposes as determining the foot of the field line that passes through the ATS satellite and the location of ground stations for the GEOS satellite. The model has also been used to successfully predict the trajectory of a rocket such that it could emit a beam of electrons and later in its flight be in the proper position to detect some of those electrons moving back along magnetic field lines after being reflected at the mirror point. It is hoped that the atmospheric density model will also become a useful tool for the research community. We firmly feel that both models will ultimately have many practical uses.

Under this contract, a program to examine the influence of the solar wind on the near earth environment was initiated. The goal of ultimately predicting the behavior of the environment was kept in mind throughout the performance of

the contract. Quantitative models of the dayside cusp, total magnetospheric magnetic field, and neutral density of the upper atmosphere were developed. We are confident that ultimately these models or their derivatives will be important inputs to a hardware/software system for quantitatively predicting environmental behavior and effects on hardware. We have also been pleased to find that these practical tools have already been used by our group and many others to perform interesting and vital basic research.

The investigators wish to thank AFOSR for its support of this work. They greatfully acknowledge computational help provided by M. B. Baker.

7.0 APPENDICES

7.1 Appendix A: SUBROUTINE BXYZ

A quantitative model of the distributed currents and their associated magnetic field has been developed (Olson 1974; Olson and Pfitzer, 1974). This model has been used together with a model of the magnetopause currents (Olson, 1969) and a dipole representation of the earth's main field to represent the total magnetospheric magnetic field, $\vec{B}$. For one of a kind calculations (constant $\vec{B}$ contours, ΔB contours, S_q patterns, etc.), $\vec{B}$ is accurately determined by direct integration over the current systems. However, for repeated usage (calculation of particle trajectories, field lines, drift shells, etc.), direct integration is too expensive and instead an analytic representation must be used with some loss of accuracy.

The subroutine BXYZ returns an analytic representation of $\vec{B}$. The components of $\vec{B}$ are given in series form. The coefficients to the series were computed by a generalized multi-variable orthonormal fitting program (Pfitzer, 1973). For both the boundary and distributed currents, the field contributions were obtained at over 600 points in one quadrant of the magnetosphere by direct integration. (The model magnetosphere considered here exhibits symmetry about the XZ and XY planes.) The fitting program was then used to find the coefficients of a series expansion for each of the components of $\vec{B}$. The average error in the three components of the field (determined by comparing $\vec{B}$ calculated by direct integration over the two current systems with the values given by the series representation) is 9.8% or .63γ.

It is necessary to use a large number of terms in the series expansion because the field from the distributed and magnetopause currents is quite structured especially in the near earth region. The expansions are:

$$BX = \sum_{i=0}^{6} \sum_{j=0}^{3} \sum_{k=0}^{3} a_{ijk} \; X^i \; Y^{2j} \; Z^{2k+1} + b_{ijk} \; X^i \; Y^{2j} \; Z^{2k+1} \; e^{-DR^2}$$

$$BY = \sum_{i=0}^{6} \sum_{j=0}^{3} \sum_{k=0}^{3} c_{ijk} \; X^i \; Y^{2j+1} \; Z^{2k+1} + d_{ijk} \; X^i \; Y^{2j+1} \; Z^{2k+1} \; e^{-ER^2}$$

$$BZ = \sum_{i=o}^{6} \sum_{j=o}^{3} \sum_{k=o}^{3} e_{ijk}\ X^i\ Y^{2j}\ Z^{2k} + f_{ijk}\ X^i\ Y^{2j}\ Z^{2k}\ e^{-FR^2}$$

$$a_{ijk} = b_{ijk} = 0 \quad \text{if} \quad i + 2j + 2k + 1 > 7$$

$$c_{ijk} = d_{ijk} = 0 \quad \text{if} \quad i + 2j + 2k + 2 > 7$$

$$e_{ijk} = f_{ijk} = 0 \quad \text{if} \quad i + 2j + 2k > 7$$

X, Y, and Z are the coordinates (in earth radii) at which the field is to be found. X is toward the sun, Z is perpendicular to X and coincident with the dipole (the model represents zero tilt). Y is such as to form a right-handed coordinate system. The constants D, E and F are adjusted to give the smallest total error to the least squares fit. $R^2 \equiv X^2 + Y^2 + Z^2$

The expansion is valid only in the following region. For points closer to the sun than X = -5 R_E the expansion is valid within a 16 R_E half sphere centered at X = -5 R_E. For points further down the tail than -5 R_E the region of validity is defined by a cylindrical surface about the X axis where the diameter of the cylinder increases with increasing X. The diameter of the cylinder is given by

$$\frac{18 \cdot (10 - 3 \cdot X)}{10 - X} + 2$$

X must be greater than -68 R_E. Since a high order series was used the series diverges rapidly outside the region of validity. The computer program contains a check on the input position where $\vec{B}$ is to be determined. If it is outside the region of validity the field is set to the dipole value and an error message is printed. The series does not accurately represent the external sources for r < 1.5 R_E and therefore should not be used for determining variations near the earth. The external sources in this region constitute less than 1% of the total field and therefore the total field is not affected by the loss of accuracy of the series.

The subroutine is written in Fortran IV. Its calling sequence is:

CALL BXYZ (X, B, BMAG)

X is a three-dimensional input array where X(1), X(2), and X(3) are respectively the X, Y, and Z coordinates (in R_E) in solar magnetospheric coordinates.

B is a three-dimensional output array where B(1), B(2), and B(3) are respectively the X, Y, and Z components of B. BMAG is the scalar magnitude of $\vec{B}$. The magnetic field is expressed in gauss and includes the contribution of the boundary and distributed currents as well as a dipole main field.

Although the data points input to the least squares program (i.e., the integration over the currents) guarantee that $\vec{\nabla} \cdot \vec{B} = 0$, the least squares program does not force $\vec{\nabla} \cdot \vec{B}$ to equal zero. Therefore, $\vec{\nabla} \cdot \vec{B} \neq 0$ in the expansion. It has been verified that $\vec{\nabla} \times \vec{B}$ of the analytic series expansion does indeed reproduce approximately the currents which were initially input into the program.

If a better representation for the main field is required the dipole representation can be replaced by a more accurate version of the main field.

A listing of BXYZ, a test program, and some sample output follow. A copy of this deck is available upon request.

```
      PROGRAM BTEST(OUTPUT,TAPE6=OUTPUT)
C   THIS PROGRAM TESTS SUBROUTINE BXYZ
      DIMENSION X(3),B(3)
      LNCNT=100
      DO 1 I=1,65,6
      X(1)=11-I
      DO 1 J=1,13,6
      X(2)=J-7
      DO 1 K=1,13,6
      X(3)=K-7
C   THE IF-TESTS DEFINE THE REGION OVER WHICH THE B-FIELD EXPANSION IS
C   DEFINED
C   EXIT IF THE POSITION IS OUTSIDE THE REGION OF VALIDITY
      IF(X(1).LT.-5.) GO TO 5
      IF(((X(1)+5.)**2+X(2)**2+X(3)**2).GT.256.) GO TO 1
      GO TO 6
 5    IF(((X(2)**2+X(3)**2).GE.((9.*(10.-3.*X(1))/(10.-X(1)))+1.)**
     *2.).OR.(X(1).LT.-68.)) GO TO 1
6     CALL BXYZ(X,B,BMAG)
      LNCNT=LNCNT+1
      IF(LNCNT.LT.55) GO TO 20
      LNCNT=0
      WRITE(6,10)
10    FORMAT(1H1,/,5X,3HXSM,7X,3HYSM,7X,3HZSM,7X,2HBX,8X,2HBY,8X,2HBZ,
     *8X,4HBMAG,//)
20    WRITE(6,100) X,B,BMAG
100    FORMAT(1H ,7F10.5)
1     CONTINUE
      END
```

```
      SUBROUTINE BXYZ(XX,BB,BMAG)
C
C  VERSION MAY 4, 1973  RECODED AUGUST 10, 1973
C  CODE MODIFIED NOVEMBER 6, 1975
C  THIS SUBROUTINE RETURNS THE MAGNETIC FIELD FROM THE MAGNETOPAUSE CURRENTS,
C  CURRENTS DISTRIBUTED THROUGHOUT THE MAGNETOSPHERE, AND A DIPOLAR
C  REPRESENTATION OF THE MAIN MAGNETIC FIELD OF THE EARTH.  A GENERALIZED
C  ORTHONORMAL LEAST SQUARES PROGRAM WAS USED TO CALCULATE THE COEFFICIENTS
C  OF A POWER SERIES THROUGH SIXTH ORDER WITH EXPONENTIAL TERMS.  THE
C  POSITION OF THE POINT WHERE THE FIELD IS TO BE FOUND IS INPUT AS A 3
C  COMPONENT ARRAY,XX.  XX(I),XX(2),AND XX(3) ARE RESPECTIVELY THE X,Y,AND
C  Z COORDINATES OF THE POINT GIVEN IN EARTH RADII IN SOLAR MAGNETOSPHERIC
C  COORDINATES.  THE MAGNETIC FIELD IS RETURNED IN THE ARRAY BB.  THE X,Y,AND
C  Z COMPONENTS OF THE FIELD ARE RESPECTIVELY BB(1),BB(2),AND BB(3).  THE
C  FIELD IS RETURNED IN GAUSS.  (X IS POSITIVE IN THE SOLAR DIRECTION.)
C  BMAG IS THE MAGNITUDE OF THE FIELD IN GAUSS.
C
C  THIS SUBROUTINE SHOULD NOT BE USED FOR X LESS THAN -68RE.  A TEMPLATE
C  CHECKS THE LOCATION OF THE POINT AND IF THE POINT IS OUTSIDE THE
C  REGION OF SERIES CONVERGENCE THE FIELD IS SET TO THE DIPOLE VALUE AND
C  AN ERROR MESSAGE IS ISSUED.
C
C  DO NOT USE THIS SUBROUTINE FOR DETERMINING VARIATIONS NEAR THE
C  EARTH.  THE LEAST SQUARES FIT DOES NOT ACCURATELY REPRESENT THE
C  EXTERNAL FIELD CONTRIBUTION FOR R LESS THAN 1.5 RE. (THE EXTERNAL
C  FIELD IS LESS THAN 1 PERCENT OF THE TOTAL FIELD IN THIS REGION).
C
C  THE VALUES FOR THE COEFFICIENTS IN THIS LISTING REPRESENT THE ENTIRE
C  EXTERNAL FIELD (BD+DS).  COEFFICIENTS REPRESENTING THE DISTRIBUTED
C  AND BOUNDARY FIELDS SEPARATELY ARE ALSO AVAILABLE.
C
C  FOR REFERENCE SEE  -THE MAGNETOSPHERIC MAGNETIC FIELD- BY W.P. OLSON
C  AND K.A. PFITZER (SEPTEMBER 74 J.G.R),  -THE DISTRIBUTED MAGNETOSPHERIC
C  CURRENTS- BY W.P. OLSON (SEPTEMBER 74 J.G.R), AND  -THE SHAPE OF THE
C  TILTED MAGNETOPAUSE- BY W.P. OLSON (J.G.R.,74,5642,1969).
C
C  PLEASE ADDRESS ANY QUESTIONS,COMMENTS OR CRITICISMS TO W.P. OLSON OR
C  K.A.PFITZER, MCDONNELL DOUGLAS ASTRONAUTICS COMPANY,
C  5301 BOLSA AVE,HUNTINGTON BEACH,CALIFORNIA,92647
C  OR PHONE (714) 896-4368 OR 896-3231
C
      DIMENSION BB(3),XX(3),A(30),B(30),C(20),D(20),E(39),F(39)          BD+DS
      DATA (A(I),I=1,30)/ 7.83174E-01, 2.88006E-03,-1.68800E-05,         BD+DS
     * 3.56869E-08,-2.28640E-03, 1.24647E-05,-1.17573E-08, 3.79774E-06, BD+DS
     *-8.62700E-09, 4.63581E-09,-8.58651E-02, 2.20713E-04, 4.41626E-07, BD+DS
     * 1.20914E-04, 3.14819E-07, 2.20886E-07,-6.07070E-03, 1.42045E-05, BD+DS
     * 6.46123E-09, 9.63390E-06, 2.63098E-09, 1.97783E-09,-1.68259E-04, BD+DS
     * 2.62119E-07, 1.80952E-07,-2.83914E-06, 1.44532E-09, 1.06634E-09, BD+DS
     *-2.97037E-08,-1.38747E-10/                                        BD+DS
      DATA (B(I),I=1,30)/-1.36002E+00, 7.80264E-02,-1.00872E-03,         BD+DS
     * 3.88102E-05, 4.68426E-02, 4.94081E-04, 3.65692E-05,-3.08892E-03, BD+DS
     * 8.27418E-05, 2.26403E-05,-2.01122E+00, 2.96513E-02,-1.50385E-04, BD+DS
     *-3.76012E-02, 3.21347E-04,-3.77516E-04, 5.42451E-01, 1.77058E-03, BD+DS
     *-6.37539E-05,-7.95695E-03,-1.02199E-04, 1.21194E-04,-2.06253E-02, BD+DS
     * 6.77865E-05,-1.37321E-03,-2.45854E-02, 2.93461E-05, 2.10455E-04, BD+DS
     *-3.88684E-04, 2.24031E-04/                                        BD+DS
      DATA (C(I),I=1,20)/-9.36032E-02, 6.97581E-05,-2.89714E-08,         BD+DS
```

```
     * 1.12435E-04,-2.29674E-07,-6.51105E-08,-9.11858E-03, 2.20257E-06, BD+DS
     *-9.71435E-10, 5.18306E-06,-4.81855E-09,-2.04812E-09,-3.78041E-04, BD+DS
     * 9.76159E-09, 9.45094E-08,-7.85671E-06,-4.81517E-11, 7.43833E-10, BD+DS
     *-8.06396E-08,-3.28896E-10/                                        BD+DS
      DATA (D(I),I=1,20)/-1.64174E+00, 2.93038E-02,-4.62707E-04,        BD+DS
     *-5.02388E-02, 3.61602E-04,-6.00587E-04, 1.19872E-01,-2.73293E-03, BD+DS
     * 3.15041E-05,-6.81062E-03, 2.00913E-05, 8.71659E-05,-3.43211E-02, BD+DS
     * 6.24163E-04,-1.74643E-03,-8.77802E-03, 2.92115E-05, 2.09335E-04, BD+DS
     *-9.57252E-04, 1.33622E-04/                                        BD+DS
      DATA (E(I),I=1,39)/ 1.00382E+02,-4.51830E-01, 2.47545E-04,        BD+DS
     * 1.13197E-07,-1.81773E-01, 3.47042E-04,-4.17901E-07, 2.60957E-04, BD+DS
     *-2.12733E-07, 1.16209E-07, 1.00713E+01,-4.30035E-02, 1.32877E-05, BD+DS
     * 1.84477E-09,-1.03666E-02, 1.09399E-05,-6.71731E-09, 1.76089E-05, BD+DS
     *-1.92875E-09, 2.53223E-09, 4.12689E-01,-1.71790E-03, 2.27366E-07, BD+DS
     *-1.05062E-04, 1.00609E-07, 3.73228E-07, 8.44098E-03,-3.48509E-05, BD+DS
     * 1.23824E-09, 3.63487E-06, 1.95769E-10, 2.45490E-09, 8.52182E-05, BD+DS
     *-3.53777E-07, 8.56056E-08, 3.32657E-07,-1.42659E-09, 4.98217E-10, BD+DS
     *-8.10951E-11/                                                     BD+DS
      DATA (F(I),I=1,39)/-1.12431E+02,-6.95878E-01,-2.82989E-03,        BD+DS
     *-1.75919E-05,-3.85656E+00, 2.21445E-02,-1.19133E-04, 5.26531E-02, BD+DS
     *-5.26914E-04,-3.10689E-04,-1.03980E+01,-3.26917E-02, 2.55292E-03, BD+DS
     *-1.85172E-06,-3.68576E-02, 3.77502E-03,-3.44933E-05, 3.25375E-04, BD+DS
     *-6.12564E-05,-2.35422E-05,-3.994445+00, 3.61904E-02, 2.27425E-04, BD+DS
     * 9.09610E-02,-1.62893E-03,-9.73721E-04,-1.14125E-02,-2.99948E-03, BD+DS
     *-8.48886E-08,-4.44055E-03,-9.02203E-05,-1.95662E-05, 1.77427E-02, BD+DS
     *-1.16655E-03,-9.74518E-04,-2.05600E-03,-3.59815E-05,-2.08878E-05, BD+DS
     *-1.58459E-04/                                                     BD+DS
      X=XX(1)
      Y=XX(2)
      Z=XX(3)
      Y2=Y**2
      Z2=Z**2
      R2=X**2+Y2+Z2
      BX=0.
      BY=0.
      BZ=0.
C   TEST FOR LOCATION OF INPUT POSITION
C   IF THE LOCATION IS OUTSIDE THE REGION OF SERIES CONVERGENCE SET
C   THE MAGNETIC FIELD TO DIPOLE AND PRINT AN ERROR MESSAGE
C   THE TEMPLATE WITHIN WHICH THE SERIES CONVERGES IS GREATER THAN THE
C   DEFINED LOCATION OF THE MAGNETOPAUSE BOUNDARY
      IF(X.LT.-5.) GO TO 5
      IF((X+5.)**2+Y2+Z2.GT.324.) GO TO 50
      GO TO 6
5     IF((Y2+Z2).GE.(9.*(10.-3.*X)/(10.-X)+3.)**2) GO TO 50
 6    EXPXY=EXP(-0.03*R2)
      EXPZ=EXP(-0.015*R2)
      II=1
      JJ=1
      KK=1
      XB=1.
      DO 30 I=1,7
      YEXB=XB
      DO 20 J=1,4
      IF(I+2*J.GT.10) GO TO 30
```

```
10      BZ=BZ+(E(KK)+F(KK)*EXPZ)*ZEYEXB
        KK=KK+1
        IF(IJK .GT.11) GO TO 20
        BX=BX+(A(II)+B(II)*EXPXY)*ZEYEXB*Z
        II=II+1
        IF(IJK .GT.10) GO TO 20
        BY=BY+(C(JJ)+D(JJ)*EXPXY)*ZEYEXB*Z*Y
        JJ=JJ+1
        ZEYEXB=ZEYEXB*Z2
        IJK=IJK+2
        IF(IJK.LE.12) GO TO 10
20      YEXB=YEXB*Y2
30      XB=XB*X
C   ADD DIPOLE FIELD AND CONVERT TO GAUSS
40      AR=-31000./(R2*R2*SQRT(R2))
        BB(1)=(3.*X*Z*AR+BX)*0.00001
        BB(2)=(3.*Y*Z*AR+BY)*0.00001
        BB(3)=((3.*Z2-R2)*AR+BZ)*0.00001
        BMAG=SQRT(BB(1)**2+BB(2)**2+BB(3)**2)
        RETURN
C   ERROR EXIT
 50     WRITE(6,60) XX
60      FORMAT 4H X= ,E10.3,4H Y= ,E10.3,4H Z= ,E10.3,76H  IS OUTSIDE THE
       *VALID REGION--POWER SERIES DIVERGES BFIELD IS SET TO DIPOLE)
        GO TO 40
        END
```

XSM	YSM	ZSM	BX	BY	BZ	BMAG
10.00000	0.00000	0.00000	0.00000	0.00000	.00101	.00101
4.00000	-6.00000	-6.00000	.00031	-.00063	.00014	.00072
4.00000	-6.00000	0.00000	0.00000	0.00000	.00086	.00086
4.00000	-6.00000	6.00000	-.00031	.00063	.00014	.00072
4.00000	0.00000	-6.00000	.00113	0.00000	-.00071	.00133
4.00000	0.00000	0.00000	0.00000	0.00000	.00462	.00462
4.00000	0.00000	6.00000	-.00113	0.00000	-.00071	.00133
4.00000	6.00000	-6.00000	.00031	.00063	.00014	.00072
4.00000	6.00000	0.00000	0.00000	0.00000	.00086	.00086
4.00000	6.00000	6.00000	-.00031	-.00063	.00014	.00072
-2.00000	-6.00000	-6.00000	-.00036	-.00082	-.00025	.00093
-2.00000	-6.00000	0.00000	0.00000	0.00000	.00100	.00100
-2.00000	-6.00000	6.00000	.00036	.00082	-.00025	.00093
-2.00000	0.00000	-6.00000	-.00127	0.00000	-.00213	.00248
-2.00000	0.00000	0.00000	0.00000	0.00000	.03856	.03856
-2.00000	0.00000	6.00000	.00127	0.00000	-.00213	.00248
-2.00000	6.00000	-6.00000	-.00036	.00082	-.00025	.00093
-2.00000	6.00000	0.00000	0.00000	0.00000	.00100	.00100
-2.00000	6.00000	6.00000	.00036	-.00082	-.00025	.00093
-8.00000	-6.00000	-6.00000	-.00036	-.00027	.00004	.00045
-8.00000	-6.00000	0.00000	0.00000	0.00000	.00037	.00037
-8.00000	-6.00000	6.00000	.00036	.00027	.00004	.00045
-8.00000	0.00000	-6.00000	-.00061	0.00000	-.00012	.00062
-8.00000	0.00000	0.00000	0.00000	0.00000	.00034	.00034
-8.00000	0.00000	6.00000	.00061	0.00000	-.00012	.00062
-8.00000	6.00000	-6.00000	-.00036	.00027	.00004	.00045
-8.00000	6.00000	0.00000	0.00000	0.00000	.00037	.00037
-8.00000	6.00000	6.00000	.00036	-.00027	.00004	.00045
-14.00000	-6.00000	-6.00000	-.00016	-.00005	.00007	.00018
-14.00000	-6.00000	0.00000	0.00000	0.00000	.00020	.00020
-14.00000	-6.00000	6.00000	.00016	.00005	.00007	.00018
-14.00000	0.00000	-6.00000	-.00023	0.00000	.00006	.00024
-14.00000	0.00000	0.00000	0.00000	0.00000	.00025	.00025
-14.00000	0.00000	6.00000	.00023	0.00000	.00006	.00024
-14.00000	6.00000	-6.00000	-.00016	.00005	.00007	.00018
-14.00000	6.00000	0.00000	0.00000	0.00000	.00020	.00020
-14.00000	6.00000	6.00000	.00016	-.00005	.00007	.00018
-20.00000	-6.00000	-6.00000	-.00009	-.00001	.00005	.00010
-20.00000	-6.00000	0.00000	0.00000	0.00000	.00007	.00007
-20.00000	-6.00000	6.00000	.00009	.00001	.00005	.00010
-20.00000	6.00000	-6.00000	-.00010	0.00000	.00005	.00011
-20.00000	0.00000	0.00000	0.00000	0.00000	.00008	.00008
-20.00000	0.00000	6.00000	.00010	0.00000	.00005	.00011
-20.00000	6.00000	-6.00000	-.00009	.00001	.00005	.00010
-20.00000	6.00000	0.00000	0.00000	0.00000	.00007	.00007
-20.00000	6.00000	6.00000	.00009	-.00001	.00005	.00010
-26.00000	-6.00000	-6.00000	-.00006	-.00000	.00004	.00007
-26.00000	-6.00000	0.00000	0.00000	0.00000	.00005	.00005
-26.00000	-6.00000	6.00000	.00006	.00000	.00004	.00007
-26.00000	0.00000	-6.00000	-.00007	0.00000	.00004	.00008
-26.00000	0.00000	0.00000	0.00000	0.00000	.00005	.00005
-26.00000	0.00000	6.00000	.00007	0.00000	.00004	.00008
-26.00000	6.00000	-6.00000	-.00006	.00000	.00004	.00007
-26.00000	6.00000	0.00000	0.00000	0.00000	.00005	.00005
-26.00000	6.00000	6.00000	.00006	-.00000	.00004	.00007

XSM	YSM	ZSM	BX	BY	BZ	BMAG
-32.00000	-6.00000	-6.00000	-.00005	-.00000	.00002	.00006
-32.00000	-6.00000	0.00000	0.00000	0.00000	.00003	.00003
-32.00000	-6.00000	6.00000	.00005	.00000	.00002	.00006
-32.00000	0.00000	-6.00000	-.00005	0.00000	.00002	.00006
-32.00000	0.00000	0.00000	0.00000	0.00000	.00003	.00003
-32.00000	0.00000	6.00000	.00005	0.00000	.00002	.00006
-32.00000	6.00000	-6.00000	-.00005	.00000	.00002	.00006
-32.00000	6.00000	0.00000	0.00000	0.00000	.00003	.00003
-32.00000	6.00000	6.00000	.00005	-.00000	.00002	.00006
-38.00000	-6.00000	-6.00000	-.00004	-.00000	.00002	.00004
-38.00000	-6.00000	0.00000	0.00000	0.00000	.00002	.00002
-38.00000	-6.00000	6.00000	.00004	.00000	.00002	.00004
-38.00000	0.00000	-6.00000	-.00004	0.00000	.00002	.00004
-38.00000	0.00000	0.00000	0.00000	0.00000	.00002	.00002
-38.00000	0.00000	6.00000	.00004	0.00000	.00002	.00004
-38.00000	6.00000	-6.00000	-.00004	.00000	.00002	.00004
-38.00000	6.00000	0.00000	0.00000	0.00000	.00002	.00002
-38.00000	6.00000	6.00000	.00004	-.00000	.00002	.00004
-44.00000	-6.00000	-6.00000	-.00003	-.00000	.00001	.00003
-44.00000	-6.00000	0.00000	0.00000	0.00000	.00001	.00001
-44.00000	-6.00000	6.00000	.00003	.00000	.00001	.00003
-44.00000	0.00000	-6.00000	-.00003	0.00000	.00001	.00003
-44.00000	0.00000	0.00000	0.00000	0.00000	.00001	.00001
-44.00000	0.00000	6.00000	.00003	0.00000	.00001	.00003
-44.00000	6.00000	-6.00000	-.00003	.00000	.00001	.00003
-44.00000	6.00000	0.00000	0.00000	0.00000	.00001	.00001
-44.00000	6.00000	6.00000	.00003	-.00000	.00001	.00003
-50.00000	-6.00000	-6.00000	-.00002	-.00000	.00001	.00003
-50.00000	-6.00000	0.00000	0.00000	0.00000	.00001	.00001
-50.00000	-6.00000	6.00000	.00002	.00000	.00001	.00003
-50.00000	0.00000	-6.00000	-.00003	0.00000	.00001	.00003
-50.00000	0.00000	0.00000	0.00000	0.00000	.00001	.00001
-50.00000	0.00000	6.00000	.00003	0.00000	.00001	.00003
-50.00000	6.00000	-6.00000	-.00002	.00000	.00001	.00003
-50.00000	6.00000	0.00000	0.00000	0.00000	.00001	.00001
-50.00000	6.00000	6.00000	.00002	-.00000	.00001	.00003

7.2 Appendix B: SUBROUTINE ATMOS

A quantitative global model of the neutral density of the upper atmosphere has been developed and is discussed in the text of this report. This model has been coded in FORTRAN IV. It can be used from 0 km to well above 500 km. The details and functions used to construct the model are discussed in the body of the text. The relationship between the mathematical symbols used in the text and the FORTRAN names are defined in Table B-1.

The calling sequence for the subroutine is CALL ATMOS (RR,XLAT,XLONG,DATE, UT,DEN)

RR is the altitude in km. The model was constructed to primarily represent the density between 120-450 km. Below 120 km a 7th order fit to CIRA 72 is included for completeness. The model can be used above 450 km; the density, however, drops off more rapidly than observed.

XLAT is the geographic latitude in degrees (-90.° to +90.°) + representing North.

XLONG is the geographic East longitude in degrees (0.° to +360.°)

DATE is the day of year (1. to 366.)

UT is the universal time in hours (0. to 24. hrs)

DEN is the output density in gm/cm^3.

Additional parameters are available thru the labeled COMMON block PARAM
COMMON/PARAM/BIGF,FBAR,CLZ,SZ,EOZ,ALPHA

These 6 variables of the COMMON are preset by a BLOCK DATA routine. Their respective meanings are given in table B-1 and their default values are given in Table B-2. The default values should be modified to suit solar cycle and particle precipitation conditions in effect at the time of the density calculation.

A listing of Subroutine ATMOS along with a test program (ATTST) and sample output follow. A copy of this deck is available upon request.

TABLE B-1

Parameter Identification

Mathematical symbols used in the text	FORTRAN name	Parameter description as used by the FORTRAN routine
z	RR	Altitude in kilometers
λ	XLAT	geographic latitude (-90 to + 90) + is north
ϕ	XLONG	East geographic longitude (0-360)
D	DATE	Day of Year (1-366)
T	UT	Universal time (0-24 hrs.)
ρ	DEN	Output density in gm/cm^3
F	BIGF	10 cm solar flux in units of 10^{-22} watts/m^2/Hz
$\overline{F}$	FBAR	3 month average 10 cm solar flux in units of 10^{-22} watts/m^2/Hz
$90 - \lambda_{mc}$	CLZ	Northern geomagnetic co-latitude in degrees of the cusp center
Σ	SZ	Half width in degrees (longitudinal) of the cusp heating region
ϵ_o	EOZ	Half width in degrees (latitudinal) of the cusp heating region
I	ALPHA	Cusp particle heating parameter. Relationship to interplanetary particle fluxes has not yet been determined. I=.15 is a value consistent with quiet conditions.

Table B-2

Default Values for Variables in COMMON block PARAM

FORTRAN Name	Math. Symbol	Default Value
BIGF	F	115.
FBAR	$\bar{F}$	115.
CLZ	$90 - \lambda_{mc}$	15.
SZ	Σ	90.
EOZ	ϵ_o	25.
ALPHA	I	0.15

```
      PROGRAM ATTST(OUTPUT,TAPE6=OUTPUT)
C   THIS PROGRAM PROVIDES A SAMPLE OUTPUT FROM THE DENSITY SUBROUTINE
      COMMON/PARAM/BIGF,FBAR,CLZ,SZ,EOZ,ALPHA
      DIMENSION ARRAY(18)
      DATE=0.
      UT=0.
      ALT=400.
      DO 50 IA=1,2
      ALT=200+(IA-1)*200
      LINE=13
 10    FORMAT(10H1ALTITUDE=,F7.2,7H  DATE=,F5.0,7H  TIME=,F6.2)
      DO 50 I=1,72,3
      IF(LINE.LT.12) GO TO 15
      LINE=0
      WRITE(6,10)ALT,DATE,UT
 15   LINE=LINE+1
      XLONG=(I-1)*5
      WRITE(6,20) XLONG
 20   FORMAT(14H0E. LONGITUDE=,F7.2,52H  LATITUDE VARIES FROM +85 TO -85
     * IN STEPS OF 10 DEG)
      DO 30 J=1,18
      XLAT=95-J*10
 30   CALL ATMOS(ALT,XLAT,XLONG,DATE,UT,ARRAY(J))
      WRITE(6,40) ARRAY
 40   FORMAT(6E11.3)
 50   CONTINUE
      END
```

```
      SUBROUTINE ATMOS(RR,XLAT,XLONG,DATE,UT,DEN)
C-----------------
C         VERSION 11/25/75
C         THIS DENSITY MODEL WAS DEVELOPED AS PART OF AIR FORCE OFFICE OF
C         SCIENTIFIC RESEARCH CONTRACT NO. F44620-72-C-0084.  IT WAS
C         CONSTRUCTED TO PRIMARILY DESCRIBE TOTAL DENSITY FOR THE
C         ALTITUDE RANGE 120-450 KM. BELOW 120 KM A 7TH ORDER FIT TO
C         CIRA 72 IS INCLUDED FOR COMPLETENESS.  ALTHOUGH USEABLE ABOVE
C         450 KM, THE DENSITY DROPS OFF MORE RAPIDLY THAN OBSERVED.
C         THE DEVELOPEMENT OF THIS FORTRAN DECK IS DESCRIBED IN DETAIL
C         IN THE FINAL CONTRACT REPORT (DEC. 75).  EARLIER INTERIM
C         CONTRACT REPORTS DETAIL THE DEVELOPEMENT OF THE FUNCTIONS AND
C         DESCRIBE THE CORPUSCULAR ENERGY SOURCE.
C         QUESTIONS CONCERNING THE MODEL SHOULD BE ADDRESSED TO
C         K.A. PFITZER MCDONNEL DOUGLAS ASTRONAUTICS COMPANY 5301 BOLSA
C         AVE. HUNTINGTON BEACH CALIFORNIA 92647
C         OR PHONE (714) 896-3231/896-4368.
C
C--------------ARGUMENTS
C         RR = ALTITUDE (IN KM)
C         XLAT = LATITUDE (0. TO +-90. DEGREES)
C         XLONG = E. LONGITUDE (0. TO 360. DEGREES)
C         DATE = DAY OF YEAR (1. TO 366. DAYS)
C         UT = TIME (0. TO 24. HRS OF UNIVERSAL TIME)
C         DEN = OUTPUT DENSITY (GM/CM**3)
C
C--------------THE FOLLOWING ADDITIONAL PARAMETERS ARE AVAILABLE THRU
C         THE COMMON BLOCK PARAM.  A BLOCK DATA ROUTINE PRESETS
C         THESE PARAMETERS -- THEY MAY BE MODIFIED TO SUIT
C         EXISTING ATMOSPHERIC CONDITIONS
C
C         BIGF  10 CM SOLAR FLUX IN UNITS OF 10**-22 WATTS/M**2/HZ
C         FBAR  3 MONTH AVERAGE SOLAR FLUX  SAME UNITS AS BIGF
C         CLZ   IS THE NORTHERN GEOMAGNETIC CO-LATITUDE OF THE CUSP CENTER
C         SZ    IS THE HALF-WIDTH (LONGITUDINAL) OF THE CUSP HEATING
C               REGION
C         EOZ   IS THE HALF-WIDTH (LATITUDINAL) OF THE CUSP HEATING
C               REGION
C         ALPHA IS THE PARTICLE HEATING PARAMETER
C
C--------------
C         SEE APPENDIX B OF THE FINAL REPORT FOR ADDITIONAL SYMBOL
C         DEFINITIONS
C-----------------
      COMMON/PARAM/BIGF,FBAR,CLZ,SZ,EOZ,ALPHA
      DATA SA1,SA2,SA3,SB1,SB2,SB3/.1427,-.1957,-.0424,.0098,-.1371,
     *-.0116/
      DATA SR1,SR2,SR3,SR4/-.02,.27E-2,-.85E-6,-.59E-9/
      DATA CR0,CR1,CR2,CR3,CR4,CR5,CR6,CR7/1.2252E-3,-.8015593E-1,
```

```
 30    IF(ABS(CMLAT-CLX).GT.E0) GO TO 80
       S=RAD*SZ
C--------DETERMINE MAGNETIC LONGITUDE
       CMLONG=0.
       IF(CMLAT.LT.0.00001)GO TO 35
       ZCOS=CT1*COLATS*PC1C-COLATC*ST1
       ZSIN=CDLATS*SIN(P-C1)
       CMLONG=ATAN2(ZSIN,ZCOS)
C--------CW = MAGNETIC LONGITUDE OF CUSP CENTER
 35    CW=PI2*((16.6-UT)/24.)
       IF(CW.GT.PI) CW=CW-PI2
C--------DLAM = DISTANCE IN MAG. LONG. FROM CENTER OF CUSP
       DLAM=CMLONG-CW
       IF(DLAM.LT.0.) DLAM=DLAM+PI2
       IF(DLAM.GT.PI) DLAM=PI2-DLAM
       IF(DLAM.GT.S) GO TO 40
       XL1=D1-G8*DLAM/S
       E=CMLAT-CLX
       GO TO 70
 40    XL1=D1-G8
       E=ACOS(CMLATC*COSCLX+SIN(CMLAT)*SINCL*COS(DLAM-S))
C--------CUSP HEATING EFFECT
 70    IF(ABS(E).LE.E0)C=ALPHA*XL1*(1.+BETA*COS(PI*E/E0))*(1.-EXP((120.-R
      *)/H))
C--------TOTAL DENSITY
 80    DEN=2.7E-11*V*(1.+C)*EXP((120.-R)/((.99+.518*UVF)*SQRT(R-103.)))
      **(1.+SEMIAN)
       RETURN
 120   CDN=1
       IF(R.LT.90.)  CON=EXP(-(R-90.)**2/200.)
C--------CALCULATE CIRA ATMOSPHERE
       ALT=((((((CR7*R+CR6)*R+CR5)*R+CR4)*R+CR3)*R+CR2)*R+CR1)*R
       DEN=CR0*EXP(ALT)*(1.+SEMIAN*CON)
       RETURN
       END
```

```
      BLOCK DATA ATMOSP
      COMMON/PARAM/BIGF,FBAR,CLZ,SZ,EOZ,ALPHA
      DATA BIGF,FBAR,CLZ,SZ,EOZ,ALPHA/115.,115.,15.,90.,25.,.15/
      END
```

ALTITUDE= 200.00 DATE= 0. TIME= 0.00

E. LONGITUDE= 0.00 LATITUDE VARIES FROM +85 TO -85 IN STEPS OF 10 DEG

.185E-12	.178E-12	.166E-12	.169E-12	.174E-12	.179E-12
.183E-12	.187E-12	.191E-12	.195E-12	.198E-12	.202E-12
.205E-12	.207E-12	.208E-12	.208E-12	.211E-12	.234E-12

E. LONGITUDE= 15.00 LATITUDE VARIES FROM +85 TO -85 IN STEPS OF 10 DEG

.186E-12	.180E-12	.165E-12	.167E-12	.171E-12	.174E-12
.178E-12	.181E-12	.185E-12	.188E-12	.192E-12	.196E-12
.200E-12	.203E-12	.205E-12	.206E-12	.209E-12	.232E-12

E. LONGITUDE= 30.00 LATITUDE VARIES FROM +85 TO -85 IN STEPS OF 10 DEG

.187E-12	.181E-12	.165E-12	.164E-12	.168E-12	.171E-12
.174E-12	.176E-12	.180E-12	.183E-12	.187E-12	.191E-12
.196E-12	.200E-12	.202E-12	.204E-12	.207E-12	.231E-12

E. LONGITUDE= 45.00 LATITUDE VARIES FROM +85 TO -85 IN STEPS OF 10 DEG

.188E-12	.182E-12	.164E-12	.163E-12	.166E-12	.168E-12
.170E-12	.173E-12	.176E-12	.179E-12	.183E-12	.188E-12
.193E-12	.197E-12	.200E-12	.204E-12	.206E-12	.230E-12

E. LONGITUDE= 60.00 LATITUDE VARIES FROM +85 TO -85 IN STEPS OF 10 DEG

.189E-12	.181E-12	.164E-12	.162E-12	.165E-12	.167E-12
.169E-12	.171E-12	.174E-12	.177E-12	.181E-12	.186E-12
.191E-12	.196E-12	.202E-12	.214E-12	.214E-12	.230E-12

E. LONGITUDE= 75.00 LATITUDE VARIES FROM +85 TO -85 IN STEPS OF 10 DEG

.191E-12	.179E-12	.163E-12	.163E-12	.166E-12	.168E-12
.170E-12	.173E-12	.175E-12	.179E-12	.183E-12	.188E-12
.192E-12	.197E-12	.217E-12	.233E-12	.224E-12	.231E-12

E. LONGITUDE= 90.00 LATITUDE VARIES FROM +85 TO -85 IN STEPS OF 10 DEG

.193E-12	.181E-12	.164E-12	.165E-12	.169E-12	.172E-12
.175E-12	.179E-12	.182E-12	.185E-12	.189E-12	.194E-12
.198E-12	.206E-12	.235E-12	.251E-12	.232E-12	.233E-12

E. LONGITUDE= 105.00 LATITUDE VARIES FROM +85 TO -85 IN STEPS OF 10 DEG

.195E-12	.184E-12	.166E-12	.170E-12	.175E-12	.180E-12
.185E-12	.189E-12	.193E-12	.197E-12	.201E-12	.204E-12
.207E-12	.217E-12	.251E-12	.264E-12	.235E-12	.236E-12

E. LONGITUDE= 120.00 LATITUDE VARIES FROM +85 TO -85 IN STEPS OF 10 DEG

.198E-12	.189E-12	.171E-12	.177E-12	.185E-12	.192E-12
.198E-12	.204E-12	.209E-12	.213E-12	.217E-12	.219E-12
.220E-12	.230E-12	.270E-12	.286E-12	.258E-12	.239E-12

E. LONGITUDE= 135.00 LATITUDE VARIES FROM +85 TO -85 IN STEPS OF 10 DEG

.201E-12	.196E-12	.178E-12	.185E-12	.195E-12	.205E-12
.214E-12	.221E-12	.227E-12	.232E-12	.235E-12	.236E-12
.235E-12	.241E-12	.286E-12	.311E-12	.289E-12	.243E-12

E. LONGITUDE= 150.00 LATITUDE VARIES FROM +85 TO -85 IN STEPS OF 10 DEG

.205E-12	.206E-12	.188E-12	.194E-12	.207E-12	.219E-12
.230E-12	.239E-12	.246E-12	.251E-12	.253E-12	.253E-12
.251E-12	.250E-12	.294E-12	.332E-12	.300E-12	.248E-12

E. LONGITUDE= 165.00 LATITUDE VARIES FROM +85 TO -85 IN STEPS OF 10 DEG

.208E-12	.218E-12	.200E-12	.202E-12	.217E-12	.232E-12
.244E-12	.255E-12	.263E-12	.268E-12	.271E-12	.270E-12
.265E-12	.259E-12	.293E-12	.331E-12	.308E-12	.254E-12

ALTITUDE= 200.00 DATE= 0. TIME= 0.00

E. LONGITUDE= 180.00 LATITUDE VARIES FROM +85 TO -85 IN STEPS OF 10 DEG
.211E-12 .231E-12 .215E-12 .209E-12 .226E-12 .242E-12
.256E-12 .268E-12 .277E-12 .283E-12 .285E-12 .283E-12
.277E-12 .269E-12 .280E-12 .317E-12 .308E-12 .258E-12

E. LONGITUDE= 195.00 LATITUDE VARIES FROM +85 TO -85 IN STEPS OF 10 DEG
.212E-12 .244E-12 .234E-12 .216E-12 .232E-12 .249E-12
.265E-12 .277E-12 .287E-12 .292E-12 .294E-12 .292E-12
.286E-12 .276E-12 .271E-12 .301E-12 .304E-12 .260E-12

E. LONGITUDE= 210.00 LATITUDE VARIES FROM +85 TO -85 IN STEPS OF 10 DEG
.212E-12 .255E-12 .252E-12 .226E-12 .235E-12 .253E-12
.268E-12 .281E-12 .291E-12 .297E-12 .299E-12 .296E-12
.290E-12 .279E-12 .267E-12 .284E-12 .295E-12 .261E-12

E. LONGITUDE= 225.00 LATITUDE VARIES FROM +85 TO -85 IN STEPS OF 10 DEG
.210E-12 .261E-12 .261E-12 .236E-12 .235E-12 .252E-12
.268E-12 .281E-12 .290E-12 .296E-12 .298E-12 .296E-12
.289E-12 .279E-12 .265E-12 .269E-12 .283E-12 .260E-12

E. LONGITUDE= 240.00 LATITUDE VARIES FROM +85 TO -85 IN STEPS OF 10 DEG
.207E-12 .250E-12 .262E-12 .244E-12 .232E-12 .248E-12
.263E-12 .275E-12 .285E-12 .290E-12 .292E-12 .290E-12
.284E-12 .275E-12 .262E-12 .257E-12 .272E-12 .259E-12

E. LONGITUDE= 255.00 LATITUDE VARIES FROM +85 TO -85 IN STEPS OF 10 DEG
.201E-12 .234E-12 .254E-12 .245E-12 .229E-12 .241E-12
.255E-12 .266E-12 .275E-12 .280E-12 .282E-12 .281E-12
.276E-12 .267E-12 .256E-12 .248E-12 .261E-12 .257E-12

E. LONGITUDE= 270.00 LATITUDE VARIES FROM +85 TO -85 IN STEPS OF 10 DEG
.196E-12 .213E-12 .238E-12 .237E-12 .223E-12 .231E-12
.243E-12 .254E-12 .262E-12 .267E-12 .270E-12 .269E-12
.264E-12 .257E-12 .248E-12 .239E-12 .253E-12 .254E-12

E. LONGITUDE= 285.00 LATITUDE VARIES FROM +85 TO -85 IN STEPS OF 10 DEG
.190E-12 .192E-12 .223E-12 .226E-12 .214E-12 .220E-12
.231E-12 .240E-12 .248E-12 .253E-12 .255E-12 .255E-12
.252E-12 .247E-12 .239E-12 .231E-12 .243E-12 .250E-12

E. LONGITUDE= 300.00 LATITUDE VARIES FROM +85 TO -85 IN STEPS OF 10 DEG
.185E-12 .183E-12 .206E-12 .206E-12 .200E-12 .209E-12
.218E-12 .226E-12 .233E-12 .238E-12 .240E-12 .241E-12
.240E-12 .236E-12 .231E-12 .224E-12 .235E-12 .247E-12

E. LONGITUDE= 315.00 LATITUDE VARIES FROM +85 TO -85 IN STEPS OF 10 DEG
.183E-12 .173E-12 .185E-12 .185E-12 .191E-12 .199E-12
.207E-12 .214E-12 .219E-12 .224E-12 .227E-12 .228E-12
.228E-12 .226E-12 .223E-12 .218E-12 .227E-12 .243E-12

E. LONGITUDE= 330.00 LATITUDE VARIES FROM +85 TO -85 IN STEPS OF 10 DEG
.183E-12 .174E-12 .170E-12 .176E-12 .184E-12 .191E-12
.197E-12 .203E-12 .208E-12 .212E-12 .215E-12 .217E-12
.219E-12 .218E-12 .217E-12 .214E-12 .220E-12 .239E-12

E. LONGITUDE= 345.00 LATITUDE VARIES FROM +85 TO -85 IN STEPS OF 10 DEG
.184E-12 .176E-12 .166E-12 .172E-12 .178E-12 .184E-12
.189E-12 .194E-12 .198E-12 .202E-12 .206E-12 .209E-12
.211E-12 .212E-12 .212E-12 .210E-12 .215E-12 .236E-12

ALTITUDE= 400.00 DATE= 0. TIME= 0.00

E. LONGITUDE= 0.00 LATITUDE VARIES FROM +85 TO -85 IN STEPS OF 10 DEG
.107E-14 .106E-14 .993E-15 .105E-14 .111E-14 .117E-14
.123E-14 .129E-14 .134E-14 .140E-14 .145E-14 .150E-14
.155E-14 .158E-14 .160E-14 .159E-14 .162E-14 .181E-14

E. LONGITUDE= 15.00 LATITUDE VARIES FROM +85 TO -85 IN STEPS OF 10 DEG
.107E-14 .106E-14 .983E-15 .101E-14 .107E-14 .112E-14
.116E-14 .121E-14 .125E-14 .131E-14 .136E-14 .142E-14
.147E-14 .152E-14 .155E-14 .156E-14 .159E-14 .179E-14

E. LONGITUDE= 30.00 LATITUDE VARIES FROM +85 TO -85 IN STEPS OF 10 DEG
.108E-14 .107E-14 .974E-15 .989E-15 .103E-14 .107E-14
.110E-14 .114E-14 .118E-14 .123E-14 .129E-14 .135E-14
.141E-14 .147E-14 .151E-14 .153E-14 .156E-14 .177E-14

E. LONGITUDE= 45.00 LATITUDE VARIES FROM +85 TO -85 IN STEPS OF 10 DEG
.108E-14 .107E-14 .965E-15 .970E-15 .100E-14 .103E-14
.106E-14 .109E-14 .113E-14 .118E-14 .123E-14 .130E-14
.137E-14 .143E-14 .148E-14 .152E-14 .155E-14 .177E-14

E. LONGITUDE= 60.00 LATITUDE VARIES FROM +85 TO -85 IN STEPS OF 10 DEG
.109E-14 .106E-14 .957E-15 .961E-15 .993E-15 .102E-14
.104E-14 .107E-14 .111E-14 .115E-14 .121E-14 .128E-14
.135E-14 .141E-14 .149E-14 .162E-14 .162E-14 .177E-14

E. LONGITUDE= 75.00 LATITUDE VARIES FROM +85 TO -85 IN STEPS OF 10 DEG
.110E-14 .105E-14 .954E-15 .969E-15 .100E-14 .103E-14
.106E-14 .109E-14 .113E-14 .117E-14 .123E-14 .130E-14
.136E-14 .143E-14 .164E-14 .180E-14 .171E-14 .178E-14

E. LONGITUDE= 90.00 LATITUDE VARIES FROM +85 TO -85 IN STEPS OF 10 DEG
.112E-14 .106E-14 .967E-15 .100E-14 .105E-14 .109E-14
.113E-14 .117E-14 .121E-14 .126E-14 .132E-14 .138E-14
.144E-14 .154E-14 .183E-14 .198E-14 .180E-14 .179E-14

E. LONGITUDE= 105.00 LATITUDE VARIES FROM +85 TO -85 IN STEPS OF 10 DEG
.114E-14 .110E-14 .100E-14 .106E-14 .113E-14 .120E-14
.126E-14 .132E-14 .138E-14 .143E-14 .149E-14 .154E-14
.158E-14 .169E-14 .202E-14 .214E-14 .184E-14 .182E-14

E. LONGITUDE= 120.00 LATITUDE VARIES FROM +85 TO -85 IN STEPS OF 10 DEG
.116E-14 .115E-14 .106E-14 .115E-14 .125E-14 .135E-14
.145E-14 .154E-14 .162E-14 .168E-14 .174E-14 .177E-14
.179E-14 .189E-14 .228E-14 .241E-14 .210E-14 .186E-14

E. LONGITUDE= 135.00 LATITUDE VARIES FROM +85 TO -85 IN STEPS OF 10 DEG
.119E-14 .122E-14 .115E-14 .126E-14 .141E-14 .155E-14
.169E-14 .182E-14 .192E-14 .200E-14 .205E-14 .207E-14
.205E-14 .210E-14 .253E-14 .273E-14 .243E-14 .191E-14

E. LONGITUDE= 150.00 LATITUDE VARIES FROM +85 TO -85 IN STEPS OF 10 DEG
.122E-14 .132E-14 .126E-14 .138E-14 .158E-14 .177E-14
.196E-14 .212E-14 .226E-14 .235E-14 .240E-14 .239E-14
.234E-14 .230E-14 .273E-14 .304E-14 .259E-14 .197E-14

E. LONGITUDE= 165.00 LATITUDE VARIES FROM +85 TO -85 IN STEPS OF 10 DEG
.125E-14 .144E-14 .139E-14 .151E-14 .175E-14 .199E-14
.222E-14 .243E-14 .259E-14 .269E-14 .274E-14 .272E-14
.263E-14 .249E-14 .281E-14 .312E-14 .271E-14 .204E-14

ALTITUDE= 400.00 DATE= 0. TIME= 0.00

E. LONGITUDE= 180.00 LATITUDE VARIES FROM +85 TO -85 IN STEPS OF 10 DEG

.128E-14	.156E-14	.155E-14	.161E-14	.190E-14	.218E-14
.245E-14	.269E-14	.287E-14	.299E-14	.304E-14	.300E-14
.288E-14	.270E-14	.274E-14	.304E-14	.276E-14	.209E-14

E. LONGITUDE= 195.00 LATITUDE VARIES FROM +85 TO -85 IN STEPS OF 10 DEG

.129E-14	.168E-14	.175E-14	.171E-14	.200E-14	.232E-14
.262E-14	.288E-14	.308E-14	.321E-14	.325E-14	.320E-14
.306E-14	.285E-14	.268E-14	.289E-14	.274E-14	.212E-14

E. LONGITUDE= 210.00 LATITUDE VARIES FROM +85 TO -85 IN STEPS OF 10 DEG

.130E-14	.177E-14	.192E-14	.182E-14	.205E-14	.238E-14
.270E-14	.297E-14	.318E-14	.331E-14	.335E-14	.329E-14
.315E-14	.292E-14	.265E-14	.272E-14	.266E-14	.212E-14

E. LONGITUDE= 225.00 LATITUDE VARIES FROM +85 TO -85 IN STEPS OF 10 DEG

.128E-14	.182E-14	.201E-14	.193E-14	.204E-14	.237E-14
.268E-14	.295E-14	.316E-14	.329E-14	.333E-14	.328E-14
.313E-14	.291E-14	.263E-14	.254E-14	.254E-14	.212E-14

E. LONGITUDE= 240.00 LATITUDE VARIES FROM +85 TO -85 IN STEPS OF 10 DEG

.125E-14	.173E-14	.199E-14	.198E-14	.199E-14	.229E-14
.258E-14	.284E-14	.304E-14	.316E-14	.321E-14	.316E-14
.303E-14	.282E-14	.256E-14	.239E-14	.240E-14	.211E-14

E. LONGITUDE= 255.00 LATITUDE VARIES FROM +85 TO -85 IN STEPS OF 10 DEG

.121E-14	.158E-14	.189E-14	.195E-14	.191E-14	.215E-14
.242E-14	.265E-14	.283E-14	.295E-14	.299E-14	.295E-14
.284E-14	.267E-14	.244E-14	.224E-14	.226E-14	.208E-14

E. LONGITUDE= 270.00 LATITUDE VARIES FROM +85 TO -85 IN STEPS OF 10 DEG

.117E-14	.140E-14	.171E-14	.183E-14	.180E-14	.198E-14
.221E-14	.241E-14	.257E-14	.267E-14	.272E-14	.270E-14
.261E-14	.247E-14	.229E-14	.211E-14	.214E-14	.204E-14

E. LONGITUDE= 285.00 LATITUDE VARIES FROM +85 TO -85 IN STEPS OF 10 DEG

.112E-14	.121E-14	.155E-14	.168E-14	.165E-14	.179E-14
.198E-14	.215E-14	.228E-14	.238E-14	.243E-14	.242E-14
.237E-14	.227E-14	.213E-14	.197E-14	.202E-14	.199E-14

E. LONGITUDE= 300.00 LATITUDE VARIES FROM +85 TO -85 IN STEPS OF 10 DEG

.108E-14	.113E-14	.138E-14	.145E-14	.147E-14	.162E-14
.177E-14	.190E-14	.202E-14	.210E-14	.215E-14	.216E-14
.213E-14	.207E-14	.198E-14	.186E-14	.191E-14	.195E-14

E. LONGITUDE= 315.00 LATITUDE VARIES FROM +85 TO -85 IN STEPS OF 10 DEG

.106E-14	.104E-14	.119E-14	.124E-14	.134E-14	.146E-14
.158E-14	.169E-14	.178E-14	.186E-14	.191E-14	.193E-14
.193E-14	.190E-14	.185E-14	.176E-14	.180E-14	.190E-14

E. LONGITUDE= 330.00 LATITUDE VARIES FROM +85 TO -85 IN STEPS OF 10 DEG

.105E-14	.104E-14	.105E-14	.114E-14	.124E-14	.134E-14
.143E-14	.152E-14	.160E-14	.166E-14	.171E-14	.175E-14
.177E-14	.177E-14	.174E-14	.169E-14	.172E-14	.186E-14

E. LONGITUDE= 345.00 LATITUDE VARIES FROM +85 TO -85 IN STEPS OF 10 DEG

.106E-14	.105E-14	.101E-14	.109E-14	.117E-14	.124E-14
.132E-14	.139E-14	.145E-14	.151E-14	.156E-14	.161E-14
.164E-14	.166E-14	.166E-14	.164E-14	.156E-14	.183E-14

7.3 Appendix C: Summary of the La Jolla Conference on Quantitative Magnetospheric Models

Introduction

The meeting was held in La Jolla Shores, California, from 6-8 May 1975. There were five sponsors: the American Geophysical Union, The American Institute of Aeronautics and Astronautics, Air Force Office of Scientific Research, the Office of Naval Research, and McDonnell Douglas Astronautics Company. The meeting was divided roughly into three parts, with one day devoted to each. Further, each day was divided such that approximately two-thirds of the time was devoted to presentation of papers, while one-third of the time was used for discussions and working group activities. The first day was devoted to magnetic fields, the second day to electric fields, and the last day to charged particles. This summary will roughly follow the order of the meeting. Many of the comments made concerning the magnetic field apply equally well to the electric field. There were 85 registered attendees with six foreign participants. One of the purposes of the meeting was to bring together those people working on the actual development of models with a cross-section of those workers collecting observational data. The data is necessary for the proper development of empirical models. There were also several model "users" present. Their current and future needs make it possible to test existing models and to suggest which future models will be most valuable. The meeting discussions were limited to quantitative models and associated observational data sets. A quantitative model was defined as one that yields numerical information which agrees well with quantitative observations of a magnetospheric feature.

Magnetic Fields

In contrast to the electric field, the magnetospheric magnetic field is relatively well-behaved and its variability fairly well understood. Modelling of magnetospheric magnetic fields is well ahead of modelling of the magnetospheric electric field and various particle structures in the magnetosphere. This is, in part, because the magnetic field is measured directly (electric fields are still typically inferred from particle motions). Also the sources of the magnetospheric magnetic field, the several magnetospheric current systems, are fairly well known and understood. The most important are: the magnetopause currents, formed by the deflection of shocked solar wind particles off of the magnetospheric

magnetic field, the tail current system, produced mainly by charged particles drifting across the plasma sheet region of the tail, and the ring current system which is formed by trapped particles drifting around the earth. Sugiura has suggested that at least most of the time, the quiet time ring current system is contiguous with the tail current system. There are many data sets that have been used to develop the current models of the magnetospheric magnetic field, $\vec{B}$. Sugiura, Hedgecock, McPherron, and Cain talked about observations of $\vec{B}$. Cain discussed the modelling of the earth's main field and its importance for magnetospheric phenomena as was described at the Zmuda Memorial Conference. A key point for magnetospheric physicists was that the present International Geomagnetic Reference Field currently only models "structures" with longitudinal extent greater than 45°. This is probably inadequate for the proper quantitative study of high latitude magnetospheric (and ionospheric) phenomena. Sugiura discussed the procedure of subtracting the magnitude of the earth's main field from the magnitude of the observed field to obtain ΔB. It has become an important tool in understanding the magnetic effects of currents flowing in the inner magnetosphere. Magnetic observations at synchronous orbit also provide excellent tests of the models in that region of the magnetosphere. McPherron pointed out that the variations seen at synchronous orbit are quite sensitive to geomagnetic longitude. The analysis of the HEOS data by Hedgecock and his colleagues has shown that in the high latitude, high altitude magnetosphere, the magnetopause is more flared than predicted by the models whose shape was determined using the pressure balance condition (specular reflection). This data also suggests that although charged particles may enter the magnetosphere at high latitudes over a cleft or cusp-like region, the magnetic field topology in that region is more like a funnel in shape and does not extend more than two hours on either side of the noon magnetic meridian. Hedgecock's group has also initiated the use of a "hinged" coordinate system that near earth is like an ordinary magnetic coordinate system, while in different regions of the magnetosphere it becomes either a solar magnetic, or solar magnetospheric coordinate system. With the use of this coordinate system, it was possible to do a much better job of organizing the magnetic field data. (This coordinate system takes into account "tilt" effects. Tilt refers to the varying angle between the geomagnetic dipole axis and the solar wind direction.)

Several models of $\vec{B}$ were presented by their authors and reviewed by Walker. These included the models of Sugiura and Poros, Mead and Fairfield, Choe and Beard and Sullivan, Olson and Pfitzer, Willis and Pratt, Alekeev and Shabansky, and Voigt. Most of these models are discussed in some detail in the accompanying extended abstracts. A general set of requirements that an all purpose model should have, include; the magnetopause, tail and quiet time ring currents must be included as must the effects of tilt. The model must be good throughout a large portion of the magnetosphere. It must be capable of predicting $\vec{B}$ during quiet to moderately disturbed conditions. None of the models of $\vec{B}$ developed to date meet all of these requirements.

In addition to these general requirements, there are some more specific details that should probably be included in any future modelling efforts. Potemra pointed out the importance of field aligned currents in the high latitude region. Although they are presently not well understood and their coupling of the magnetospheric current systems not presently known, it is clear that at high latitudes they exert some influence on the structure of the magnetic field. Likewise, at high latitudes, Hedgecock showed that the observed magnetospheric boundary is more distant than that given by the older models. Either a better theory for the shape of the magnetopause should be developed or these observations be input to an empirical model. It is also becoming increasingly obvious that several magnetospheric phenomena are directly linked to the interplanetary magnetic field. It is therefore appropriate to develop a model that at once includes both the magnetospheric and interplanetary fields. However, the difficulties with the mathematical representation of such a field are formidable. Another requirement of these models is that they be differentiable. This is necessary if they are to be used to interpret the drift and energization of charged particles. It was suggested that specialized models might be developed for various local regions of the magnetosphere. However, such models cannot be used conveniently with other models. Since adding them together and truncating outside their region of validity causes severe problems with their differentiability. The same is true of trying to represent the interplanetary field and $\vec{B}$ simultaneously. It was agreed that any future model should be "global", differentiable, and include at least the magnetopause, tail, and quiet time ring current system contribution, and the tilt effect.

There were some talks given on model uses. Seely reported that the Stanford group has used the Olson-Pfitzer model to locate the crossing of whistler ducts in the equatorial plane. McPherron showed the importance of including both the magnetic effects of the trapped currents and the effects of the tilt of the geomagnetic axis to the solar wind direction for the proper description of the variations in $\vec{B}$ seen by ATS-1 and ATS-6 at synchronous orbit. The Mead-Fairfield model accurately represents daily variations in the observed field perpendicular to the northward direction which is most sensitive to tilt. Hendrickson told of several model tests provided by an electron echo experiment in which electrons were accelerated away from a rocket and later mirroring along magnetic field lines, detected by the same rocket. In order to observe the "echo" it was necessary to accurately predict both the bounce time and the drift rate of the electrons. The Olson-Pfitzer model worked well for this purpose.

A general conclusion on the magnetic field modelling was that further advances should be directed toward increasing the general understanding of the magnetospheric magnetic field and increasing the gross accuracy of the models. Efforts that dwell on refining some of the details of present models might profitably be redirected.

It now appears to be well established that magnetically, the magnetosphere is open. That is, a portion of the earth's magnetic field is not contained in the magnetosphere but passes through the magnetopause and is connected to interplanetary magnetic field. It therefore would not, at first glance, appear profitable to try to develop closed magnetic field models (in which all field lines emanating from the earth's surface return to the earth's surface in the opposite hemisphere without going outside the magnetopause. However, in order to accurately determine magnetic field properties and particle behavior near the boundary of the magnetosphere, it may be worthwhile to assume a fixed shape through which no field lines can penetrate as was suggested by Roederer (this technique has been employed by Shabansky and his colleagues). An alternative to this method is to abandon the assumption of specular reflection off the magnetopause but retain the pressure balance assumption and use pressures obtained from a hydrodynamic flow model such as developed by Spreiter's group from wind tunnel tests of flow past an object shaped to represented the magnetopause. Preliminary work on this problem has been reported by Olson.

Electric Fields

The current situation with the magnetospheric electric field, $\vec{E}$, is far different from that of $\vec{B}$. Good empirical models of $\vec{B}$ and the source currents for $\vec{B}$ are fairly well understood. Progress on the development of theoretical $\vec{B}$ models is also substantial. However, new empirical models of $\vec{E}$ are just now emerging and the overall picture of $\vec{E}$ is still cloudy enough that no good theoretical models seem to be on the horizon. There are several reasons for this. Throughout the magnetosphere, $\vec{E}$ is quite variable in both space and time, so it is difficult to use data to determine average characteristics of $\vec{E}$. Second, most work on $\vec{E}$ relies heavily on its indirect measurement using particle data and inferring $\vec{E}$ from the $\vec{V} \times \vec{B}$ drift. Third, there has only been limited success in "mapping" the electric field from one region of the magnetosphere to another. Typically, measurement of the scalar potential associated with $\vec{E}$ is determined in the ionosphere. The assumption that field lines are equipotentials is then made in order to map this electric field to the equatorial regions of the magnetosphere. There are at least three possible sources of difficulty associated with this mapping procedure. First, models of the magnetic field may not correctly predict the observed magnetic field line geometry. Second, if induced electric fields are present, the assumption that field lines are equipotentials is no longer valid, and third, anomalous resistivity may be present which allows electric fields to have a component parallel to the direction of the magnetic field. Cauffman assessed the status of experiments in operation or planned for the direct measurement of dc electric fields using double probes. Many long boom-double probe experiments will become operational during the IMS era, greatly increasing the number of observations of $\vec{E}$.

However, at present, most dc electric field observations are inferred from particle data. These measurements can roughly be divided into those made in the magnetosphere and in the ionosphere. Higby and Hones have used solar particle motions in order to infer magnetospheric electric fields, while Carpenter and Rycroft have used whistler data in the plasmasphere to infer motions that are more dynamo-like than convection-like. In the ionosphere, Hellis has used Atmospheric Explorer data to develop three-dimensional particle velocity measurements and from them high latitude convection patterns. The Chatanika

data was discussed in some detail by the USCD group. Measurements of ion velocities with the Chatanika radar should make it possible to determine the role of discrete auroral arcs in the convection process at high latitudes. In a paper read by Murayama for Mezeawa, work on a reverse current flows over the polar cap was reported. This suggests motions that are reverse of the standard convection patterns inferred at high latitudes. Thus, polar cap work and plasmasphere studies have suggested deviations from the classical magnetospheric convection patterns and indicate once more the high degree of variability in the magnetospheric electric field and also possibly some physical processes that are currently not well understood.

On the summary panel, Wolf indicated that there is now a fairly complete picture of the ionospheric electric field and it may be possible to develop an empirical model of $\vec{E}$ in the ionospheric regions. This model might be similar to McIlwain's electric field model that is useful in equatorial regions of the magnetosphere and would have as inputs to it such variables as the boundary locations of the polar cap. Again, the usefulness of such a model would depend on the user needs. Any empirical model will not directly help to further our understanding of magnetospheric processes. However, deviations between such a model and observations may isolate important physical processes currently unobserved. Also, such a model could be used in conjunction with available magnetic field models in order to study charged particle phenomena in the inner magnetosphere and ionosphere.

In the outer magnetosphere, the electric field situation is much more complex both from a spatial and a temporal point of view. It was mentioned before that mapping between the ionosphere and outer magnetosphere is complicated for several reasons. It may be reasonable to try to couple the various regions of the magnetosphere and ionosphere with a semiempirical model in which magnetospheric, ionospheric and plasmasphere (whistler) data are used together. There was a consensus, however, that there is no chance that in the next few years a theoretical model of $\vec{E}$ in the polar cap and outer magnetospheric regions will be developed.

Another way to contrast $\vec{B}$ and $\vec{E}$ is in terms of their sources. Although the source currents responsible for $\vec{B}$ are well known (but not directly measured) to date most work on $\vec{E}$ has looked only at the total field with little regard for its

sources. Basically, there can only be three sources for $\vec{E}$; charge separation, time varying magnetic fields, and the relativistic transformation of the solar wind magnetic and electric fields into a magnetospheric reference frame. In order to develop theoretical models of the magnetospheric electric field, it will be necessary to understand these sources of $\vec{E}$. Of these three source mechanisms, probably those electric fields induced by time varying magnetic fields are most amenable to understanding and quantitative modelling. Several sources of time varying magnetic fields in the magnetosphere are known; changes in the standoff distance of the magnetopause current system, substorm related changes in the tail current system, storm time changes in the ring current, and the daily variation in the magnetic field produced by tilt effects. Hones and Burgeson, and Birmingham and Northrup did early work in general problem areas. Recent procedures for calculating induced electric fields developed by Olson and Pfitzer have shown that even the daily wobble of the earth's magnetic field plus the corresponding wobble in the magnetopause currents can produce a substantial induced electric field. The same sort of comments made on $\vec{B}$ apply to $\vec{E}$ as regards user needs. The models of $\vec{E}$ should be "global", analytic, etc.

Emphasis is shifting from the static magnetosphere to the study of its dynamic properties. It is therefore necessary that both $\vec{E}$ and $\vec{B}$ be capable of representing observed temporal variations. The magnetospheric substorm is an example. In order to properly model the injection of charged particles during substorms, it is necessary to employ both a time varying magnetic field model and a time varying electric field model. Also, during time varying situations, the $\vec{E}$ and $\vec{B}$ models are coupled in that the time variations in $\vec{B}$ will induce a component that must be included in the total model of $\vec{E}$. Because of this coupling another requirement must be made on all future magnetic field models and that is, in addition to computing $\vec{B}$, these models should also include $\vec{A}$, the vector magnetic potential. (The induced electric field is best computed by taking the time derivative of $\vec{A}$.) The need for having a time varying electric field model again points out the importance of understanding its source mechanisms since input parameters to both $\vec{E}$ and $\vec{B}$ must be well understood if the models are to generate meaningful results.

Charged Particles

In the session on charged particles, it became apparent that the current lack of understanding of magnetospheric boundary phenomena limits the use of field models describing charged particle behavior. This is true for both the high and low energy charged particles. The access of low energy charged particles is not well understood, nor is the coupling of the magnetospheric magnetic field with the magnetosheath and interplanetary fields. This coupling influences the entry of energetic particles and their subsequent motions in the magnetosphere. It is possible, however, that the higher energy particles, which do not contribute significantly to the current systems that produce $\vec{B}$ can be used to study some of the gross properties of the magnetospheric magnetic field.

Masley reported work on comparisons of observed solar cosmic ray phenomena and model prediction. Particle trajectories and cutoffs obtained using the Olson-Pfitzer model were in good agreement in the noon and midnight meridian planes when observations were used for the same range of K_p values as the model is intended. His studies of cosmic ray entry and propagation also suggest that energetic particle access to the polar cap regions is strongly influenced by the interplanetary magnetic field direction. Other papers on high energy particles also suggested the importance of accurate magnetic field models and tests that these particles can offer for the development of such models. It was suggested that observations of high energy particle fluxes be correlated with substorm time to help develop dynamic models of the magnetic field. Hoffman and Smith showed that particle fluxes observed from 1 to 872 kilovolts can account for most of the depression of the inner magnetosphere observed in the magnetic field data by Sugiura and his colleagues. Buck and West presented detailed pitch angle distributions from which they derive drift shell splitting and determine, indirectly, the shape of magnetic field lines. Buck has examined the motions of energetic particles near noon and suggests that the observed pitch angle spectra can be explained in terms of a magnetic field that has minima along the field lines displaced from the equatorial region as much as 60°. Both Konradi and McIlwain suggested that the region between 6 and 10 earth radii where particle injection occurs needs more detailed study in order that it be properly modelled.

It is in this region, at least near local midnight, where the magnetopause, quiet time ring and tail current systems all contribute similar amounts to the total magnetic field. Murayama discussed energetic electrons that were observed near the high latitude dayside magnetopause several hours after observed substorm activity.

All of these particle observations must eventually be accounted for by improved field models. However, it appears at present that only the more gross features of the particle and field phenomena observed in the magnetosphere are being fit by the models. These detailed magnetospheric particle features will provide tests for the more sophisticated models that should be developed in the near future.

There was also discussion on the definition of the last closed or first open field line. It was argued that this was best done using charged particle data. A magnetometer on a polar orbiting satellite cannot by itself distinguish open from closed field lines. Magnetometer data can best be used to define average magnetic field models and then use the model geometry to define the boundary between open and closed lines. However, electrons present during solar events can be used to accurately determine the position of the first open field line, although this technique is limited because of the infrequent occurrence of solar events, it nevertheless can be used to determine the average position (possibly as a function of K_p) of the first open field line.

The question of open versus closed magnetosphere as regards charged particle entry must also be answered in the affirmative. That is, the magnetosphere appears to be always "open" to the entry of both low and high energy particles over some portions of the magnetopause. This is true even if the magnetosphere is magnetically closed. This is possible because some particles incident upon the magnetopause enter it and drift through the magnetosphere because of gradients in the magnetic field parallel to the boundary. For low energy particles these regions include clefts on the high latitude dayside magnetopause and in the equatorial (plasma sheet) regions of the tail. Solar and galactic cosmic rays penetrate all regions of the magnetopause. It was concluded that the magnetosphere is open, both in the magnetic sense and from the standpoint of entry of

charged particles. However, present models do not explicitly attempt to represent this open nature of the magnetosphere. In order to do this a much better quantitative understanding of the magnetopause must be obtained. Such a quantitative model of the magnetopause must self-consistently account for a (small?) component of magnetic field normal to the boundary and a determination of which particles are deflected from this boundary and which particles are able to move through it.

Conclusions

The goal of the meeting was to make an assessment of what quantitative models are now available and how good they are, to determine generally what data sets are available, or will become available during the IMS era, and then to determine the limitations of existing models. These items were then used to make recommendations to model developers and model users for work that should be undertaken during the IMS period to extend existing models and to develop new ones. A summary of the present situation regarding quantitative models is given in this section and recommendations for work in the near future given in the next.

Modelling efforts in magnetic fields, electric fields, and charged particles were described. Clearly, efforts to model the magnetospheric magnetic field has made the most progress. However, it is clear that an "international" reference model" is not yet at hand. There are several models available that do specific things well, but no single model that meets all of the user requirements. The current models range from physical to entirely empirical. The utility of a given model depends on the needs of the user. This was one of the key problem areas isolated at the meeting. Although different users typically would ask for the same output from a model, the inputs might vary considerably. For example, a user who is trying to understand a particular magnetospheric phenomenon may only require that a model input parameter becomes available several weeks, or even months, after the time in question (for example, K_p or many of the other indicies of magnetic activity) while there are many "more practical" users who require input parameters which can themselves be monitored in real time (for example, the solar wind dynamic pressure, the

direction of the interplanetary magnetic field). Thus, determining the proper input parameters for a model is not a trivial problem is the needs of these several users are to be met. It is necessary that general input parameters for the models be developed. This means that in addition to the location in question, inputs to a model that will give back the vector magnetic field must also include parameters like the standoff distance of the magnetopause which can be related either to K_p (after the fact) or in real time to solar wind parameters. Both model and data user communities indicated that a data sampling rate of 1 per minute suffices for most tests and applications. Some users, of course, use much lower sampling rates. Power suggested a rate of 1 per hour for some practical applications.

Many indices and real time input parameters were discussed. They included the location of the auroral oval and the electron trough, the size of the polar cap, the Q index K_p, A_E, D_{st}, the vector specification of the interplanetary magnetic field, the various solar wind parameters, and the tilt angle. For input parameters to the models to have general utility, it is necessary that they relate both to parameters that are readily available (such as K_p) but not necessarily in real time, and to other environmental features that can be monitored in real time (such as the dynamic solar wind pressure). Thus the standoff distance (which gives an indication of the size of the magnetosphere and concurrently the strength of the magnetopause current systems) might be an appropriate model input parameter. It would be then left to the user to relate this particular model input parameter to another quantity convenient for his particular use (for example, K_p, or the solar wind dynamic pressure). Many such input

parameters must be decided upon. This must be done with both user needs and data availability kept in mind.

Although there were several complaints about availability of good data for use in the construction of empirical models, and as a monitored input to some models, it is apparent that the modelling community must make the best of what is available. For example, it was suggested that vector ΔB measurements (ΔB is the difference between the observed magnetic field and that portion produced by the earth's magnetic field as given by an accurate model of the main field) be used instead of scalar ΔB measurements. When vector $\Delta \vec{B}$ measurements become generally available, they will be used as inputs to models and also to test models. To date, however, the scalar ΔB measurements have been used effectively to understand current systems in the inner magnetosphere and to develop quantitative models of the inner magnetospheric magnetic field.

The general availability of data and the fact that $\vec{B}$ can be measured directly has served to expedite efforts to quantitatively model magnetospheric magnetic fields. Efforts to model the electric field, on the other hand, have suffered from a lack of direct measurement of $\vec{E}$ and its extreme variability, both in time and space. Efforts to "map" the electric field between different regions of the magnetosphere and thus compare simultaneous data sets, have met with only partial success, due, in part, to this variability. Hopefully, as several double probe experiments become available to directly measure the dc electric field, some of these problems will be resolved, and the effort to model $\vec{E}$ in terms of its various sources can be accelerated.

For the future development of models, the various users should be kept in mind. Users vary from those interested only in an understanding of the magnetosphere (and an interest only in completely physical theoretical models) to those practical users who are interested in models simply as "black boxes" that yield quantitatively accurate information. Between these two extremes there is an almost continuous spectrum of users. These include, for example, the experimenter who needs to know the location of the foot of the magnetic field line that passes through his satellite, and some monitoring activities that can be done within several hours of real time observations. Some of the practical uses of

magnetospheric models include the understanding and prediction of spacecraft charging and arcing, coupling of the magnetosphere to ionosphere and associated radio communications problems, the coupling of the magnetosphere and ionosphere to the upper atmosphere and the influence of the upper atmosphere on satellite trajectories and lifetimes, and the effects of trapped radiation and radiation present during solar cosmic ray events on various space hardware. Hildebrand suggested that the scientific community keep in mind the needs of the practical users because they can exert considerable influence on the determination of funding levels in several government agencies.

Recommendations

In order to best meet current and future user needs for quantitative models of magnetospheric phenomena, several recommendations are made here that should have special significance during the IMS era. During the IMS, increased attention will be focused on all aspects of magnetospheric phenomena. These efforts will include sets of satellite and ground based experiments and monitoring stations the procurement of many observational data sets and the development of both physical and empirical quantitative models. The first, and probably most general recommendation, is that a model situation center be formed - in the same manner as the experiment situation center. Such a center would serve two important purposes. First, it would permit a means for closely monitoring progress in the development of models and a means for evolving new sets of modelling recommendations as better data sets become available and more sophisticated quantitative models are developed. Second, such a center would provide a means for interaction between the magnetospheric physics community and the many users who need to know quantitatively the effects of the magnetosphere (possibly coupled with the ionosphere and/or atmosphere) on their hardware systems. It should be remembered that these users can provide much needed incentive to various agencies to continue their support of magnetospheric research. In the eyes of these users, the quantitative model is the end result of the magnetospheric research. The model is employed by the user to cost effectively find solutions to environmental effects on his hardware systems. A modelling situation center would also provide an interface between modelling and observational data collection efforts.

More specific recommendations concerning the future development of quantitative magnetospheric magnetic field models were also made. Several of these recommendations apply as well to the development of electric field models and some even to the development of charged particle models. These recommendations can be roughly divided into two categories; requirements that future models should meet and quantitative tests that they should satisfy. General requirements that any future quantitative magnetospheric magnetic field model should satisfy include:

1. It should represent the magnetic field contributions from all important magnetospheric current systems including those currents distributed throughout the inner magnetosphere (the quiet and disturbed ring currents) and in the plasma sheet region of the tail (the tail current system).

2. The dependence of each of these current systems on the tilt angle (the complement of the angle between the solar wind direction and the geomagnetic dipole axis) should be included.

3. Variability in each of the current systems should be taken into account (e.g., the shape and strength of the magnetopause current systems as a function of standoff distance).

4. The representation of $\vec{B}$ should be analytic.

5. The magnetic vector potential $\vec{A}$ should be computed together with $\vec{B}$.

6. The model should be valid over a large portion of the observed magnetosphere.

In addition, there are some specific user requirements:

7. The amount of computer time needed to represent $\vec{B}$ should be minimized.

8. Input parameters to the computer subroutine should be easily obtainable from user chosen indices or monitored parameters.

The first three requirements would satisfy most of the complaints made against existing models: they do not include the effects of all current systems and/or tilt effects, and most important, they do not do a good job of describing dynamic magnetospheric behavior. A dynamic model must of necessity have input parameters that are related to the variability of the several current systems contributing to $\vec{B}$. In order to use the model to describe charged particle behavior, it is necessary that it be both analytic and differentiable. Such a model of $\vec{B}$ should then yield both the motions of charged particles (from $\nabla\vec{B}$) and currents distributed throughout the magnetosphere (from $\nabla\times\vec{B}$). It is necessary to compute the vector potential $\vec{A}$ in order to determine the electric field induced by temporal variations in $\vec{B}$. $\vec{A}$ can also be used to determine $\vec{B}$ if it is demanded that $\nabla\cdot\vec{B}$ be precisely 0. A computer representation of $\vec{B}$ must be extremely fast if it is to be used to compute magnetic field lines, low energy particle motions and drift shells, and the precise trajectories of high energy particles.

In order to assess the quantitative accuracy of any model meeting the above criteria, it is necessary to have available quantitative tests. It is recommended that a standard set of tests be applied to all $\vec{B}$ models (it is understood that some specialized models would not do as well as others in satisfying these tests but still be the most useful for certain specific user needs). Several existing models have been tested by comparing their output with quantitative observational data of known magnetospheric phenomena. These data include:

1. Magnetic field observations in different regions of the magnetosphere (scalar $\vec{B}$ plots, the decay of the tail field in its equatorial and lobe regions, the field geometry at high latitudes - especially near the magnetopause, the latitude of the last closed magnetic field line).

2. The daily variations in the synchronous magnetic field during quiet and disturbed periods.

3. The trapping boundary of adiabatic particles.

4. The low latitude cutoff boundary for solar cosmic rays.

5. Field line shape as determined from barium releases.

Other observational data sets that should be used to test models in the near future include:

6. Vector ΔB measurements

7. Detailed pitch angle information on trapped particle phenomena.

Several of the same requirements can be applied to the electric field modelling efforts. The greatest problem with the electric field to date appears to be the lack of data in the inner and outer regions of the magnetosphere. However, because there is currently a fair amount of data on the ionospheric electric field, it is recommended that an empirical model of the ionospheric electric field be developed. Such a model would at least indirectly help the understanding of electric fields throughout the magnetosphere. The problem of data in the inner and outer magnetosphere regions should largely be overcome by the deployment of several long boom, double probe experiments to measure the dc electric field. As this data becomes available, it is recommended that the various sources of $\vec{E}$ be kept in mind in trying to explain and model the magnetospheric electric field. For example, magnetospheric electric field observations could be checked for the existence of a longitudinal component which is dependent on universal time. Such a component in the total field could be induced by the daily wobble of the earth's dipole field. The availability of simultaneous data from different regions of the magnetosphere and ionosphere will also shed light on the mapping problem.

It is probably the lack of understanding of the various boundaries in the magnetosphere and ionosphere that causes the largest problem for the physical modelling of electric fields. Thus the proper determination of the properties of the magnetopause again appears important (it was mentioned above that the magnetopause properties must be understood in detail in order to understand the coupling of the interplanetary magnetic field with the geomagnetic field and in order to properly understand and model the entry of charged particles into the magnetosphere). Thus it is recommended that some attention be directed toward the magnetopause, such that electric and magnetic fields and particles phenomena both on and through that boundary can be quantitatively understood.

There are now many data sets that detail charged particle behavior in the magnetosphere. It would be of general help to the electric and magnetic field contingent of the magnetospheric community if models were to be developed of several of the gross particle features in the magnetosphere (e.g., the properties of the plasma sheet and the plasmasphere). It is probably necessary to have a first order set of models (of the electric, and magnetic field, and of charged particle structures) in order to finally consider their mutual interaction and begin the development of a true quantitative magnetospheric model. It might be argued that models of the magnetic field, or of charged particle phenomena, are merely different ways of representing the same magnetospheric phenomena. A quantitative magnetospheric model, then, may at least be defined as one that self-consistently and simultaneously considers the magnetospheric magnetic and electric fields and charged particle phenomena.

It was also recommended that considerable effort be devoted toward the determination of proper input parameters to all of the models. This is imperative if the models are to meet the various user needs. These input parameters must be chosen so as to make the models dynamic. In the case of $\vec{B}$, input parameters are needed to describe each of the various current systems. It may be that for some user applications existing indices are adequate (e.g., D_{st} as an input to described ring current strengths). However, it appears that no parameters presently are adequate to describe the dynamics of the tail current during magnetospheric substorms. It was suggested that the size of the polar cap might provide a good indication of the strength and location of the tail currents. It is clear that a given model "can be no better than its input parameters". Thus the selection and use of the proper indices and/or monitored data for input parameters must be considered an important part of the development of quantitative models of magnetospheric phenomena.

Acknowledgements

The "author" wishes to thank the many meeting attendees who made suggestions regarding this summary. The chairman of the working groups and the technical sessions especially provided significant inputs. No attempt was made here to mention all of the papers presented at the meeting as they are covered in greater detail in the extended abstracts which follow.

MEMORANDUM

10 April 1975
A3-254-AJEO-300

Subject: IMPROVED REPRESENTATION OF THE DIURNAL VARIATION AT LOW LATITUDES

To: W. P. Olson, A3-254

Copies To: AJEO File

The thermospheric model in our August 1974 report to AFOSR [Olson et al., 1974] includes a quantity, f(t), which represents the diurnal density variation at the equator. In Table 1 of that report, f(t) is represented by low-latitude data collected by OGO-6 [Hedin, at al., 1974]. This table has now been compared with measurements obtained by accelerometers on the two equatorial satellites, San Marco II [Broglio, 1971] and III, [Broglio et al., 1974], and with the Paetzold [1963] model, which was based on data from seven early satellites. All four data sets were compared at an altitude of 450 km (in the case of the two San Marcos, this required a moderate amount of extrapolation). The four data sets have been averaged to obtain the values plotted as open circles in Figure 1.

By using Karl Pfitzer's universal fitting program, ORTHON, the following Fourier series has been fitted to the points:

$$f(t) = 0.994 + 0.545 \cos C(t - 14.745) + 0.102 \cos 2C(t - 1.838)$$
$$+ 0.0154 \cos 3C(t - 23.098) - 0.00667 \cos 4C\,t + 0.0161 \cos 5C(t - 0.777)$$

where $C = \pi/12$ and t is local time in hours.

The equation is also shown in Figure 1.

O. K. Moe
Space Physics Branch
Biotechnology & Space Sciences Department
Engineering Division

M. B. Baker
Space Physics Branch
Biotechnology & Space Sciences Department
Engineering Division

OKM:MBB:sp

Attachments - Reference List
Figure 1

References

Broglio, L., C. Arduini, C. Buongiorno, U. Ponzi, and G. Ravelli, Diurnal Density Variations Measured by the San Marco III Satellite in the Equatorial Atmosphere, Institute di Construzioni Aeronautiche, University of Rome, Italy, 1974.

Broglio, L., San Marco II Measurements of Equatorial Atmospheric Density, J. Atm. Terr. Phys., 33, 1473-'80, 1971.

Hedin, A. E., H. G. Mayr, C. A. Reber, N. W. Spencer, and G. A. Carignan, Empirical Model of Global Thermospheric Temperature and Composition, J. Geophys. Res., 79, 215-'25, 1974.

Olson, W. P., O. K. Moe, and K. A. Pfitzer, Response of the Magnetosphere and Atmosphere to the Solar Wind, interim scientific report for contract F44620-72-C-0084, McDonnell Douglas Astronautics Company, August, 1974.

Paetzold, H. K., Solar Activity Effects in the Upper Atmosphere Deduced from Satellite Observations, in Space Research III, edited by W. Priester, North-Holland Publ. Co., Amsterdam, 1963, pp. 28-52.

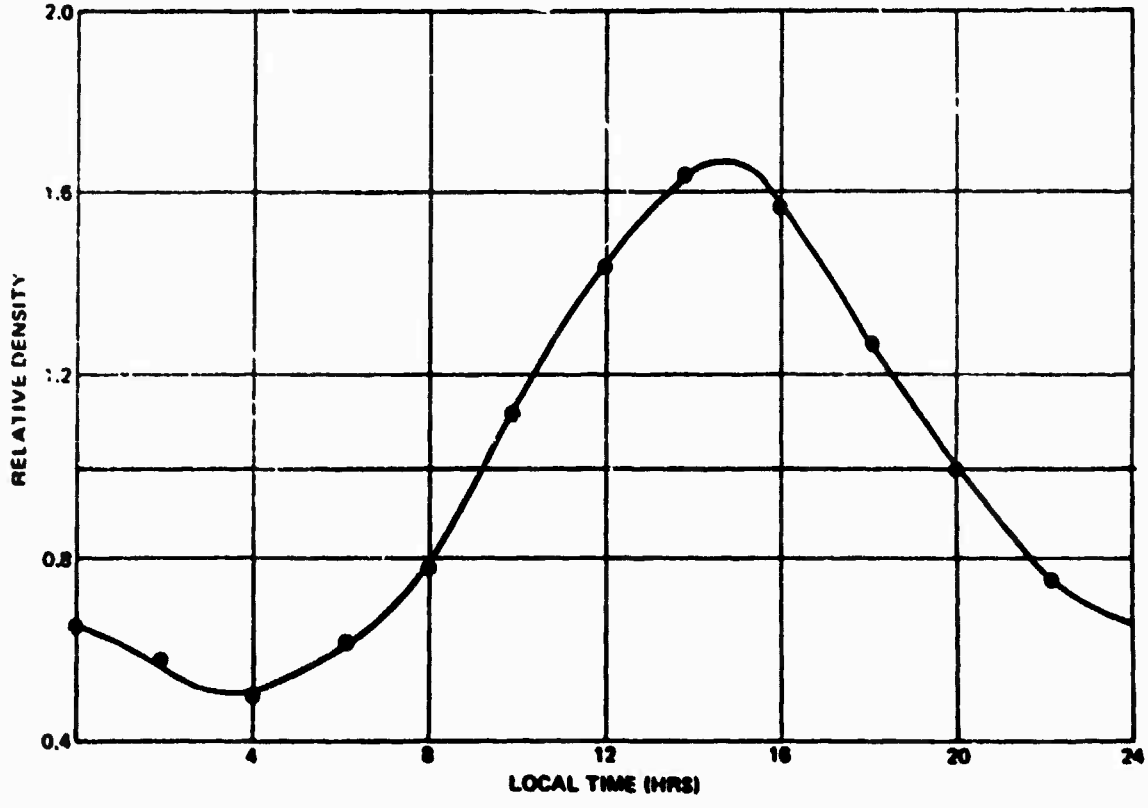

Figure 1. Diurnal Variation of Atmospheric Density

7.5 Appendix E

MEMORANDUM

A3-254-AJEO-289
26 March 1975

Subject: ANALYTIC EXPRESSION FOR SEMIANNUAL VARIATION IN THERMOSPHERIC DENSITY

To: W. P. Olson, A3-254

Copies To: AJEO File

From: M. B. Baker, O. K. Moe, A3-254; Ext. 4923/4668

In addition to the seasonal variation, there is a semiannual variation in atmospheric density which was discovered by Paetzold and Zschorner [1961]. Its existence was at first denied by Jacchia and some other workers, but it is now firmly established. The semiannual variation has been detected from 90 km well into the exosphere. Some measurements of the ratio of the October maximum to the July minimum are shown in Figure 1.

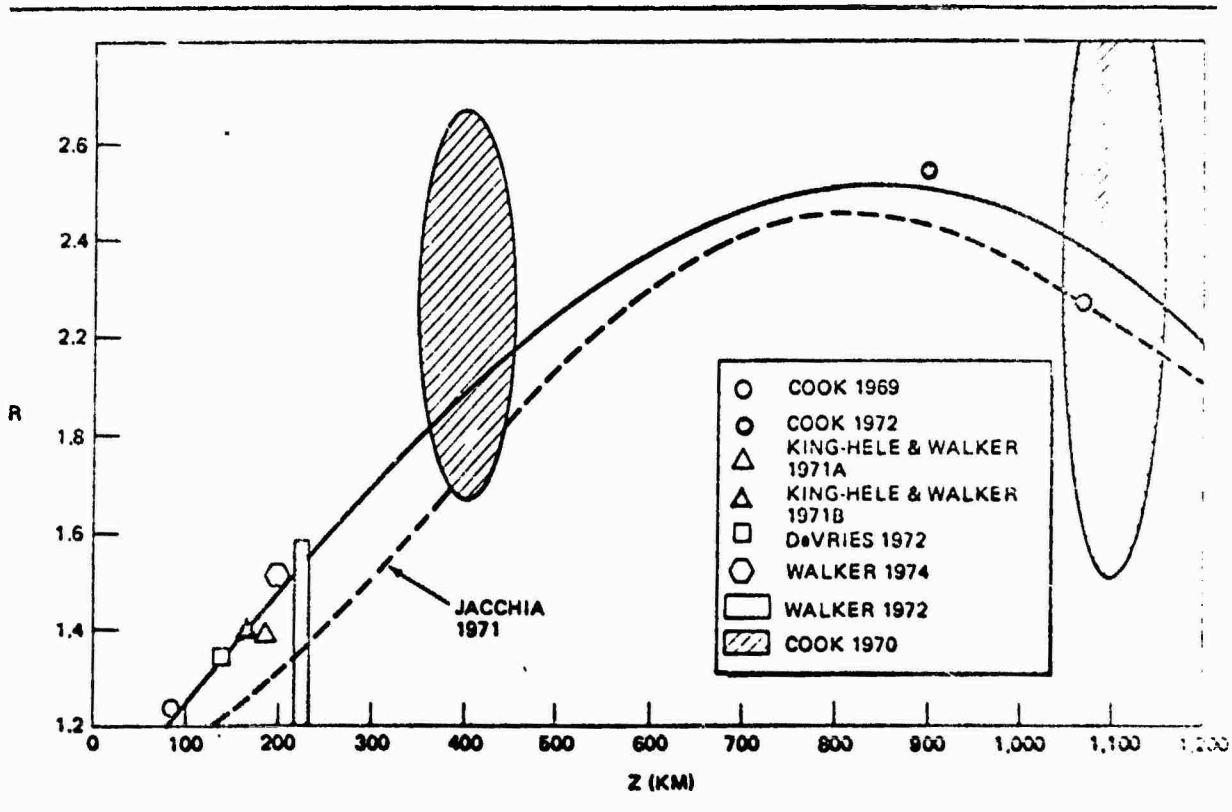

Figure 1. Ratio of Density at October Maximum to July Minimum, Plotted as a Function of Altitude

Jacchia's [1971] analytic approximation, which is based on data from seven satellites and Cook's rocket data, is shown dashed. Measurements between 90 and 215 km, which were largely lacking from Jacchia's data sample are shown; also the range of data near 400 and 1100 km for a number of years reported by Cook [1970], and three-year averages at 900 and 1070 km published by Cook [1972]. Jacchia's formula does not fit the data below 200 km. Even at higher altitudes, the variability of the measured values does not justify the elaborate formula constructed by him. A simpler formula, represented by the solid curve, has therefore been constructed using K. A. Pfitzer's routine ORTHON.

In the revised formula, R(Z) represents the ratio of the October density maximum to the July minimum.

$$R(Z) = 0.98 + 0.27 \times 10^{-2} Z - 0.85 \times 10^{-6} Z^2 - 0.59 \times 10^{-9} Z^3.$$

The time dependence is approximated by a sum of cosines of period 1 year, 1/2 year, 1/3 year, etc. The phases of the cosine terms are adopted from Volland et al. [1972]. The result plotted in Figure 2, using ORTHON, is:

$$G(D) = 0.143 \cos (K(D-4)) + 0.239 \cos (2K(D-109)) + 0.044 \cos (3K(D-66))$$

where $K = \frac{2\pi}{365}$, and D is the day number in the year.

Adding a fourth harmonic term does not significantly improve the fit. The semiannual variation of density is then represented by multiplying the expression for density by the factor

$$[1 + (R(Z) - 1) G(D)].$$

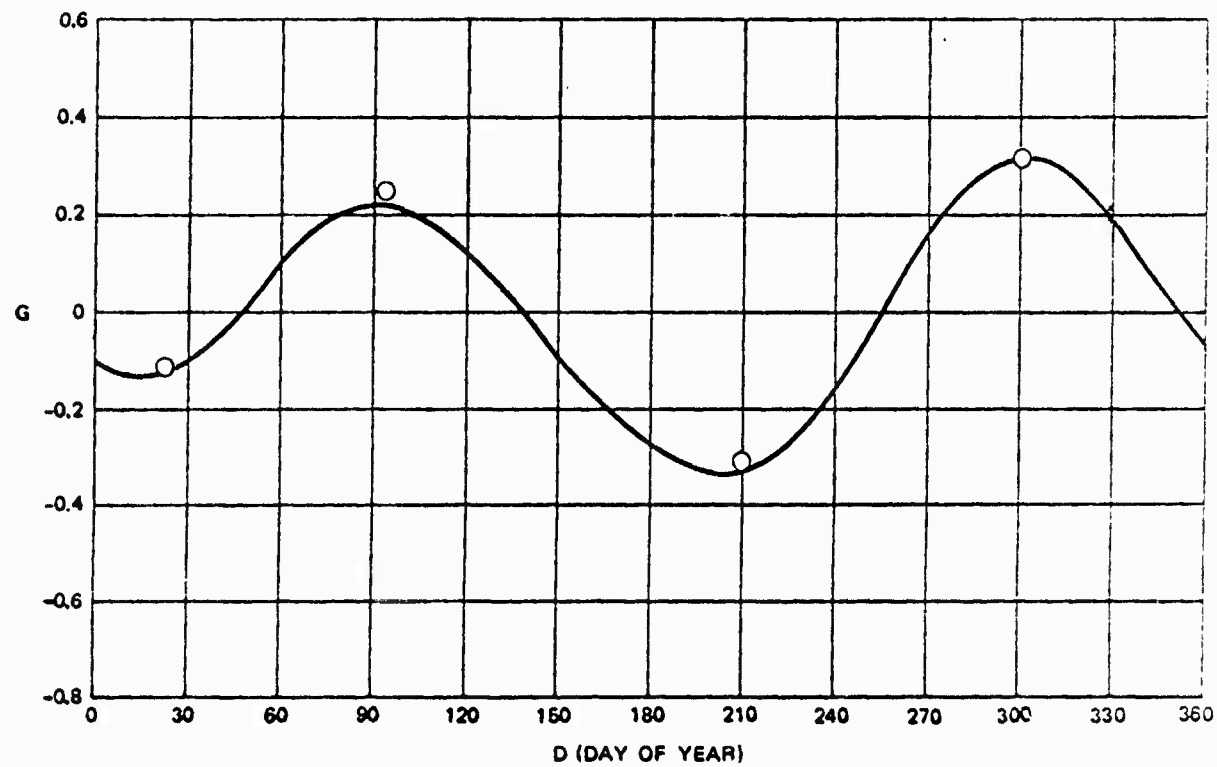

Figure 2. Time Dependence of the Density When the Amplitude Ratio, R = 2.

M. B. Baker
Space Physics Branch
Biotechnology and Space Sciences Department

O. K. Moe
Space Physics Branch
Biotechnology and Space Sciences Department

MBB:OKM:sp

Attachment

REFERENCES

Cook, G. E., Semiannual variation in density at a height of 90 km, Nature, 222, 969-'71, 1969.

Cook, G. E., The semiannual variation in the upper atmosphere during 1967 and 1968, Planet. Space Sci., 18, 1573-'88, 1970.

Cook, G. E., Density variations in the exosphere from June 1968 to December 1970, Planet. Space Sci., 20, 473-'82, 1972.

DeVries, L. L., L. Schusterman, and R. W. Bruce, Atmospheric density variations at 140 km deduced from precise satellite radar tracking data, J. Geophys. Res., 77, 1905-'13, 1972.

King-Hele, D. G., and Doreen M. C. Walker, Air density at heights near 180 km in 1968 and 1969, from the orbit of 1967-31A, Planet. Space Sci., 19, 297-311, 1971A.

King-Hele, D. G., and Doreen M. C. Walker, Air density at heights near 150 km in 1970, from the orbit of Cosmos 316 (1969-108A), Planet. Space Sci., 19, 1637-'51, 1971B.

Jacchia, L. G., Semiannual variation in the heterosphere: a reappraisal. J. Geophys. Res., 76, 4602-'7, 1971.

Paetzold, H. K., and H. Zschörner, An annual and a semiannual variation of the upper air density, Geofisica Pura e Applicata, 48, 85-92, 1961.

Volland, H., C. Wulf-Mathies, and W. Priester, On the annual and semiannual variations of the thermospheric density, J. Atm. Terr. Phys., 34, 1053-'63, 1972.

Walker, Doreen M. C., Air density at heights near 200 km from the orbit of 1969 - 20B, Planet. Space Sci., 20, 2165-73, 1972.

Walker, Doreen, M. C., Air density at height near 200 km from the orbit of 1970 - 65D, Planet. Space Sci., 22, 403-'11, 1974.

8.0 TECHNICAL REFERENCES

Adamson, D., C. L. Fricke, S. A. T. Long, W. F. Landon, and D. L. Ridge, Preliminary analysis of NASA optical data obtained in barium ion cloud experiment of September 21, 1971, J. Geophys. Res., 78, 5769, 1973.

Axford, W. I., H. E. Petschek, and G. L. Siscoe, Tail of the magnetosphere, J. Geophys. Res., 70, 1231, 1965.

Barrish, F. D., and J. G. Roederer, Experimental test of magnetospheric model, J. Geophys. Res., 78, 5795, 1973.

Bruce, R. W., Upper atmosphere density determined from a low-g accelerometer on satellite 1967-50B, Rep. TOR-0158 (3110-01)-16, Aerospace Corp., El Segundo, Calif., 1968.

Bruce, R. W., Upper atmosphere density determined from LOGACS, Space Res., 12, 1972.

Ching, B. K., and V. L. Carter, High-latitude density variations from magnetron gauge measurements from the satellite 1972-32A, Space Physics Laboratory No. SPL-74(4260-10)-7, 1974.

Clark, M. A., and P. H. Metzger, Auroral lyman-alpha observations, J. Geophys. Res., 74, 6257, 1969.

DeVries, L. L., Analysis and interpretation of density data from the Low-g accelerometer calibration system (LOGACS), Space Res., 12, 1972.

Frank, L. A., Plasma in the earth's polar magnetosphere, J. Geophys. Res., 76, 5202, 1971.

Hedin, A. E., and C. A. Reber, Longitudinal variations of thermospheric composition indicating magnetic control of polar heat input, J. Geophys. Res., 77, 2871, 1972.

Hedin, A. E., H. G. Mayr, C. A. Reber, and N. W. Spencer, Empirical Model of global thermospheric temperature and composition based on data from the OGO 6 quadrupole mass spectrometer, J. Geophys. Res., 79, 215, 1974.

Heikkila, W. J. and J. D. Winningham, Penetration of magnetosheath plasma to low altitudes through the dayside magnetospheric cusps, J. Geophys. Res., 76, 883, 1971.

Heikkila, W. J., Auroral emissions and particle precipitation in the noon sector, J. Geophys. Res., 77, 4100, 1972.

Jacchia, L. G., New static models of the thermosphere..., Special Rept. 313, Smithsonian Astrophysical Observatory, 1970.

Jacchia, L. G., and J. W. Slowey, A supplemental catalogue of atmospheric densities, Special Rept. 348, Smithsonian Astrophysical Observatory, Cambridge, Mass., 1972.

Jacchia, L., Revised static models of the thermosphere and exosphere with empirical temperature profiles, Special Report No. 332, Smithsonian Astrophysical Observatory, Cambridge, Mass., 1971.

Jacobs, R. L., Atmospheric density derived from the drag of eleven low-altitude satellites, J. Geophys. Res., 72, 1571, 1967.

King-Hele, D. G., and Eileen Quinn, Upper-atmosphere density, determined from the orbits of cosmos rockets, Planet, Space Sci., 14, 1023, 1966.

Masley, A. J., W. P. Olson, and K. A. Pfitzer, Charged particle access calculations, Conf. Papers, 13th International Cosmic Ray Conferences, Denver, Colorado, 2, 1973.

Mead, G. D., Deformation of the geomagnetic field by the solar wind, J. Geophys. Res., 69, 1181, 1964.

Metzger, P. H., and M. A. Clark, Auroral lyman-alpha observations, 2. Event of May 1967, J. Geophys. Res., 76, 1756, 1971.

Moe, O. K., A review of atmospheric models in the altitude range 100 to 1000 km, AIAA Paper 69-50, 1969; Reprinted in The Earth's Atmosphere, 1972.

Moe, O. K., Indirect energy sources and sinks in the thermosphere and mesosphere, McDonnell Douglas Astronautics Company, Report MDC-G2280, 1971.

Moe, K., Density and composition of the lower thermosphere, J. Geophys. Res., 78, 1633, 1973.

Moe, K., D. Klein, G. Maled, and L. Tsang, Density scale heights at sunspot maximum and minimum, Planet. Space Sci., 16, 409, 1968.

Olson, W. P., The shape of the tilted magnetopause, J. Geophys. Res., 74, 5642, 1969.

Olson, W. P., A scalar representation of the tilted magnetopause and neutral sheet magnetic fields, McDonnell Douglas Astronautics Co., Paper WD-1332, 1970.

Olson, W. P., Study of particle precipitation as an energy source in the atmosphere, McDonnell Douglas Rept. MDC G2281, 1971.

Olson, W. P., Corpuscular radiation as an upper atmospheric energy source, Space Research XII, Akademie-Verlag, Berlin, GDR, 1972a.

Olson, W. P., Distributed magnetospheric currents and their magnetic effects, EOS Trans. Amer. Geophys. Un., 53, 1089, 1972b.

Olson, W. P., A model of the distributed magnetospheric currents, J. Geophys. Res., 79, 3731, 1974.

Olson, W. P., and K. A. Pfitzer, A quantitative model of the magnetospheric magnetic field, J. Geophys. Res., 79, 3739, 1974.

Olson, W. P., Distributed magnetospheric currents and their magnetic effects, McDonnell Douglas Rept. MDC WD 2038, 1973.

Pfitzer, K. A., Analysis of inner and outer zone OGO 1 and OGO 3 electron spectrometer and ion chamber data, McDonnell Douglas Astronautics Co., Report MDC G2960, 1972.

Pfitzer, K. A., and W. P. Olson, The entry of low energy charged particles into the magnetosphere, EOS, Trans. Amer. Geophys. Un., 54, 432, 1973.

Pfitzer, K. A. and W. P. Olson, B, $\bar{L}$ - an improved B, L coordinate system, EOS, Trans. AGU, 56, 1045, 1975.

Sarabhai, V., and K. N. Nair, Daily variation of the geomagnetic field and the deformation of the magnetosphere, Nature, 223, 603, 1969.

Shepherd, G. G., and F. W. Thirkettle, Magnetospheric dayside cusp: At topside view of its 6300A emission, Science, 180, 733, 18 May 1973.

Siscoe, G. L., A unified treatment of magentospheric dynamics, Planet Space Sci., 14, 947, 1966.

Siscoe, G. L., Models of the geomagnetic tail, EOS, Trans. AGU,52, 900, 1971.

Sugiura, M., Equatorial current sheet in the magnetosphere, J. Geophys. Res., 77, 6093, 1972.

Sugiura, M., and D. J. Poros, A magnetospheric field model incorporating the Ogo 3 and Ogo 5 magnetic field observations, Planet Space Sci., 21, 1763, 1973.

Sugiura, M., G. G. Ledley, T. L. Spillman, and J. P. Heppner, Magnetospheric field distortions observed by OGO 3 and 5, J. Geophys. Res., 76, 7552, 1971.

Taylor, H. A., Observed solar geomagnetic control of the ionosphere, Preprint X-621-71-232, NASA Goddard Space Flight Center, 1971.

SECTION 9.0 PUBLICATIONS, REPORTS AND PRESENTATIONS

Moe, K., A Mathematical Description of the Disturbed Thermosphere, EOS, Trans. AGU, 56, 1031, 1975.

Moe, K., and M. M. Moe, A Dynamic Model of the Neutral Thermosphere, MDAC Interim Scientific Report to this contract, 1975.

Moe, M. M., K. Moe, V. L. Carter, and M. B. Ruggera, Jr. The correlation of densities at high southern latitudes with charged particle precipitation, EOS, Trans. AGU, 54, 1146, 1973.

Moe, K., W. P. Olson, and M. M. Moe, A New Global Model of the Thermosphere, EOS, Trans. AGU, 56, 1155, 1974.

Moe, K., W. P. Olson, M. M. Moe, and G. Oelker, A Thermospheric Model which includes Magnetospheric, Tropospheric, and Ultraviolet Energy, EOS, Trans. AGU, 56, 614, 1975.

Moe, M. M., A. Rice, K. Moe, H. R. Mukherjee, and K. L. Chan, Ionospheric Response to Precipitation through the Magnetospheric Cleft, EOS, Trans. AGU, 56, 1038, 1975.

Olson, W. P., Cleft Magnetic Fields and Currents, invited review presented to the Magnetospheric Cleft Symposium, Dallas, 1973.

Olson, W. P. Corpuscular Heating of the Upper Atmosphere, presented to the Symposium on Dynamics, Chemistry and Thermal Processes in the Ionosphere and Thermosphere, IAGA, Kyoto, 1973.

Olson, W. P., Quiet Magnetospheric Currents and Fields, presented at the Chapman Memorial Symposium on Magnetospheric Motions, Boulder, June, 1973.

Olson, W. P., Self-consistent Study of Magnetospheric Particle and Field Structures, presented to the Symposium on Magnetospheric Configuration, IAGA, Kyoto, 1973.

Olson, W. P., The Sources of Magnetospheric Currents, EOS, Trans. AGU, 54, 1185, 1973.

Olson, W. P. The Tail Magnetic Field to 100 R_E, EOS, Trans. AGU, 54, 428, 1973.

Olson, W. P. Variations in Magnetic Conjugacy and Related Effects on Low Energy Particles, presented to the Symposium on Magnetospheric Configuration, IAGA, Kyoto, 1973.

Olson, W. P., A model of the distributed magnetospheric currents, J. Geophys. Res., 79, 3731, 1974.

Olson, W. P., Dayside Cusp Structure and Magnetic Field, EOS, Trans. AGU, 55, 402, 1974.

Olson, W. P., Solar Wind Influence on the Earth's Atmosphere and Magnetosphere, invited paper presented to the 12th Aerospace Sciences Meeting of the AIAA, January, 1974.

Olson, W. P., A Summary of the LaJolla Conference on Quantitative Magnetospheric Models, presented to the 10th ESLAB Symposium, Vienna, June 1975.

Olson, W. P., Electromagnetic Coupling of the Lower Atmosphere and Magnetosphere, invited review presented to the Symposium on Global Effects of Interplanetary Medium - Magnetosphere - Lower Atmosphere Interactions, Grenoble 1975.

Olson, W. P., Numerical Magnetospheric Modelling, invited review presented to the IMS workshop, Grenoble, September 1975.

Olson, W. P., Quantitative Magnetospheric Models, invited paper presented to the Annual Meeting of the AGU, EOS, Trans. AGU, 56, 422, 1975.

Olson, W. P., The Contributions of Ionospheric and Magnetospheric Currents to the Earth's Surface Field, invited review presented to the Zmuda Memorial Conference, Colorado Springs, March 1975.

Olson, W. P., and K. Moe, Response of the Magnetosphere and Atmosphere to the Solar Wind, MDAC Interim Scientific Report to this contract, 1973.

Olson, W. P., and K. Moe, Influence of precipitating charged particles on the high-latitude thermosphere, J. Atm. Terr. Phys., 36, 1715, 1974.

Olson, W. P., K. Moe, and K. Pfitzer, Response of the Magnetosphere and Atmosphere to the Solar Wind, MDAC Interim Scientific Report to this contract, 1974.

Olson, W. P., and K. A. Pfitzer, A Quantitative Model of the Magnetospheric Magnetic Field, J. Geophys. Res., 79, 3739, 1974.

Olson, W. P., K. A. Pfitzer, and K. Moe, Response of the Magnetosphere and Atmosphere to the Solar Wind, Final Scientific Report to this contract, 1975.

Pfitzer, K. A., Magnetospheric Magnetic Field Expansions, EOS, Trans. AGU, 54, 1186, 1973.

Pfitzer, K. A., and W. P. Olson, The Entry of Low Energy Charged Particles into the Magnetosphere, EOS, Trans, AGU, 54, 432, 1973.

Pfitzer, K. A., and W. P. Olson, Particle Entry to a Model Magnetosphere, EOS, Trans. AGU, 56, 1174, 1974.

UNCLASSIFIED
SECURITY CLASSIFICATION OF THIS PAGE (When Data Entered)

REPORT DOCUMENTATION PAGE	READ INSTRUCTIONS BEFORE COMPLETING FORM
1. REPORT NUMBER: AFOSR TR-76-0083	2. GOVT ACCESSION NO. / 3. RECIPIENT'S CATALOG NUMBER: (9) Final rept. Jul 72 - Sep 75
4. TITLE (and Subtitle): Response of the Magnetosphere and Atmosphere to the Solar Wind.	5. TYPE OF REPORT & PERIOD COVERED: Final 7/'72 - 9/'75
	6. PERFORMING ORG. REPORT NUMBER
7. AUTHOR(s): W. P. Olson, K. A. Pfitzer — O.K. / Moe	8. CONTRACT OR GRANT NUMBER(s): F44620-72-C-0084
9. PERFORMING ORGANIZATION NAME AND ADDRESS: McDonnell Douglas Astronautics Co., 5301 Bolsa Avenue, Huntington Beach, California 92647	10. PROGRAM ELEMENT, PROJECT, TASK AREA & WORK UNIT NUMBERS: AF-9751-06, 61102F, 9751-06
11. CONTROLLING OFFICE NAME AND ADDRESS: Air Force Office of Scientific Research/NP, 1400 Wilson Boulevard, Arlington, Virginia 22209	12. REPORT DATE: December 1975
	13. NUMBER OF PAGES: 120 pp.
14. MONITORING AGENCY NAME & ADDRESS (if different from Controlling Office)	15. SECURITY CLASS. (of this report): UNCLASSIFIED
	15a. DECLASSIFICATION/DOWNGRADING SCHEDULE

16. DISTRIBUTION STATEMENT (of this Report)

Approved for public release, distribution unlimited.

17. DISTRIBUTION STATEMENT (of the abstract entered in Block 20, if different from Report)

18. SUPPLEMENTARY NOTES

Tech., other

19. KEY WORDS (Continue on reverse side if necessary and identify by block number)

Solar wind, magnetosphere, atmosphere, quantitative models, data correlations.

20. ABSTRACT (Continue on reverse side if necessary and identify by block number)

This report summarizes work performed during the entire contract period. The general goal was to obtain a better quantitative understanding of the interaction of the solar wind with the magnetosphere and atmosphere. Several scientific goals were formulated and meet. They included the fabrication of quantitative models of the shape and location of the davside cusps, the total magnetospheric magnetic field, and of total neutral atmospheric density. These models, together with others developed or under development with other DoD support, should provide a first set of software capable of being used to

DD FORM 1 JAN 73 1473 EDITION OF 1 NOV 65 IS OBSOLETE

404 770

SECURITY CLASSIFICATION OF THIS PAGE (When Data Entered)

20. ABSTRACT

specify environmental behavior, with emphasis being given to those aspects which influence the performance of hardware systems.